New Jersey Institute of Technology

Digital Commons @ NJIT

Dissertations   Electronic Theses and Dissertations

Fall 1-31-2007

Reactive modification and crystallization behavior of foamed poly(butylene terephthalate)

Byeong Joon Jeong
New Jersey Institute of Technology

Recommended Citation

ABSTRACT

REACTIVE MODIFICATION AND CRYSTALLIZATION BEHAVIOR OF FOAMED POLY(BUTYLENE TEREPHTHALATE)

by
Byeong Joon Jeong

The objective of this study is to investigate the feasibility of preparing low density foams based on poly(butylene terephthalate) (PBT) through modification of its molecular structure and rheological characteristics by reactive extrusion. The scientific and/or engineering interpretation of the experimental data was based on fundamentals of extrusion, crystallization mechanisms, as well as information on reactivity and tendency toward degradation of PBT.

As a preliminary study, the extrusion foaming behavior of a commercial linear semi-crystalline PBT with a chemical blowing agent (CBA) was investigated. Foam characteristics were functions of extrusion operational variables, such as die set temperature and screw speed. Gas solubility and CBA decomposition kinetics were found to be key elements for controlling and optimizing the quality of the foamed polymer.

Initially, the linear PBT polymer was reactively modified using a tri-functional epoxide in a batch mixer to produce a branched structure with a higher molecular weight (MW) and a broader molecular weight distribution (MWD) as evidenced by rheological analysis. These experiments provided information on the PBT/modifier reaction kinetics. Chain branching was then carried out by single screw extrusion, where the competing degradative chain scission reaction needed to be taken into account.

Applications of fundamentals of extrusion theory to the reactive extrusion process enabled the optimization of the extrusion operational conditions. The optimization led to

the production of a branched polymer with viscoelastic characteristics suitable for low density extrusion foaming by injection of a physical blowing agent (PBA).

The branched product made under the optimized conditions could be foamed to densities as low as 0.33 g/cc and showed high expansion ratio of 4.0 and cell structure resistant to coalescence. The possibility of overlap of the polymer crystal formation with the nucleation/growth of gaseous cells was investigated based on theoretical predictions. Slow pressure drop rate was shown to decrease cell nucleation rate. Fast crystallization rate stabilized cell morphology.

The occurrence of flow induced crystallization during bubble formation was investigated, to our knowledge, for the first time. Smaller size spherulitic structures at the bubble walls of the branched PBT compared with the linear polymer, suggested longer crystal nuclei lifetime, which may indicate that the formation of the crystalline structures was affected by the bi-axial deformation occurring during bubble growth.

REACTIVE MODIFICATION AND CRYSTALLIZATION BEHAVIOR OF FOAMED POLY(BUTYLENE TEREPHTHALATE)

by
Byeong Joon Jeong

A Dissertation
Submitted to the Faculty of
New Jersey Institute of Technology
in Partial Fulfillment of the Requirements for the Degree of
Doctor of Philosophy in Chemical Engineering

Otto H. York Department of Chemical Engineering

January 2007

APPROVAL PAGE

REACTIVE MODIFICATION AND CRYSTALLIZATION BEHAVIOR OF FOAMED POLY(BUTYLENE TEREPHTHALATE)

Byeong Joon Jeong

Dr. Marino Xanthos, Dissertation Advisor   Date
Professor, Otto H. York Department of Chemical Engineering, NJIT

Dr. Costas G. Gogos, Dissertation Co-Advisor   Date
Distinguished Research Professor, Otto H. York Department of Chemical Engineering, NJIT

Dr. Kun S. Hyun, Dissertation Co-Advisor   Date
Research Professor, Otto H. York Department of Chemical Engineering, NJIT

Dr. David Todd, Committee Member   Date
President, Todd Engineering, West Windsor, NJ

Dr. Dana E. Knox, Committee Member   Date
Professor, Otto H. York Department of Chemical Engineering, NJIT

Dr. Jing Wu, Committee Member   Date
Assistant Professor, Otto H. York Department of Chemical Engineering, NJIT

BIOGRAPHICAL SKETCH

Author: Byeong Joon Jeong

Degree: Doctor of Philosophy

Date: January 2007

Undergraduate and Graduate Education:

- Doctor of Philosophy in Chemical Engineering,
  New Jersey Institute of Technology, Newark, NJ, 2007

- Master of Science in Chemical Engineering,
  University of Korea, Seoul, Republic of Korea, 1996

- Bachelor of Science in Chemical Engineering,
  University of Korea, Seoul, Republic of Korea, 1994

Major: Chemical Engineering

Presentations and Publications:

Byeong Joon Jeong, Marino Xanthos and Kun S. Hyun, "Rheological and crystallization behavior of linear and branched PBT", Proceedings of SPE Annual Techn. Conf. (2007) (submitted).

Byeong Joon Jeong and Marino Xanthos, "Reactive modification of PBT with applications in low density extrusion foaming,", *Polym. Eng. Sci.*, (2006) (in press).

Byeong Joon Jeong, Marino Xanthos and Kun S. Hyun, "Reactive extrusion of PBT for low density foaming,", Proceedings of SPE Annual Techn. Conf. Vol. I, 983 (2006).

Byeong Joon Jeong, Marino Xanthos and Yoon S. Seo, "Extrusion foaming behavior of PBT resins,", J. Cell. Plast., **43**, 656 (2006).

Byeong Joon Jeong, Yoon S. Seo and Marino Xanthos, "Extrusion foaming behavior of PBT resins,", Proceedings of SPE Annual Techn. Conf. Vol. II, 2605 (2005)

Dedicated to my cherished memories with my parents and three sisters,
and invaluable current moments with my wife, son and ......

ACKNOWLEDGMENTS

I would like to thank my advisor, Prof. Marino Xanthos, for giving me advising and encouragement. Without his enthusiastic devotion to guiding my research and academic activities, this work would not have been presented. The contributions of Prof. Xanthos would be fundamental to my further professional career. I am thankful to Dr. Costas Gogos for his efforts to provide me a thorough way to look at polymer processing. I am also thankful to Dr. Kun Sup Hyun for his kind care of my family as well as constructive suggestions on my research. I am indebted to Dr. David Todd for sharing his knowledge and experiences with me. Many thanks to Dr. Dana Knox and Dr. Jing Wu for their suggestions on improving this dissertation.

Financial support provided by Prof. Marino Xanthos from various research grants and by the Polymer Processing Institute (PPI) are highly appreciated. I am grateful to the Tech Center at LG Chemical Ltd. to allow me to have a chance to be a Ph.D. candidate of NJIT as well as a visiting engineer at PPI.

I would thank to all the ex- and current PPI members for their suggestions and discussion. In particular, I would like to thank Dr. Victor Tan for helpful discussions and advising on polymer characterization. Also, to Dr. Steve Kim for his guidance on SEM operation. I am thankful to Mr. Dale Conti and Dr. Chen Wan for setting up the extrusion foaming line.

My wife's endurance and understanding enabled me to complete this work; my parents-in-law are also appreciated for their encouragement. Talking with my sisters is always joyous and supportive. I cannot overstate my gratitude to my parents, whose presence and best wishes are always fundamental to whom and what I am.

TABLE OF CONTENTS

LIST OF TABLES

LIST OF FIGURES

A	Area
A_{micro}	Area of micrograph
c	Concentration
D	Diffusivity
f	Correction factor
$f(\theta)$	Geometric correction factor
G	Crystal growth rate
G'	Storage modulus
G''	Loss modulus
g	Source term
H_f	Heat of fusion
J	Nucleation rate
K_f	Crystal growth rate induced by flow
K_w	Henry's law constant
k	Avrami crystallization kinetic constant
k_{batch}	Reaction kinetic constant from batch mixer
k_{Boltz}	Boltzmann constant
k_m	Mass transfer coefficient
L	Length of die
l_c	Size of crystal
M_{micro}	Magnification of micrograph
m	Power low consistency

N	Number of nuclei per volume
N_0	Number of cells per unit volume
N_f	Number of nuclei per volume created by flow
n	Avrami exponent
n_c	Cross model constant
n_p	Power low exponent
n_{cell}	Number of cells in micrographs
P	Pressure
Q	Volumetric flow rate
R	Radius of die
R_c	Radius of boundary between gas and polymer matrix
r	Radius`
r^*	Critical radius for nucleation
S	Entropy
S_c	Radius of interface of a unit cell
S_g	Solubility
T	Temperature
T_m	Melting temperature
T_g	Glass transition temperature
T_∞	Temperature where chain mobility is frozen
T_m^0	Equilibrium melting temperature
$\Delta T_{g,CO_2}$	Depression of glass transition temperature by CO_2

$\Delta T_{m,CO2}^{0}$	Depression of equilibrium melting transition temperature by CO_2
U^*	Activation energy for the segment jump of polymer molecules
X_c	Relative crystallinity in Avrami equation
x	Molar content
V	Volume
V_f	Void fraction of foam
W	Work
Δ	Difference or change
$\dot{\gamma}$	Shear rate
$\dot{\gamma}_w$	Wall shear rate
μ	Chemical potential
λ	Stretching or deformation
μ_0	Newtonian viscosity in Cross model
ν	Frequency factor
θ_c	Relative crystallinity
ρ	Density
ρ_ϕ	Foam density
σ	Surface tension
σ_{ij}	Interfacial tension between i and j
τ_{batch}	Toque of batch mixer

$\left(\tau_{rr} - \tau_{\theta\theta}\right)$ Normal stress difference in foam growth

ω Frequency

superscript

$*$ Critical condition for nucleation

subscript

f Fusion or melting

g Gas phase

hom Homogeneous nucleation

het Heterogeneous nucleation

o Initial condition

r Function of radius

s Polymer cell in bubble growth model

x Function of molar content

∞ Ambient

LIST OF ACRONYMS

APET	Amorphous poly(ethylene terephthalate)
BGPM	N,N'-bis[3(carbo-2',3' epoxypropoxy)phenyl] pyromellitimide
BTDA	3,3',4,4'-benzophenone tetracarboxylic anhydride
CAS No.	Chemical abstract number
CBA	Chemical blowing agent
cc	Cubic centimeter
CFC	Chlorofluorocarbon
Con G'	Contribution of G' to the magnitude of the complex viscosity
CPET	Nucleated poly(ethylene terephthalate)
DDC	Dynamic decompression and cooling
DGEBA	Glycidyl ether of bisphenol-A
DSC	Differential scanning calorimeter
E-GMA	Ethylene-glycidyl methacrylate
FIC	Flow or deformation induced crystallization
HBR	Helical barrel rheometer
GPC	Gas permeable chromatography
HCFC	HydroChlorofluorocarbon
HDPE	High density polyethylene
iPP	Isotactic polypropylene
LDPE	Low density polyethylene
MFI	Melt flow index

MW	Molecular weight
MWD	Molecular weight distribution
PBA	Physical blowing agent
PBT	Poly(butylene terephthalate)
PET	Poly(ethylene terephthalate)
PMDA	Pyromellitic dianhydride
PS	Polystyrene
PP	Polypropylene
5-PT	5-phenyltetrazole
phr	Part per hundred
PTT	Phan-Thien Tanner (viscoelastic model)
RMS	Rheometrics Mechanical Spectrometer
rpm	Revolutions per minute
SAXS	Small angle X-ray scattering
SEM	Scanning electron microscope
TGDDM	Tetraglycidyl diamino diphenyl methane
TGIC	Triglycidyl isocyanurate
TGG	Triglycidyl glycerol
WAXD	Wide angle X-ray diffraction
XRD	X-ray diffraction

CHAPTER 1

INTRODUCTION

In general, thermoplastic foams fall into two categories in terms of density: high and low density. The density reduction of high density foams is usually 10~25% versus the unfoamed polymer, and they are used in applications where weight reduction without loss of strength or rigidity is desired (such as furniture, windows, doors and appliances and automotive parts). Injection molding in the presence of chemical blowing agents (CBAs) is the major manufacturing method to produce high density foams. On the other hand, up to 90% of density reduction versus the unfoamed polymer can be achieved by low density foaming with physical blowing agents (PBAs) such as volatile hydrocarbons, CFCs, HCFCs and atmospheric gases. Applications of low density foams are in heat and sound barriers, cushioning, shock absorbents and floating devices. Extrusion by gas injection and gas-impregnated expanding polymer beads are the primary methods to produce low density foams (Throne, 2004a).

There exist several foamable polymers. Amorphous polymers, e.g., polystyrene (PS), and semi-crystalline vinyl polymers, such as high density polyethylene (HDPE), low density polyethylene (LDPE) and polypropylene (PP) are considered as foamable polymers.

However, foaming of aromatic polyesters, such as poly(ethylene terephthalate) (PET) and poly(butylene terephthalate) (PBT) has been mostly limited to high density products. Low density foaming of such polyesters is achieved with difficulties, although there exists a potential usage in packaging, construction and transportation applications, in which they may provide advantages such as high temperature dimensional stability,

good mechanical properties and recyclability. Difficulties in low density foaming are related to the relatively low molecular weight (MW) and narrow molecular weight distribution (MWD), inherent in polycondensation polymers. The typical low MW and narrow MWD of polyesters result in a rheological behavior at processing temperatures that is not compatible with processes such as low density foaming, thermoforming or extrusion blow molding, where high elastic properties are required.

In order to overcome this limitation, reactive modification has been introduced; polyfunctional coupling agents (or chain structure modifiers) with suitable electrophilic functionality have been shown to react with nucleophilic end groups (hydroxyl and/or carboxyl) present in polyesters, within relatively short times. Through the reaction, the structure of the linear polyesters is modified with a resulting improved rheology suitable for low density foaming; PET is well known to respond to such modifications (Xanthos and Dey, 2000; Xanthos et al. 2004).

PBT, the second in importance aromatic polyester, has numerous applications mostly in unfoamed injection molding products due to its good thermal and electrical resistance, dimensional stability and mechanical strength. One can expect that the PBT advantages could extend to applications of foamed PBT products; however, there have been only limited attempts to investigate low density foaming even after reactive modification. Reasons for such limited attempts may be related to difficulties arising from the faster crystallization kinetics and higher crystallinity of PBT versus PET. The tetra-methylene groups in the PBT repeating units provide more flexibility and facilitate the crystallization process, resulting in faster crystallization kinetics as well as a higher crystallinity, as compared to PET containing the more rigid bi-methylene groups.

It should be noted that the effects of crystallization on foaming have only been investigated with polymers of low crystallinity and/or slow crystallization kinetics, and mostly in batch foaming.

Polymer foaming is a complicated process. Nucleation, induced by a thermodynamic driving force, creates nuclei as the seeds for foaming, which grow to a final size under the balance between the hydrodynamic driving force and forces related to the viscoelasticity of the matrix polymer. Thus, theoretical and experimental knowledge on thermodynamics, hydrodynamics and viscoelasticity are to be considered. In addition, extrusion foaming involves more complexity, since the variables that govern the foaming process are determined by selection and control of the extruder equipment and processing conditions. Furthermore, nucleation and growth behavior deviate from theoretical predictions based on static and equilibrium conditions. Considering these complexities, one cannot expect a well-established relationship between extrusion foaming behavior and crystallization behavior, in particular, with polymers having fast crystallization kinetics and high crystallinity such as PBT.

1.1 Objectives of This Thesis

Among the objectives of this study is the investigation of the reactive modification of PBT for chain branching, by introducing a triepoxide in a conventional extrusion system, followed by optimization of the process parameters to produce polymers with defined viscoelastic characteristics for low density foaming. As a preliminary study, both unmodified and modified PBT are foamed with a chemical blowing agent (CBA) to high density foams, and the possibility of using the modified resin in low density extrusion

foaming is then examined, after thorough rheological analysis of the modified products. Crystallization behavior as a function of molecular chain structure is investigated and related to the characteristics of the foaming processes. This is of significant importance, considering the fast crystallization kinetics of PBT and the possible overlapping effects of crystallization and bubble nucleation/growth on the process and product characteristics.

1.2 Preview of This Thesis

In Chapter 2, information on reactive modification and foaming of polyesters that are currently available are presented. After a brief summary of the fundamentals of extrusion foaming, two crystallization mechanisms – flow induced and gas induced - are introduced, since they are apparently related to the crystallization behavior in extrusion foaming. In Chapter 3, experimental processing and characterization methods including reactive processing and foaming are discussed. In Chapter 4, after a preliminary experimental work with CBAs, reactive modification to obtain the desired viscoelastic property is presented, and optimization of the operational parameters of the reactive extrusion process is discussed. Extrusion foaming of the modified PBT by gas injection to low density products is then discussed, considering the effects of crystallization. Finally, the possibility of the occurrence of flow induced crystallization in extrusion foaming and its effects are discussed in detail.

CHAPTER 2

BACKGROUND

2.1 Polyester Foams

The rheological behavior and viscoelastic characteristics of commercial linear polyesters produced by polycondensation reactions are generally inadequate for low density foaming; thus, the production of foams from linear polyesters are limited to: (I) conventional extrusion foaming with CBA, (II) batch foaming or injection molding foaming using supercritical fluids as blowing agents, and, (III) non-conventional foaming processes. The linear polyesters can be foamed by these processes, since the resin viscoelasticity has little or no effect on their foamability.

CBAs are used in extrusion foaming to produce medium to high density foams (> 0.5 g/cc). Extrusion foaming with CBAs usually requires less modification of the extrusion system, and the operational window is wider as compared to that with PBA. However, CBAs are relatively expensive, and the residue of CBA may involve undesired changes of the matrix polymer characteristics (Xanthos and Dey, 2000).

Xanthos et al. (1998) evaluated extrusion foamability of a variety of PET resins with different rheological characteristics using several CBAs and found that an exothermic CBA (Expandex 5-PT) performed better than two other endothermic ones. They produced high to medium density PET foams (> 0.6 g/cc). The foam densities varied with respect to the material variables (type and concentration of CBA) and the operational variables (die set temperature and screw rpm). In order to obtain improved foamability of PET with PBA, they suggested the use of PET with modified viscoelastic characteristics.

A batch foaming process with PBAs, known as microcellular foaming, is adaptable to linear polyesters. The procedure of microcellular foaming is as follows: polymer samples are first placed in a pressure vessel, the pressure vessel is then charged with the saturation gas (blowing agent) to a constant saturation pressure at room temperature using a pressure regulator while maintaining isobaric conditions throughout the sample saturation, and the samples are maintained at room temperature during the blowing agent saturation step. After the saturation time, the polymer/gas solution is discharged from the pressure vessel, and the solution is foamed at higher temperatures in a temperature controlled glycerin bath. The final structure of the foamed samples is fixed by quenching, following the foaming step. A detailed description of the process is found elsewhere (Martini et al. 1984; Colton and Suh, 1987; Kumar and Suh, 1990; Kumar and Weller, 1994)

Baldwin et al. (1996a; 1996b) performed microcellular foaming with a commercial PET. They used cell density as a representative variable to describe the foam characteristics, and the higher cell densities of $10^{10} \sim 10^{12}$ cells/cc were obtained with the semi-crystalline PET rather than APET (amorphous PET) or CPET (nucleated PET).

The published information on foaming of aromatic polyesters is mostly about PET foaming rather than PBT, which is the topic of the current study. This may also be related to the lower cost of the PET resin vs. PBT and the recent penetration of PET foams in competitive packaging markets that are currently served by low cost commodity resins.

To our knowledge, very few reports were available on foaming PBT to low or medium densities by conventional polymer processes such as extrusion. Klotzer et al.

(1997) performed extrusion foaming of PBT with PBA, using a conventional extrusion system. Their motivation of producing such foams was to prepare membranes with good thermal stability; however, the coarse cell morphologies that appear in their publication would suggest poor quality of the foamed products. Information on the foam characteristics such as density and expansion ratio was not included in their published article.

Other references using PBAs (CO_2, N_2) involved foaming of highly filled or reinforced PBT by injection molding processes such as Mucell® (Technical brochure by GE Plastics) or Optifoam® (Technical brochure by Pollmann Austria). Both technologies produce relatively high density structural foams (density reduction of about 30% or less) similar to those of commercially available PBTs (highly filled or reinforced injection molding grades) foamed with chemical blowing agents (CBA).

It should be noted that an unconventional foaming method, the so called "dynamic decompression and cooling (DDC)", has also been used for PBT foaming as reported by Song et al. (1999). The DDC involved heating and mixing of materials under high pressure in the presence of a volatile blowing agent. A rapid expansion of the mixture induced the volatile phase to evaporate causing the melt to cool down and expand, resulting in a porous structure. The PBT foam produced by this method showed open cell structures with an increased crystallinity as compared to foams by the conventional foaming processes.

2.2 Reactive Modification of Polyesters for Foaming Applications

Polyesters have been used in wide applications such as fibers, biaxially-oriented film, stretched blow-molded bottles, electronic housings and automotive parts. In a usual melt polycondensation, it is difficult to obtain a polyester with a high MW and broad MWD, and as a result, the products have low viscosity and elasticity. This is due to the competing degradation reaction occurring during polycondensation; in the reactor, the MW of the intermediate polymers are increasing with respect to time as a result of polycondensation. However, as the MW reaches a certain level, it is difficult to remove the polymerization by-products, and this may result in hydrolytic degradation. In addition, after reaching this MW level, the rates of degradation and side reactions are faster than that of the polycondensation reaction (Yoon and Park, 1995). As a result, application of polyesters in polymer processing operations, where higher viscoelasticity is required, is limited.

In order to overcome this limitation, post-polycondensation in a solid phase has been introduced, in spite of slow reaction rates and need for specialized equipment for large scale operations (Inata and Matsumura, 1985). Another method is to use a chain extender, which can react with the polymer end groups, resulting in polyesters with higher MW. In earlier work on reactive chain extension, reactions involved by-products, such as phenol and ethylene carbonate, which may have resulted in contamination of the final product. Examples of such chain extenders are diphenyl carbonate, diphenyl terephthalate, diphenyl oxalate and phenyl orthocarbonate (Inata and Matsumura, 1985; Loontjens, 2003). Addition type chain extenders, which involve no by-product formation, started being used and favored over the past 30 years. The addition type chain extenders

currently available are diepoxy compounds, bis(cyclic carboxylic anhydride), diisocyanates and bis-2-oxazolines. Furthermore, by introducing chemicals with more than two functionalities, branching and (partially) crosslinking are possible during reactive melt modification.

The products of the chain extension/branching have an increased MW and broadened MWD. These structural changes result in different rheological behavior as compared to the unmodified polymer, and such changes in rheological behavior favor extrusion foaming to low densities. The importance of the rheological characteristics on foaming will be discussed in the following section.

With respect to PET, there exist many technical and scientific articles on chain extension/branching used to modify its structure as well as applications of the modified PET in extrusion foaming. PET modifiers and examples of their use have been recently reviewed (Xanthos and Dey, 2000; Zhang and Xanthos, 2004).

By its versatility, the reactive modification of PET has been applied to recycled post-consumer PET with the intent of producing extrusion foamed products. Xanthos et al. (2000a; 2000b) showed the improvement of foamability of the recycled PET by rheological modification with pyromellitic dianhydride (PMDA) in a comparative study of unmodified and modified (post-consumer) PET using PBAs. They delineated the rheological characteristics of the modified PET as higher MFI, higher melt viscosity, early shear thinning with high shear sensitivity, and higher extrudate swell ratio as compared to the unmodified PET. They could obtain low density foams (< 0.5 g/cc) with the modified PET, while foams with density below 0.7 g/cc could not be achieved with the unmodified polymer.

Japon et al. (2000) used a tetraepoxide to reactively modify recycled PET. They obtained branched structures with broadened MWD, and highly increased elongational viscosity. Their application of the modified PET to extrusion foaming with PBA resulted in foams with high density of 0.85 ~ 1.0 g/cc.

The most important element in selecting a modifier is the possibility to obtain the desired viscoelastic properties for foaming. There exist many multifunctional anhydrides and multi-epoxides that have been shown to be efficient modifiers reacting with the polyester terminal carboxyl and/or hydroxyl groups. However, the reaction time is always of concern particularly in continuous polymer processing such as extrusion. The availability and cost of the modifiers may be another concern.

Xanthos et al. (2001) showed that glycidyl functionalized additives such as a diepoxide and an ethylene-glycidyl methacrylate (E-GMA) copolymer reacted readily with the functional groups of PET, acting as chain extending/branching agents. The modified product showed promising rheological characteristics for low density foaming. They also found that the diepoxide had higher reactivity than E-GMA and could be used at much lower concentrations to produce resins with the desired characteristics.

Dhavalikar and Xanthos (2003) performed a comparative study of four different multi-epoxides, N,N'-bis[3(carbo-2',3' epoxypropoxy)phenyl] pyromellitimide (BGPM), glycidyl ether of bisphenol-A (DGEBA), triglycidyl isocyanurate (TGIC) and triglycidyl glycerol (TGG), as PET rheology modifiers. They found that TGIC and BGPM were most efficient in the modification reactions; however, a limitation of BGPM was that it was not commercially available. As shown in their subsequent work (Dhavalikar et al.

2003), the melt modified PET by TGIC showed an increase in relaxation time and broadening of relaxation times distribution with corresponding effects on MW and MWD.

Recently, a comprehensive comparison study was published by Xanthos et al. (2004) Low molecular weight multifunctional anhydrides and epoxides were evaluated as rheological modifiers for PET by reactive extrusion under controlled conditions. The dianhydrides, used in the study, were: pyromellitic dianhydride (PMDA) and 3,3',4,4'-benzophenone tetracarboxylic anhydride (BTDA). The multi-epoxides were BGPM, TGIC and tetraglycidyl diamino diphenyl methane (TGDDM). Correlations of die pressure with extrudate swell and melt flow index with melt strength by off-line testing showed that the most reactive modifiers were PMDA, TGDDM, and TGIC.

The multi-epoxides are good candidates in terms of availability. There exist commercial epoxides with various numbers of functional groups whereas some of the multifunctional anhydrides are only available in small quantities. A schematic of the assumed reaction mechanism between an epoxide and polyester terminal groups (Dhavalikar and Xanthos, 2003) is shown in Figure 2.1. The glycidyl functional group of the epoxide has been suggested to react with carboxyl end groups (esterification) preferentially, followed by reaction with hydroxyl groups (etherification) in the melt processing temperature range.

Esterification:

$$\text{\Large\textasciitilde\textasciitilde\textasciitilde} \; \underset{\underset{O}{\|}}{C} - OH \; + \; \underset{\underset{O}{\diagdown\diagup}}{CH_2 \; CH \; CH_2} - R$$

$$\downarrow$$

$$\text{\Large\textasciitilde\textasciitilde\textasciitilde} \; \underset{\underset{O}{\|}}{C} - O - CH_2 \; \underset{\underset{OH}{|}}{CH} \; CH_2 - R$$

Etherification:

$$\text{\Large\textasciitilde\textasciitilde\textasciitilde} \; CH_2 - OH \; + \; \underset{\underset{O}{\diagdown\diagup}}{CH_2 \; CH \; CH_2} - R$$

$$\downarrow$$

$$\text{\Large\textasciitilde\textasciitilde\textasciitilde} \; CH_2 - O - CH_2 \; \underset{\underset{OH}{|}}{CH} \; CH_2 - R$$
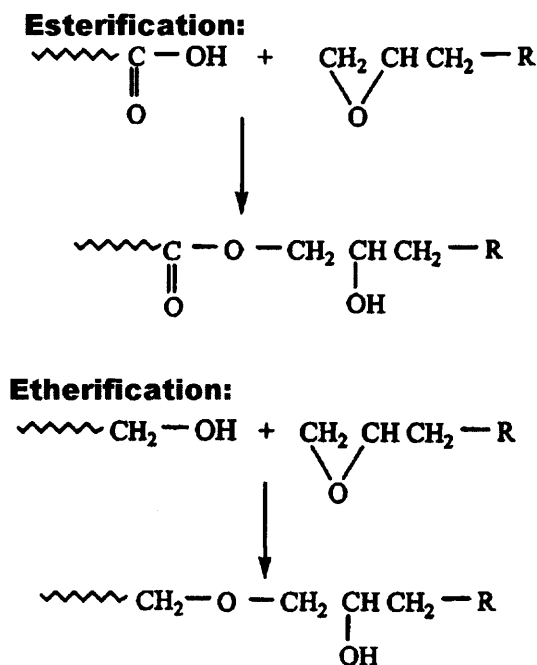
Figure 2.1 Schematic of reaction between epoxide and polyester terminal groups (Dhavalikar and Xanthos, 2003).

A batch mixer is normally used for the investigation of the kinetics of the reactive modification reactions. The torque change as a consequence of the reaction is monitored, and the reaction time is extracted from the results. However, the reaction kinetics data from this method are applicable only in processes with similar mixing kinematics and diffusion behavior as with the batch mixer. An interesting approach for evaluating the reaction kinetics was suggested by Dhavalikar and Xanthos (2004). They prepared two types of PET/modifier samples and performed chemorheological measurements; the chemorheology of the samples prepared by the solution casting method represented the kinetic data of the reaction at the interfaces only, eliminating the effects of diffusion. The results of the samples prepared by the powder cake method gave information under a "segregated" condition, where the reaction kinetics were affected by the reactions at the

interfaces and the diffusion of the reactant through PET. Note that mixing effects were eliminated in both cases. It should also be noted, however, that the kinetic data obtained by these methods were equivalent to those obtained under static conditions. Thus, a direct application to real processing is limited, since the dynamics of processing induce a change of the interfacial area as well as a change in the diffusion behavior.

By contrast to PET, there exists limited information on the reactive modification of PBT. The following examples of reactive modification of PBT focus on the reactivity of the modifiers and/or the improvement of mechanical properties. So far, there was no attempt to widen the PBT applications via reactive modification.

Bikiaris and Karayannidis (1995; 1996) synthesized three types of diepoxides and performed chain extension reactions with PBT in a batch mixer. An increase of the intrinsic viscosity and a decrease in the carboxyl content of PBT, as a result of the chain extension reactions, were obtained. The reaction times in the batch mixer were a function of the type and concentration of the modifiers. Under some conditions, the time for the completion of the reaction was up to 60 min, which seems to be impractical in an industrial environment; however, the authors concluded that a different appropriate modifier could be chosen in order to produce the chain extended PBT within reasonable residence times.

Inata and Matsumara (1985; 1986a; 1986b; 1987a; 1987b; 1987c) used several types of oxazolines, such as 2,2'-bis(2-oxazoline) and 2,2'-bis(4H-3,1-benzoxazin-4-one), as chain extenders of PBT as well as PET. Depending on the type of the oxazolines, the modifier reacted with either hydroxyl or (preferentially) carboxyl groups of PBT. The

reaction time was about 5 min, which is applicable to a conventional polymer processing operation.

Guo and Chan (1999) performed chain extension of PBT with a diepoxide (diglycidyl tetrahydrophthalate) by reactive extrusion. They found that the diepoxide was highly reactive, resulting in the completion of the reaction within 3 min at temperatures above $250^{\circ}C$. The mechanical properties of the chain extended PBT, which were the major objectives of their study, were improved by showing an increased notched Izod impact strength and increased elongation at break.

2.3 Fundamentals of Extrusion Foaming

Foaming consists of two processes; nucleation and growth of bubbles. Nucleation is driven by thermodynamic driving forces, resulting in the formation of seeds that will grow as bubbles. Growth occurs by hydrodynamic forces, which determine bubble size and bubble size distribution. The characteristics of nucleation and growth of bubbles in extrusion foaming are discussed in the following sections.

2.3.1 Bubble Nucleation

Nucleation is defined as a transformation from a metastable phase to a stable two phase system. Metastable mixtures are either superheated liquids or supersaturated vapors, which exist between the equilibrium locus (the binodal curve) and the limit of stability (the spinodal curve). Metastable phases can form new phases by a finite size fluctuation. The process is called homogeneous nucleation when the fluctuation occurs within the mixture; homogeneous nucleation occurs when a secondary phase is nucleated from the

bulk phase in the absence of impurities or solid surfaces. By contrast, the process of heterogeneous nucleation is induced by a fluctuation at an interface: when dispersed impurities or imperfectly wetted solid boundaries are present, heterogeneous nucleation takes place from nuclei formed at the interface between the bulk metastable liquid and these impurities. In order to form stable bubbles, nuclei need to overcome energy barriers, thus, nucleation rate depends on this free energy barrier (Blander and Katz, 1975; Han and Han, 1990). In this section, a brief summary of the basic equations, which characterize both homogeneous and heterogeneous nucleation, is introduced in order to obtain a concept of the nucleation process. Detailed description can be found elsewhere (Lee, 2000; Spitael 2003).

In homogeneous nucleation, three types of work (or free energy changes) are required: to create a spherical cavity with volume V, to create surface area A and to transport blowing agent molecules into this cavity. The work, $W_{r,x}$, as a function of bubble radius, r and its molar content, x, can be described by Equation (2.1) (Blander and Katz, 1975).

$$W_{r,x} = \sigma A - \Delta P V + x \Delta \mu \tag{2.1}$$

where A is the new surface created, σ is the surface tension, V is the volume of a sphere formed, ΔP is the pressure difference between the bulk and inside the bubble, and $\Delta \mu$ is the difference of the chemical potentials of the nucleated component (gas molecules) between the gas and liquid phases. A schematic representation of the variables for homogeneous nucleation is shown in Figure 2.2, where the subscript "hom" refers to homogeneous.
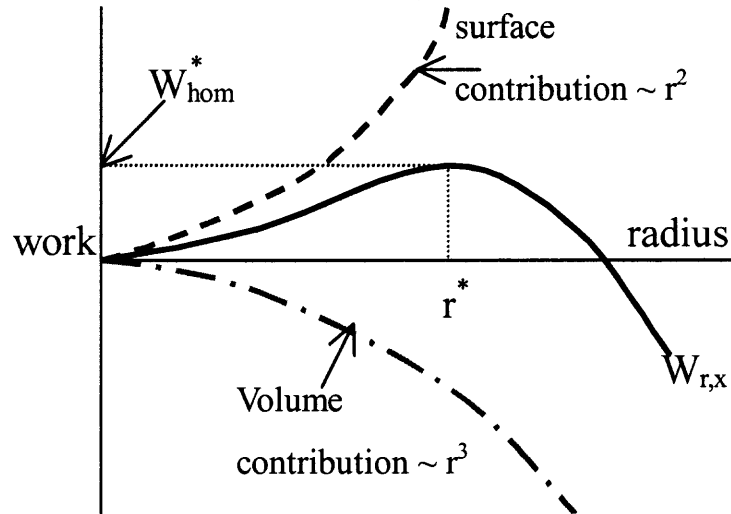
Figure 2.2 Schematic representation of the work to create a critical bubble from a metastable mixture (Spitael, 2003).

There exists a unique radius at which the formed bubble is in both chemical and mechanical equilibrium with its surroundings. This is defined as the critical radius, r^*. Formed bubbles with smaller than the critical radius would collapse, while bubbles whose size reach the critical radius would grow spontaneously. An illustration of the critical radius concept is shown in Figure 2.2, where the work is maximum at the critical radius. Thus, the critical radius, which satisfies $\partial W_{r,x} / \partial r = 0$, can be determined as:

$$r^* = \frac{2\sigma}{\Delta P} \qquad (2.2)$$

Goel and Beckman (1994) calculated the size of the critical radius in the batch foaming process of poly(methyl methacrylate) by CO_2. They found that the critical radius was about 30 nm at a low saturation pressure, and it was decreased to less than 1 nm with respect to the increase of the saturation pressure. By using Equation (2.2), the energy barrier for occurrence of the homogeneous nucleation, W_{hom}^*, which is usually defined as

the minimum work to reach equilibrium condition, can be obtained by combining

Equation (2.2) with Equation (2.1).

$$W_{hom}^{*} = \frac{16\pi\sigma^3}{3\Delta P^2} \qquad (2.3)$$

The nucleated bubbles with same or larger sizes that the critical radius can

overcome the barrier to grow further. A prediction of the number density of gas

molecules, which are able to overcome the barrier, requires an expression introduced by

Gibbs (1961); the number density of gas clusters (bubbles) of radius r containing x

molecules can be expressed as:

$$n_{r,x} = N \exp\left[-\frac{W_{r,x}}{k_{Boltz}T} \right] \qquad (2.4)$$

where $W_{r,x}$ is the minimum work to sustain a bubble, N is the number of

molecules per unit volume, k_{Boltz} and T are the Boltzmann constant and absolute

temperature, respectively. Thus, the critical radius of the bubbles can be derived by

substituting $W_{r,x}$ with Equation (2.3). Furthermore, an equation of the nucleation rate, J,

can be obtained by introducing a frequency factor as follows:

$$J = \nu N \exp\left[-\frac{W_{hom}^{*}}{k_{Boltz}T} \right] \qquad (2.5)$$

where ν is a frequency factor, which depends on the kinetics of bubble growth.

For example, Blander and Katz (1975) defined the frequency factor as $(2\sigma/(\pi m))^{1/2}$

where m represents the mass of a gas molecule.

In heterogeneous nucleation, three types of work are required in analogy with

homogeneous nucleation. However, the terms representing the volume change and the

surface area change are different, since heterogeneous nucleation occurs at pre-existing

interfaces between matrix and solid surfaces. Solid surfaces may be provided by solid particles (catalyst residue, residue of chemical blowing agent, dust, unmelted or degraded polymer), and/or vessel walls containing the metastable mixture. With an assumption that the interface is flat as shown in Figure 2.3, a horizontal balance of the interfacial tensions between polymer (1), gas (2) and solid (3) gives the Young's equation:

$$\sigma_{13} = \sigma_{23} + \sigma_{12} \cos\theta \tag{2.6}$$

and Equation (2.6) can be rearranged as:

$$\cos\theta = \frac{(\sigma_{13} - \sigma_{23})}{\sigma_{12}} \tag{2.7}$$

Work to form nuclei for heterogeneous nucleation, $W_{(het)r,x}$, can be defined as:

$$W_{(het)r,x} = S_{12}\sigma_{12} + S_{23}(\sigma_{23} - \sigma_{13}) - \Delta P V_2 + x\Delta\mu \tag{2.8}$$

where S_{12} is the surface area of the polymer/gas interface, S_{23} is the surface area of the gas/solid interface, V_2 is the volume of gas.
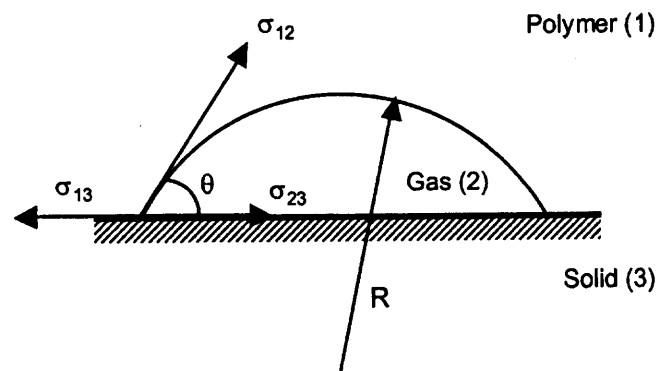
Figure 2.3 Schematic of bubble formation on a flat surface in heterogeneous nucleation.

The critical radius for heterogeneous nucleation can be determined in the same way as for the homogeneous nucleation above:

$$r_{het}^* = \frac{2\sigma_{12}}{\Delta P} \tag{2.9}$$

By combining Equation (2.9) and Equation (2.8), the minimum work in heterogeneous nucleation is defined as:

$$W_{het}^* = \frac{16\pi\sigma_{12}^3}{3\Delta P^2} f(\theta) \tag{2.10}$$

where the geometric correction factor, $f(\theta)$ is:

$$f(\theta) = \frac{\left(2 - 3\cos\theta + \cos^3\theta\right)}{4} \tag{2.11}$$

It should be noted that the critical radius for heterogeneous nucleation is identical to that for homogeneous nucleation and W_{het}^* is primarily lower than W_{hom}^*, since $0 \le f(\theta) \le 1$. The reduced minimum work (energy barrier) enhances nucleation, and this is how particles added intentionally work as nucleation agents. The heterogeneous nucleation rate can be derived similarly to the homogeneous nucleation rate.

$$J_{het} = \nu_{het} N_{het} \exp\left[-\frac{W_{het}^*}{k_{Boltz}T}\right] \tag{2.12}$$

where ν_{het} is the frequency factor and N_{het} is the number of heterogeneous sites.

Cavitation, known as a phenomenon that induces nucleation, occurs in the areas of discontinuity in the fluid due to external disturbance-induced pressure variation. For example, one can observe vigorous foaming during pouring or shaking an opened soda can. Pouring or shaking is an external disturbance that may induce local pressure

variation and/or local velocity differences. Nucleation would occur where a severe superheated condition is locally produced by these external disturbances.

Micro-cavities at surfaces of a (flow) channel may also induce cavitation. It is distinguishable from classical heterogeneous nucleation, since there is no pre-existing nucleation site at the interface. Further information on this topic can be found in the review by Lee (2000).

Han and Han (1988) suggested that bubble nucleation in extrusion foaming does not follow classical nucleation theories by showing the occurrence of nucleation in a shear flow field at unsaturated conditions. They found that bubble nucleation might be induced either by flow or shear stress. They suggested that nucleation was induced by flow (stress) dominantly at positions near the die wall, whereas bubbles near the die wall might be generated by cavitation, induced by the surface roughness of the wall and by thermal fluctuations due to the heat transfer between the metal and the mixture of polymer and volatile component. Lee (1993) suggested a cavity model in order to describe the increased nucleation by a shear flow. He also concluded that shear stress reduced the energy barrier and enhanced nucleation in extrusion foaming. Chen et al. (2002) found that the number of nucleated bubbles (equivalent to cell density) was significantly increased by applying a shear stress. They suggested that the nuclei were stretched by the shear stress, and the stretched nuclei were easier to grow owing to reduced energy barrier by the increased surface area. They concluded that the stress (flow) induced nucleation was the transformation of mechanical energy into surface energy.

In spite of the work described above, the nucleation mechanism in extrusion foaming seems to be controversial and needs further investigations. For example, the experimental and corresponding modeling by Chen et al. (2002), described above, was based on morphology of oval shaped bubbles. They explained that the oval shape of bubbles was a sign of cell formation with oriented (stretched) nucleation sites. It can be argued that extruded foams, which have experienced shear stresses, normally do not show the oval shaped bubbles; This may be due to the instability of elongated domains dispersed in a viscous matrix in a given flow field (Grace, 1982). However, the heterogeneous nucleation and cavitation are generally accepted as the nucleation mechanisms in extrusion foaming, while batch foaming is governed by homogeneous nucleation. Pressure drop rate should be considered in investigating nucleation in extrusion foaming. The minimum work given by Equation (2.3) and Equation (2.10) above, is based on an instantaneous pressure drop. In extrusion foaming, the pressure drop takes place in a region between before and after the die exit; however, the pressure drop in a real process takes place during a finite time period rather than instantaneously. Thus, there exists competition between the nucleation and the growth in extrusion foaming (Martini, 1981). A brief description of this competition is as follows: in the earlier stages of the nucleation, there are initially nucleated bubbles. Gas molecules near these bubbles are available for further nucleation. However, if the pressure drop is not fast enough, the gas molecules are able to diffuse into the nearby bubbles already nucleated, resulting in bubble growth (in an instantaneous pressure drop, gas molecules do not have time to diffuse). Therefore, higher pressure drop rate (faster pressure drop) is

preferred in order to enhance the nucleation (rate). Park et al. (1995) provided experimental data to prove the above behavior.

2.3.2 Bubble Growth

The characteristics of extruded foams are usually determined by cell density, foam density, expansion ratio, bubble size and bubble size distribution. These variables are related to bubble growth, bubble collapse and coalescence. Bubble collapse and coalescence (which are to be avoided) limit bubble growth; bubble collapse is failure of growth and bubble coalescence is the result of excessive and uncontrollable bubble growth. Thus, bubble growth is a key element to control the morphology of bubbles as well as the characteristics of the final foam products.

Parameters used in the optimization of bubble growth are various; material parameters such as solubility, surface tension and viscoelasticity, and operational parameters such as temperature, throughput and extrudate cooling rate. The only limitation in the optimization of the bubble growth is the initial condition (number of nuclei), already determined by the nucleation step. Among the parameters, viscoelasticity is the most important element in determining the foamability of a polymer. A certain level of strength is required from the molten polymer chains to sustain the stress and the strain imposed by the biaxial deformation during bubble formation, which would result in an equilibrium diameter of bubbles during low density foaming. Such strength may be represented by values of extensional viscosity under biaxial deformation. However, due to measurement difficulties, the extensional viscosity under biaxial deformation is inferred from the extensional viscosity under uniaxial deformation and other measurable

parameters such as extrudate swell and melt strength. Strain hardening behavior, which is a transient increase in the extensional viscosity above its limits predicted by linear viscoelasticity, is also a key element controlling foamability. Note that these properties depend on melt elasticity, which is a response of a material with high MW, broad MWD and/or branched structure.

Bradley and Philips (1990) showed that a low density foam could not be made with a linear PP even with a blowing agent with high solubility (CFC 114). By introducing a branched PP with high melt strength, they produced a low density foam with a significant expansion ratio and density reduction.

Park and Cheung (1997) showed that a branched PP polymer retarded cell coalescence, although a reduced cell density was found in the resultant foam. They concluded that cell coalescence was retarded by strain hardening of the branched PP.

Experimental investigations on bubble growth have experienced some difficulties in obtaining a bubble radius as a function of time, since: 1) the deformation occurs during a very short time period and 2) no on-line experimental technique is available to measure the radius of a particular bubble during extrusion foaming. Thus, the bubble morphology of the final foamed product is usually considered as corresponding to the ultimate size of the grown bubbles. Available data on bubble growth that were obtained experimentally are: transient radius of bubble in batch foaming (Ramesh et al. 1991), transient thickness of sheet extrudate (Lee et al. 1996) and transient diameter of cylinder extrudate.

Due to the experimental difficulties, investigations on bubble growth have mostly focused on modeling. Before the concept of the single cell was introduced, the models

were based on a single bubble in an infinite sea. Since the single bubble could be provided with gas available for its growth, the models seemed to be unrealistic, although in some cases complicated thermal and viscoelastic effects were introduced. The concept of the single cell was introduced by Amon and Denson (1984). In this model, bubbles were represented as separate unit cells, consisting of a polymer envelope surrounding a single bubble (gas). Afterwards, the model became more realistic, since the final radius yielded to a finite radius due to the limited supply (diffusion) of the gas molecule available for its growth. Attempts for realistic models such as introduction of viscoelasticity and/or gas loss from extrudate have been made or are in progress. An excellent summary of the historical development of bubble growth models has been presented by Ramesh (2000).

The section below attempts to facilitate the understanding of the governing equations and parameters in the bubble growth model and how thermodynamic and hydrodynamic theories are applied. Most of the models were developed based on information given below. A schematic of a single polymer cell model is shown in Figure 2.4.
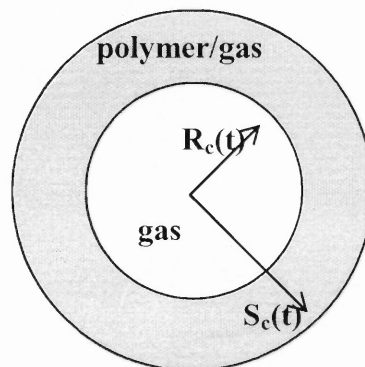
Figure 2.4 Schematic representation of a single polymer cell model.

The source of bubble growth is the diffused gas, and it follows Fick's law. In spherical coordinates, the diffusion equation is simplified as Equation (2.13) with the boundary conditions of Equations (2.14) – (2.17)

$$\frac{\partial c}{\partial t} = \frac{D}{r^2} \frac{\partial}{\partial r}\left(r^2 \frac{\partial c}{\partial r}\right), \quad R_c \leq r \leq S_c \tag{2.13}$$

where c is the concentration of gas molecules in the bubble and D is diffusivity. R_c and S_c are the radii of the bubble and cell, respectively. In addition, R_c defines the boundary between gas (bubble) and polymer matrix (cell), and S_c is the interface of cells that are adjacent to each other. Initially, the concentration of gas inside the bubble follows Henry's law, and the gas pressure is determined by the nucleation step, thus:

$$c(r,0) = K_w P_{g0} \tag{2.14}$$

where K_w is the Henry's law constant and P_{g0} is the initial gas pressure. At the outer radius of the polymer film (Equation 2.15), there is no diffusion between cells that are adjacent to each other. This means limited supply of gas, which is distinguished from the single bubble models. If a given cell is located at the surface of the foamed extrudate, Equation (2.16) is applied instead of Equation (2.15).

$$\frac{\partial c}{\partial r} = 0, \text{ at } r = S_c, \text{ for all } t \geq 0 \tag{2.15}$$

$$\frac{\partial c}{\partial r} = k_m(c_s - c_\infty), \text{ at } r = S_c, \text{ for all } t \geq 0 \tag{2.16}$$

where k_m is the mass transfer coefficient, c_s is the gas concentration in the polymer film and c_∞ is the ambient gas concentration. No gas loss can be assumed by setting k_m equal to zero. The gas concentration at the interface between the bubble and the film is determined by Henry's law, thus:

$$c(R,r) = K_w P_{g0}, \text{ at } r = R_c, \text{ for all } t \geq 0 \tag{2.17}$$

The momentum equation requires a constitutive equation, and provides the information of the gas pressure inside the bubble, P_g:

$$P_g - P_\infty - \frac{2\sigma}{R_c} + \int (\tau_{rr} - \tau_{\theta\theta}) \frac{dr}{r} = 0 \tag{2.18}$$

where P_∞ is the ambient pressure, σ is the surface tension, τ is the stress. This equation explains and helps the evaluation of the effects of viscoelasticity on foaming. The sensitivity of bubble growth model on the viscoelastic behavior depends on the selection of an appropriate constitutive equation in order to evaluate the normal stress difference term in Equation (2.18). The mass balance gives the bubble radius, R_c, as:

$$\frac{d}{dt} \left(\frac{4}{3} \pi R_c^3 \rho_g \right) = D \frac{\partial c}{\partial r} \bigg|_{r=R} \left(4\pi R_c^2 \right) \rho \tag{2.19}$$

The solutions of the three coupled governing equations [(2.13), (2.18) and (2.19)] would provide information on the transient behavior of bubble growth as a function of thermodynamic and various material parameters.

For example, Ramesh (2000) used the Maxwell model to evaluate the normal stress difference term, and obtained the solution of the extruded foam radius as shown in Figure 2.5 (solid line). Note that the extruded foam radius is obtained by multiplying the transient radius of a cell by the average number of cells growing across the diameter of the extrudate.
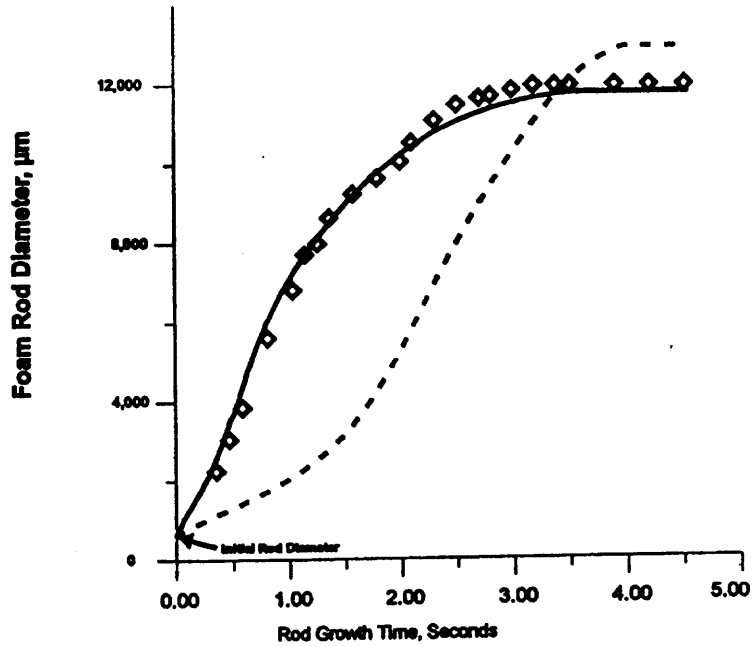
Figure 2.5 Comparison of bubble growth with respect to time between experimental data (symbols) and model predictions by Ramesh (solid line) and Arefmanesh and Advani (dashed line) (Ramesh, 2000).

The dashed line is the prediction by the model suggested by Arefmanesh and Advani (1991), which excludes the effect of gas loss from the extrudate. The solution of the model by Ramesh shows a faster diffusion initially and reaches an equilibrium radius earlier than the model by Arefmanesh and Advani due to the early depletion of gas by losses. The model of Ramesh appears to match well with experimental data, confirming the importance of the gas loss effect. It should be noted that the deformation takes place during a very short time.

2.4 Flow Induced Crystallization

It has been found that elastomers can crystallize by stretching at temperatures where no crystallization can be induced in the unstretched condition (Flory, 1947; Andrews et al. 1971). This phenomenon is explained in terms of entropic changes in the system (Flory, 1951). The entropy of the chains in the stretched system is lower than in the quiescent state, since chain orientation of the elastomer by stretching reduces the number of possible conformations available to the chains. The melting point is generally given by:

$$T_m(\lambda) = \frac{\Delta H_f}{\Delta S(\lambda)} \qquad (2.20)$$

where λ is the relative extension of the chains, ΔH_f is the heat of fusion (not affected by stretching), and $\Delta S(\lambda)$ is the entropy change by stretching λ. Thus, an increased melting point is induced by stretching via the reduced entropy, and a melting temperature higher than that of the system can be accomplished and crystallization should occur.

The same tendency is found with polymer solutions and melts under flow and/or deformation conditions. Crystallization from flowing polymer solutions results in a shish-kebab morphology having a threadlike backbone from which lamellar crystals grow laterally (Schultz, 2001b). Crystallization from melts under flow and/or deformation which involve shearing and extension produces a row structure (oriented, extended or twisted chain lamellae). Keller (1955) identified the row structure first from morphologies of long stacks of crystalline lamellae of isotactic polystyrene films. He found that the row structures were formed during the stretching of the films. In a series of publications on the flow and/or deformation induced crystallization (FIC) of polymer melts (Andrews et al. 1963; Schultz and Petermann, 1984; Eder et al. 1990), it is shown

that growth of row structures start from a precursor or nucleus and the density of such precursors increases with increasing molecular strain (deformation).

The distinctive features of FIC are as follows (Kumaraswamy et al. 1999; Jerschow and Janeschitz-Kriegl, 1997; Kornfield et al. 2002; Li and de Jeu, 2004): (i) flow accelerates the crystallization kinetics and forms a crystalline phase with an oriented lamellar structure, (ii) the enhancement of the crystallization kinetics is attributed to an increase in the nucleation rate caused by orientation of the polymer chains in the melt, and (iii) the MW and the MWD have a pronounced effect. High molecular weight chains play an important role in orienting the melt and in the observed enhancement of the crystallization kinetics.

Similarly to Equation (2.20), an increase of the melting temperature of a polymer melt under flow is calculated from:

$$\frac{1}{T_m(\lambda)} = \frac{1}{T_m^0} + \frac{\Delta S(\lambda)}{\Delta H_f}$$

(2.21)

where T_m^0 is the equilibrium melting temperature under a quiescent condition whose physical meaning is the melting point of a pure single (boundless) crystal and its determination was shown by Hoffman and Weeks (1965). By inserting the melt temperature, $T_m(\lambda)$, of Equation (2.21) into an equation for calculating the growth rate, for example, the Hoffman-Lauritzen equation (Hoffman et al. 1976), the modified equation for growth rate (velocity) of FIC dependent on deformation and temperature, $K_f(\lambda, T)$, is derived as follows:

$$K_f(\lambda, T) = G_0 \times \exp\left(\frac{-U^*}{R(T - T_\infty)}\right) \times \exp\left(-\frac{K_g}{T(T_m(\lambda, T) - T)f}\right)$$

(2.22)

$$f = \frac{2T}{T + T_m(\lambda, T)}$$

where f is the correction factor for the reduction in the latent heat of fusion as the temperature is decreased, R is the universal gas constant, U^* is the activation energy for the segmental jump of polymer molecules, T_∞ is the temperature where chain mobility is frozen and identified empirically as $T_g + 30K$. K_g and G_0 are constants and their detailed expressions and values are found elsewhere (Hoffman et al. 1976; Schultz, 2001c). From Equation (2.22), enhancement of growth rate and higher onset temperature of crystallization are expected from the increase of the crystallization driving force (the degree of supercooling) as a consequence of the increased melting temperature by flow.

The FIC models described below were published recently and show the trends and progresses of the FIC modeling. The calculation of $\Delta S(\lambda)$ in Equation (2.21) requires an introduction of a constitutive equation as well as the solutions of given flow fields, i.e., strain and strain rate. Therefore, the quantitative prediction of FIC has been limited to ideal flows such as simple shear or elongational flows. However, a constitutive equation, which is adopted in modeling, evaluates the entropy changes from the response of the polymer melt under strain and strain rate as a function of MW and MWD per se, and thus, the effects of MW and MWD on FIC can be predictable by modeling. The necessity of the description of the conformational changes (orientation) of chain segments demands a viscoelastic model. In addition to calculation of the melt temperature, modeling of the nucleation rate and the number of nuclei formed by flow also depends on the selection of the constitutive equation, since the chain orientation is related to the formation of the precursors of FIC. The viscoelastic models frequently used and appearing in FIC

modeling are: the Phan-Thien Tanner (PTT) model (Dai et al. 2006), the upper convected Maxwell model (Koscher and Fulchiron, 2002) and the Leonov model (Kim et al. 2005).

Dai et al. (2006) derived a first order differential equation, which relates the nucleation rate to the relaxation time of the material and the flow fields.

$$\frac{dN_f}{dt} + \frac{N_f}{\lambda_N} = g \tag{2.24}$$

$$g \propto \left| \dot{\gamma} \right|^p \left(\dot{\gamma} t \right) \tag{2.25}$$

where N_f is the number of nuclei created by flow, λ_N is the largest (relaxation) time, $\dot{\gamma}$ is the shear rate, and g is the source term and p is a parameter. According to this equation, the (enhanced) nucleation rate was a function of both the strain, $\left(\dot{\gamma} t \right)$, and the strain rate. The equation was solved by fitting the measurements of the first normal stress difference.

The model by Koscher and Fulchiron (2002) defined "additional nuclei" by flow as a function of the first normal stress difference in addition to the nucleation under quiescent conditions. They evaluated the additional nuclei by adopting the upper convected Maxwell model. The solution of their model predicts the general trend of FIC: the higher shear rate forms more nuclei as well as reduces the induction time (Figure 2.6), and the shearing time, t_s, which is equivalent to the total shear, determines the number of additional nuclei at a given shear rate (Figure 2.7).
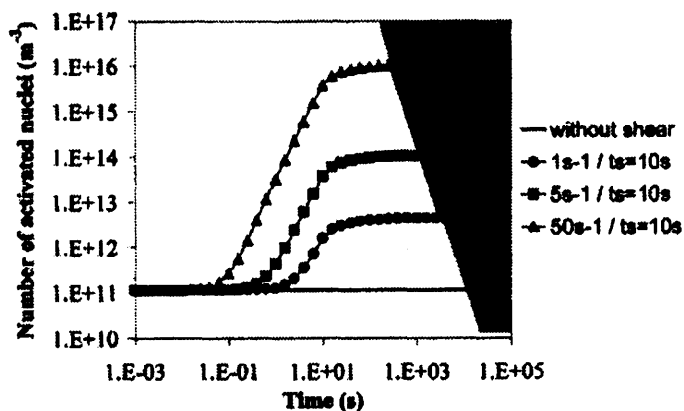
Figure 2.6 Calculated number of nuclei as a function of time for different shear rates (Koscher and Fulchiron, 2002).
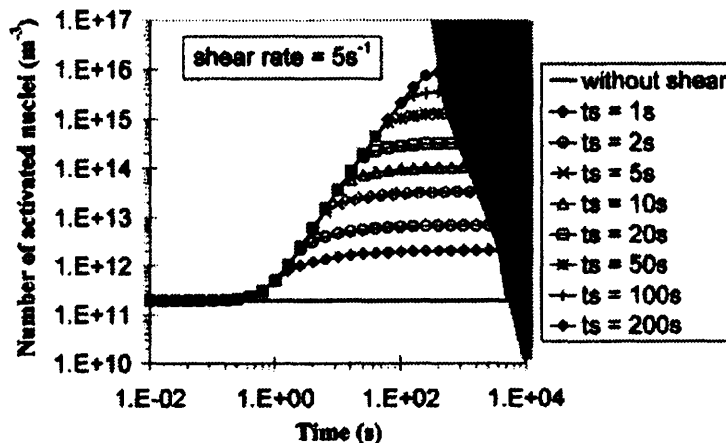
Figure 2.7 Calculated number of nuclei as a function of time for different shearing times (Koscher and Fulchiron, 2002).

Kim et al. (2005) introduced the Leonov multimode equation for calculating the entropy reduction in a simple shear flow. The calculated entropy was used in evaluating the growth rate (K_s in their notation) equation similar to Equation (2.22). A model for the overall crystallization kinetics by FIC was formulated by applying K_s and modifying Nakamura's equation, which is a kinetic model for nonisothermal crystallization (Nakamura et al. 1972). The resulting equation is

$$\frac{D\theta_c}{Dt} = nK_s(T)(1-\theta_c)[-\ln(1-\theta_c)]^{(n-1)/n} \qquad (2.26)$$

where θ_c is the relative crystallinity, n is the Avrami exponent, and $K_s(T)$ is the growth rate by FIC. They used three isotactic polypropylenes (iPP) in injection molding experiments and their corresponding material parameters in modeling. The effects of MW (and MWD) on FIC were more pronounced with iPP of the highest molecular weight (whose grade name was PP6523) due to the largest entropy change by shear flow. A typical calculated result shown in Figure 2.8 shows the enhanced overall crystallization kinetics as a function of shear rates. The major objective of their work was to predict the skin layer, which is distinguishable from the core by its different crystalline structure, formed by FIC. They found appreciable agreement between the prediction of their model and their experimental data on injection molded products with a simple geometry (dumbbell shaped bar).
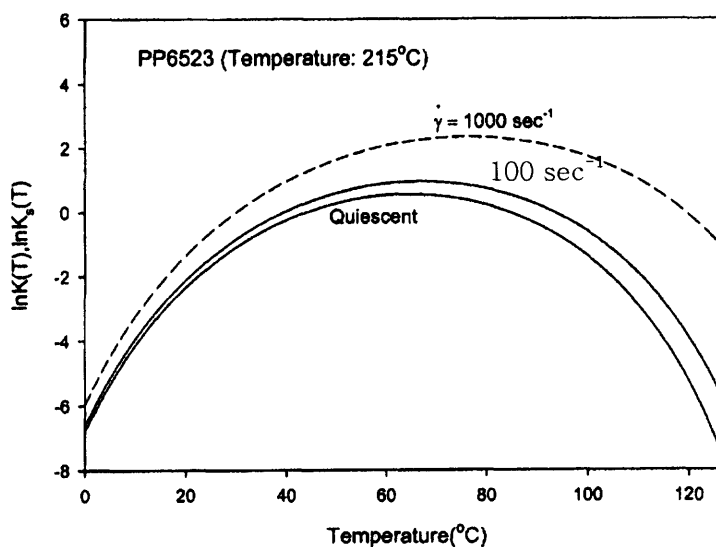
Figure 2.8 Crystallization rate constant as a function of the crystallization temperature at different shear rates (Kim et al. 2005).

The (oriented) skin layer is usually of importance in the injection molding process since the presence of the skin layer contributes to the enhancement of the mechanical properties such as flexural modulus, tensile yield strength and heat distortion temperature. The skin layer of injection molded products is formed during the filling stage where a high shear rate near the wall takes place; the alignment of molecules along the flow direction may act as FIC nuclei.

The formation of the skin layer is known as a good example of FIC and a complete explanation of this phenomenon has been provided by Tan and Kamal (1978). Figure 2.9 shows the following four distinct morphological zones developed in injection molding. Type I is a non-spherulitic structure formed by FIC (no Maltese cross pattern), and interpreted as stacks of lamellae. Type II contains very fine asymmetric spherulites of almost uniform size which were formed under a large thermal gradient, and consequently at a fast nucleation rate. The crystalline structures of type I and II are formed during the filling stage. Note that Type I and II were considered as skin layers by Kim et al. (2005) Type III contains asymmetric oblate spherulites with axes of symmetry in the depth direction, i.e., the direction of the thermal gradient. Type IV contains randomly nucleated spherulites as under quiescent conditions. The crystalline structures of types III and IV are thought to be formed during the packing and the pressure holding stages.
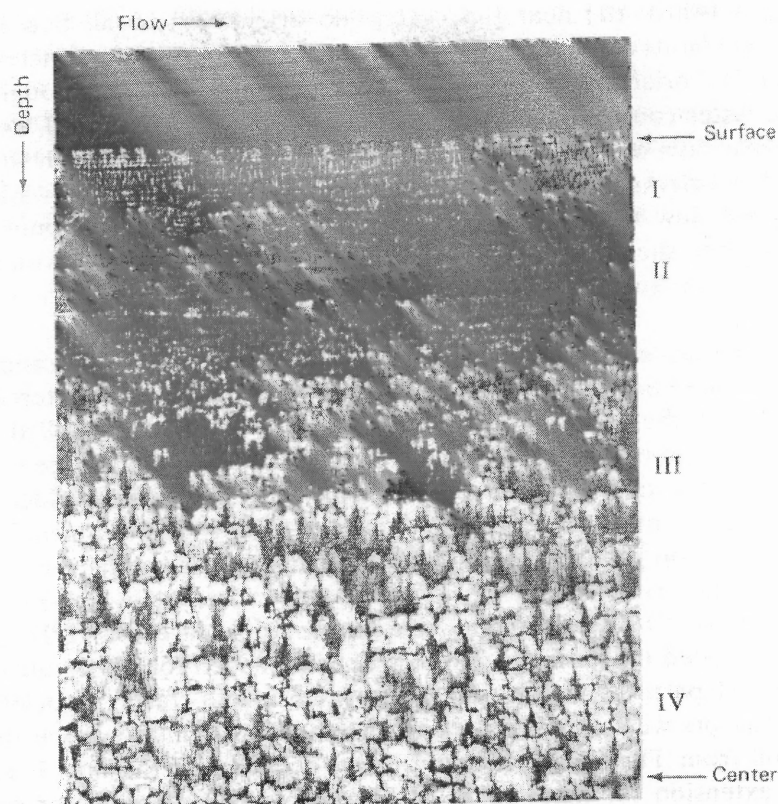
Figure 2.9 Birefringence microscopy of a cross section of injection molded LDPE, depicting various morphological regions (Tan and Kamal, 1978).

Various experimental methods were developed to investigate the formation of nuclei and the overall crystallization kinetics of FIC. Examples of recently reported methods are as follows: rheometry (Pogodina et al. 1999), polarized microscopy (Duplay et al. 1999; Jay et al. 1999; Koscher and Fulchiron, 2002), small angle X-ray scattering (SAXS) (Nogales et al. 2001; Li and de Jeu, 2004), wide-angle X-ray diffraction (WAXD) (Moitzi and Skalicky, 1993), and rheo-SAXS and rheo–WAXD (Agarwal et al. 2003).

FIC experimental studies use iPP because of its large-scale (spherulitic) crystalline structure. There exist few references on the FIC behavior of polyesters, presumably due to the difficulty of handling experiments involving high melt

temperatures and the consequent possibility of degradation (Li and de Jeu, 2004). On the other hand, work on the changes of crystalline structure by stretching of solid polyester (PET) fibers at lower temperature have been reported, e.g., by Schultz et al. (2000). Caution should be used in applying the results of iPP to the FIC of polyesters such as PET and PBT. These polyesters have rigid chains and their stress relaxation behavior will be different from that of iPP having flexible chains (Dimitrakopoulos et al. 2001); furthermore, as condensation polymers they differ from iPP significantly in their MW and MWD.

2.5 Gas Induced Crystallization

The presence of dissolved gas in a polymer matrix affects its crystallization behavior. This is due to an increase of the free volume and a decrease of the inter-chain interactions of the polymer/gas solution as compared with the polymer without gas. The increased mobility induced by the gas results in a reduction of viscosity as well as the transport process at the interface between the amorphous and crystalline phases during the crystallization process. The reduced viscosity was investigated by several research groups; however, only work performed by Dey and Todd (2004) using a versatile on- and off-line rheometer, the Helical Barrel Rheometer (HBR) developed by Todd et al. (1998), seems to be reliable in measuring viscosities under the high pressure conditions found in extrusion foaming. A detailed description of the device and the results are presented in the above references.

The glass transition temperature, T_g, may be depressed by the dissolution of gas; due to the increase of the mobility of polymer chain segments, the increased mobility may also result in enhanced crystallization kinetics.

Chiou et al. (1985a, 1985b) investigated the crystallization of PET after the dissolution of CO_2 at temperatures below its normal T_g. Handa et al. (1997) measured the depression of T_g by up to 30°C by dissolving CO_2 into syndiotactic polystyrene (sPS). They observed a depressed melting temperature of sPS under CO_2 as well. The measured crystallization kinetics showed apparent increases as a result of the dissolution of CO_2. Furthermore, the presence of CO_2 induced morphological modification of the sPS crystals as suggested by XRD measurements. However, the modification of the crystalline morphology with other polymer/gas system has not been shown so far. For example, Takada et al. (2001) and Takada and Oshima (2003) presented the effects of CO_2 on the crystallization kinetics of PP and PET, respectively. They observed no change of the crystalline structure (no modification of the crystalline morphology) by CO_2 as a result of their extensive experimental work.

In order to numerically describe the effects of gas dissolution on the crystallization kinetics, a mathematical model was proposed by Ishizuka and Koyama (1977). It begins with the Avrami equation (Avrami, 1939; 1940; 1941), which is the basis of the analyses of the isothermal crystallization kinetics:

$$X_c(t) = 1 - \exp\left[-kt^n\right] \qquad (2.27)$$

where X_c is the relative crystallinity and defined by the crystallinity at certain time divided by the crystallinity of the sample, k is the crystallization kinetic constant for nucleation and growth rate and n is the Avrami exponent that reflects the mechanisms of

nucleation and growth, i.e., the dimensionality of nucleation and growth processes. For a two-dimensional heterogeneous nucleation, the crystallization kinetic constant, k, is given by:

$$k = \pi \cdot l_c \cdot N \cdot G^2 \tag{2.28}$$

where N is the number of nuclei, G is the rate of linear crystal growth, and l_c is the size of crystal. The nucleation (number of nuclei, N) and growth rate (G) depend on temperature; thus, equations considering the temperature dependency are introduced as shown below (Ishizuka and Koyama, 1977):

$$\log G(T) = \log G_0 - \frac{\rho C_1 C_2 T}{\left(T - T_g + C_2\right)^2} - \frac{C_3 T_m^0}{T\left(T_m^0 - T\right)} \tag{2.29}$$

$$\log N(T) = \log N_0 - \frac{C_4 T_m^0}{T\left(T_m^0 - T\right)} \tag{2.30}$$

Combining Equations 2.29 – 2.30 gives:

$$k(T) = k_0 \times \exp\left(-\frac{C_5 T}{\left(T - T_g + C_2\right)^2}\right) \times \exp\left(-\frac{C_6 T_m^0}{T\left(T_m^0 - T\right)}\right) \tag{2.31}$$

where $C_1 - C_6$, ρ and G_0, N_0 and k_0 are constants, whose detailed explanations and evaluations may be found elsewhere (Ishizuka and Koyama, 1977; Takada et al. 2001; Takada and Oshima, 2003]. Note the similarity of Equation 2.31 and the Hoffman-Lauritzen equation, introduced in the previous section as Equation (2.22). The first exponent term describes the mobility of chains. At relatively lower temperature (i.e., $T_g < T << T_m^0$), the first exponent term dominates $k(T)$. This temperature range, where the overall crystallization is mainly determined by the chain mobility (diffusion of chains) is

called the diffusion controlled region. Meanwhile, at higher temperatures (i.e., $T_g << T < T_m^0$), the overall crystallization kinetics are mostly determined by the second term, which refers to nucleation. It should be mentioned that the term, $T_m^0 - T$, represents the degree of supercooling, the thermodynamic driving force for nucleation of a given system. This temperature range is called the nucleation rate controlled region.

As mentioned earlier, T_g and T_m of a polymer decrease by gas dissolution. Takada and Oshima (2003) quantified the depression of T_g and T_m of PET/CO$_2$ systems as in Figure 2.10. Solid lines represent linear regressions of the experimental data. Note that the depression of T_g is much larger than that of T_m.
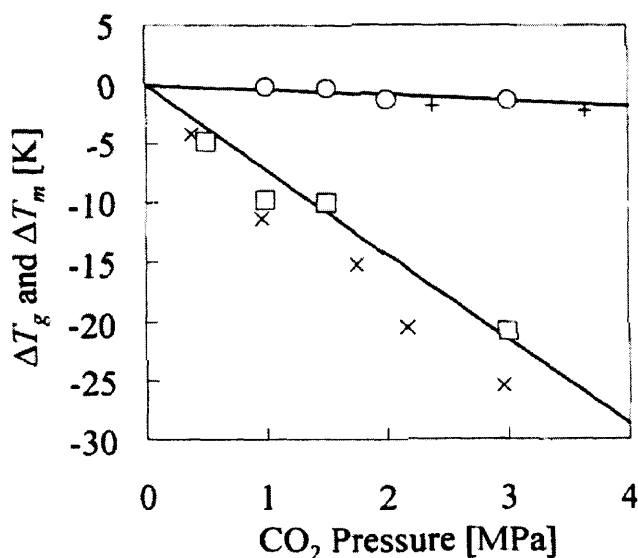
Figure 2.10 Depression of T_g (cross and square symbols) and T_m (plus and circle symbols) of PET by CO$_2$ (Takada and Oshima, 2003).

They also obtained experimental data of isothermal crystallization kinetics of the system and compared the calculated results. The calculation was based on the assumption that the equilibrium melting temperature, T_m^0 would be depressed as T_m by gas

dissolution. $k(T)$ in Equation 2.31 is converted to $k(T)_{CO2}$ in Equation 2.32, considering the depression of T_g and T_m^0 by CO_2. The depression of the temperatures was evaluated from the regressions (solid lines in Figure 2.10).

$$k(T)_{CO2} = k_0 \times \exp\left(-\frac{C_5 T}{\left(T - [T_g - \Delta T_{g,CO2}] + C_2\right)^2}\right) \times \exp\left(-\frac{C_6 T_m^0}{T\left([T_m^0 - \Delta T_{m,CO2}^0] - T\right)}\right) \quad (2.32)$$

As shown in Figure 2.11 for PET in the presence of gases, both experimental and theoretical results from Equation (2.32) show enhanced crystallization kinetics over the entire temperature range. This is due to the larger depression of T_g as compared to T_m^0, which resulted in domination of the first exponent term in Equation 2.32. In other words, the crystallization of PET/CO_2 and PET/N_2 systems was enhanced by the increased mobility over all the temperature ranges.

In the PP/CO_2 system, Takada et al. (2001) found that the depressions of T_g and T_m were almost of the same magnitude; by contrast to the PET/ CO_2 system described above the crystallization of PP showed slower kinetics at high temperature and faster at low temperature in the presence of CO_2. The unexpected results considering the increased mobility of polymer chain segments by CO_2 could be explained by the model for the crystallization kinetics including the depression of T_g and T_m, Equation (2.32). The same magnitude of the temperature depression was equivalent to a curve shifting along the temperature axis as shown in Figure 2.12. Thus, the crystallization rate at the nucleation controlled region (high temperature) might be decreased while it was increased in the diffusion controlled region (low temperature), and this is in agreement with experimental data by Takada et al. (2001).
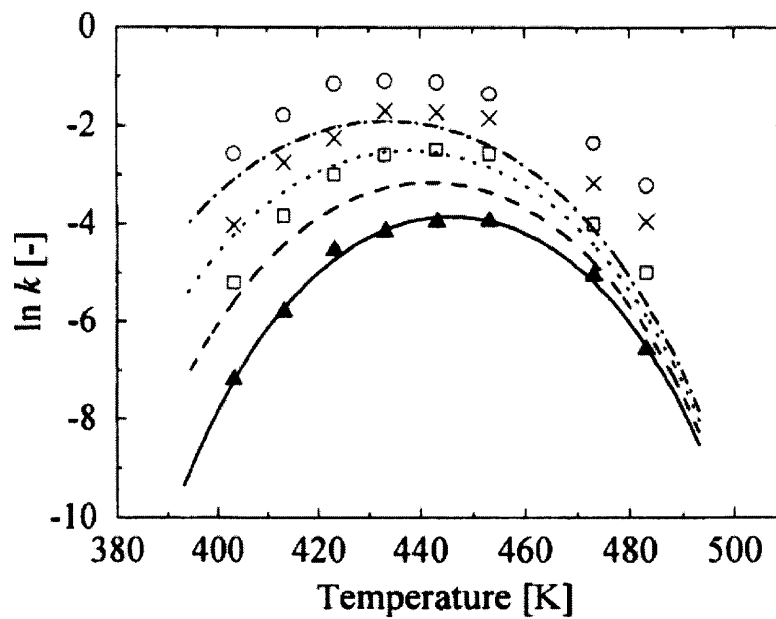
Figure 2.11 Comparison between experimental data (symbols) and calculated crystallization rate curve (lines), triangles and solid line at 0.1 MPa in N_2, square and dashed line at 1.0 MPa in CO_2, cross and dotted line at 2.0 MPa in CO_2, and circle and dashed-dot at 3.0 MPa in CO_2 (Takada and Oshima, 2003).
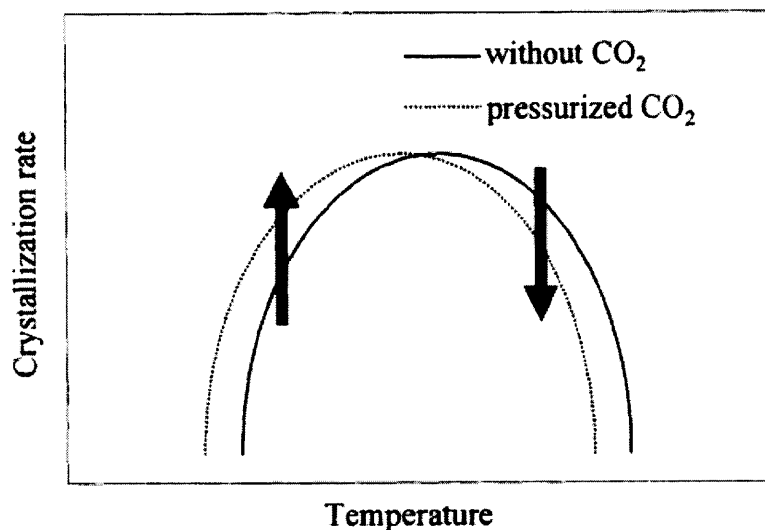
Figure 2.12 Estimated change in the crystallization rate when the magnitude of CO_2 induced depression of T_g is almost the same as the in T_m^0 as in PP/ CO_2 system (Takada and Oshima, 2003).

CHAPTER 3

EXPERIMENTAL

3.1 Materials

Two commercial PBT resins, provided by LG Chemical Ltd., were chosen. Both resins were extrusion grades with different molecular weights. The higher molecular weight PBT was an extrusion grade with MFI of $12\pm2g/10min$ at $250°C/2.16kg$ (designated as PBT1), and was used in the extrusion foaming with a chemical blowing agent. The lower molecular weight resin was designated as PBT2 with MFI of $21\pm1g/10min$ measured under the same conditions. PBT2 was used in the reactive modification and the extrusion foaming with a physical blowing agent. In all the experiments, PBT was pre-dried overnight to a moisture content of less than 0.04% by weight.

A reactive modifier with tri-functional epoxide groups was selected: triglycidyl isocyanurate (TGIC, Sigma-Aldrich, CAS No. 2451-62-9). It is white powder at room temperature. The molecular weight and boiling point are 297 and $100°C$, respectively. The structure of TGIC is shown in Figure 3.1.
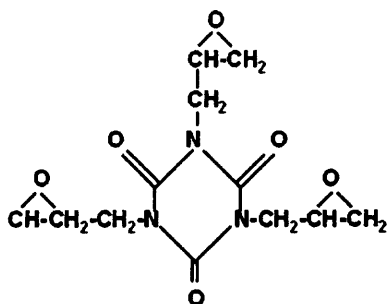
Figure 3.1 Structure of TGIC.

A chemical blowing agent (CBA) suitable for high temperature foaming, 5-Phenyltetrazole was used. The commercial name of 5-Phenyltetrazole is Expandex 5-PT (Crompton) and its structure is shown in Figure 3.2. Expandex is a white, crystalline powder with a density of $1.42 g/cm^3$. Nitrogen release was expected to begin at $215\,^{\circ}C$; an average gas yield of 210 ml/g would occur at an experimental temperature of 260 to 265 $^{\circ}C$ in air. The main decomposition products of Expandex 5-PT are heterocyclic nitrogen compounds, such as triphenyl-s-triazine, 3,5-diphenyl-1,2,4-triazole, 4-N-amino-3,5-diphenyl-1,2,4-triazole (Hurnik, 2001).
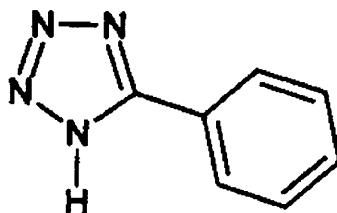
Figure 3.2 Structure of 5-Phenyltetrazole.

In extrusion foaming, isobutane (CAS No. 75-28-5, Matheson Tri-Gas) was used as a physical blowing agent (PBA). The boiling point of isobutane is -12°C.

3.2 Reactive Processing

3.2.1 Reactive Processing in Intensive Batch Mixer

An intensive batch mixer (Brabender Plasticorder PL2000) was used for initial experiments of the chain branching reaction under a nitrogen blanket. The temperature and the rotor speed of the mixer were set at $235\,^{\circ}C$ and 50 rpm, respectively. Torque and temperature were recorded during the experiments. PBT pellets were added in the mixer

and 3min 30sec later, when fusion of PBT was assumed to be complete, the reactive modifier (TGIC) at a predetermined amount (0.0 ~ 0.26 phr) was added. For 13~17min after the modifier addition, the reaction was monitored through the change of torque. Samples were then removed and hot-pressed to thin sheets for rheological measurements.

3.2.2 Reactive Processing in Single Screw Extruder

Reactive extrusion was performed using a single screw extruder (D: 32mm, L/D: 40, Killion). A segmented screw with conveying and several mixing elements was used. The temperature profile of the barrel was 210/230/235 °C. The PBT and the reactive modifier were dry-blended before extrusion. The single screw extruder was operated under starved feeding conditions using a single screw feeder. Feed rate and rpm were the operational variables used to control the residence time and the degree of fill. The extrudate from a 5.0 mm rod die attached to the extruder was cooled in a water bath, and then pelletized.

3.3 Extrusion Foaming

Two extruders with different size were used in the extrusion foaming. The foamed sample was cut continually and collected during extrusion and the cut samples were allowed to cool down at room temperature.

3.3.1 Extrusion Foaming with a Chemical Blowing Agent

A lab-scale single screw extruder (D:19mm, L/D:20, C.W. Brabender) with a conventional rod die was used in the extrusion foaming. The zone temperature profile of the extruder was set to be 190/240/235°C. The die temperature and the screw rpm were

the operational variables in this study. The die temperature was varied from 230 to 250°C, and the screw rpm was set to be either 30 or 50. The extruder was operated under flood feeding conditions. At 30 rpm, the extrusion minimum residence time was about 2min 20 s, while at 50 rpm it was about 1min 10 s. Before extrusion, the CBA was pre-mixed in a small batch mixer at room temperature.

3.3.2 Extrusion Foaming with a Physical Blowing Agent

The segmented single screw extruder, described in Section 3.2.2, was used as in the extrusion foaming with a PBA, after installing a gas injection port at a length of 19D. A rod die with a nozzle diameter of 2.2 mm was attached to the extruder. Barrel temperatures were set at 220~235°C, and the screw speed was 20 rpm. The feed rate of PBT was 3.70 ± 0.08 kg/hr (starved feeding conditions). Before and after a length of 19D, appropriate mixing elements with low conveying capacity to ensure the fusion of PBT and to create a melt seal for mixing and homogenization of the PBT and the physical blowing agent, respectively, were installed. A volumetric pump was attached to the gas injection port at a length of 19D. The concentration of the physical blowing agent was controlled by the pump to about 6~7 phr with respect to the feed rate of PBT.

3.4 Rheological Characterization

3.4.1 MFI

Melt flow index (MFI) was measured in a Tinius-Olsen Plastomer following ASTM D1238 with a standard die of 0.21 cm diameter and 0.8 cm length at $250^{\circ}C/2.16kg$.

3.4.2 Rheometrics Mechanical Spectrometer

An oscillatory rheometer (RMS 800) was used with a plate-plate fixture at 250 $^{\circ}$C. Dynamic moduli and complex viscosity were measured by a frequency sweep from 0.1 to 100 rad/s. All samples used for the measurements were prepared with the same thermal history. In the case of the modified samples, a time sweep at a constant frequency (10 rad/sec) was carried out to confirm the absence of unreacted modifier in the sample before each frequency sweep.

3.4.3 Capillary Rheometer

A capillary rheometer was used for the viscosity measurements with a 1.2mm diameter die (L/D of 33) at 250 $^{\circ}$C. The Rabinowitsch correction was applied on each measurement to calculate true shear rate and viscosity.

3.4.4 Extrudate Swell and Melt Tension

The extrudate swell and the melt strength were measured with the capillary rheometer. Extrudate swell (2.5 mm die diameter with L/D of 8.4) was determined by measuring the diameter of the extrudate and dividing by that of the die. The extrudate swell was determined from the averaged value of at least nine measurements: three positions per

extrudate times three extrudates per sample. For the measurement of melt tension, a tension meter with winding rolls was used. Melt tension was determined from the force applied to the tension meter when the extrudate was pulled by the winding rolls at a pre-set speed. Draw ratio was calculated from the ratio of the line speed of the take-up rolls and that of the extrudate from the capillary die. Some PBT samples showed poor viscoelastic behavior, which resulted in a narrow measurable range of draw ratios. At a draw ratio of 2.81, extrusion of all samples achieved a steady state without breaking of the strand; the melt tension of all samples was then measured and compared at this draw ratio.

3.5 Thermal Analysis

A differential scanning calorimeter (DSC7, Perkin Elmer) was used for the thermal analysis. The temperature range and the heating/cooling rate of the measurements were 50~240 °C and +/- 20 °C / min., respectively. Crystallinity, X_c, defined as the ratio of the heat of fusion of the sample (ΔH_m, obtained in the first heating scan) over that of a 100% crystalline PBT (ΔH_{mc}=140 J/g) (Illers, 1980) was calculated after the first heating scan. The onset temperature of crystallization and the crystallization (peak) temperature were obtained from the first cooling scan. In the measurements of the foamed samples, 3~5 mg DSC samples (cut from the foamed extrudates) were prepared carefully so as not to contain any microscopic cells that could affect thermal conductivity during measurements.

Isothermal experiments were performed using the DSC mentioned above in order to obtain information of the crystallization kinetics of the extruded PBT samples. The loaded sample was heated to 235°C at a heating rate of 20°C/min. After the melting was

assumed to be complete (in 3 min after reaching 235°C), the sample was cooled down to the pre-set crystallization temperature. Change of heat flow indicating the progress of the crystallization of the sample was measured at three different temperatures; 190, 195 and 200°C.

3.6 Off-line Foam Characterization

3.6.1 Foam Density and Swell Ratio

Foam density was determined by volume displacement. A cylindrical sample with known weight was submerged into a graduate cylinder filled with water, and then the volume of the displaced water was measured to calculate density. The foam density was determined by averaging at least 5 samples. Expansion ratio of the foamed sample was determined by the ratio of the diameter of the foamed extrudate over that of the die. It was also averaged from at least nine measurements as in the extrudate swell measurements (Section 3.4.3).

3.6.2 X-Ray Diffraction

X-ray diffraction patterns were measured using a Philips X'Pert-MPD XRD system with PC-APD software. X-rays were generated with a Cu Kα X-ray source operating at 45kV and 40mA. Thin slices for the measurement were prepared by cutting from the foamed extrudate. The XRD data were collected over the 2Θ range of 5 to 60°.

3.6.3 Microscopic Observation

Microscopic observations were performed with an optical microscope (Zeiss) for bubble size and bubble size distribution, and a scanning electron microscope (SEM, LEO-1530VP) for morphology of the crystallized material. Fractured foam samples were prepared by freezing in liquid nitrogen and sputter-coating with carbon.

CHAPTER 4

RESULTS AND DISCUSSION

4.1 Extrusion Foaming with CBA

The PBT1 shows the typical rheology of linear polyesters; a Newtonian viscosity behavior, and lower storage modulus (G') than loss modulus (G") by more than an order of magnitude (Figure 4.1). As discussed in Sections 2.1 and 2.2, low density foaming of PBT1 seems hardly achievable without any molecular structural modification. However, in order to obtain preliminary information on the foaming behavior of PBTs, extrusion foaming experiments using a CBA were performed. CBAs typically produce foamed structure with medium to high densities.
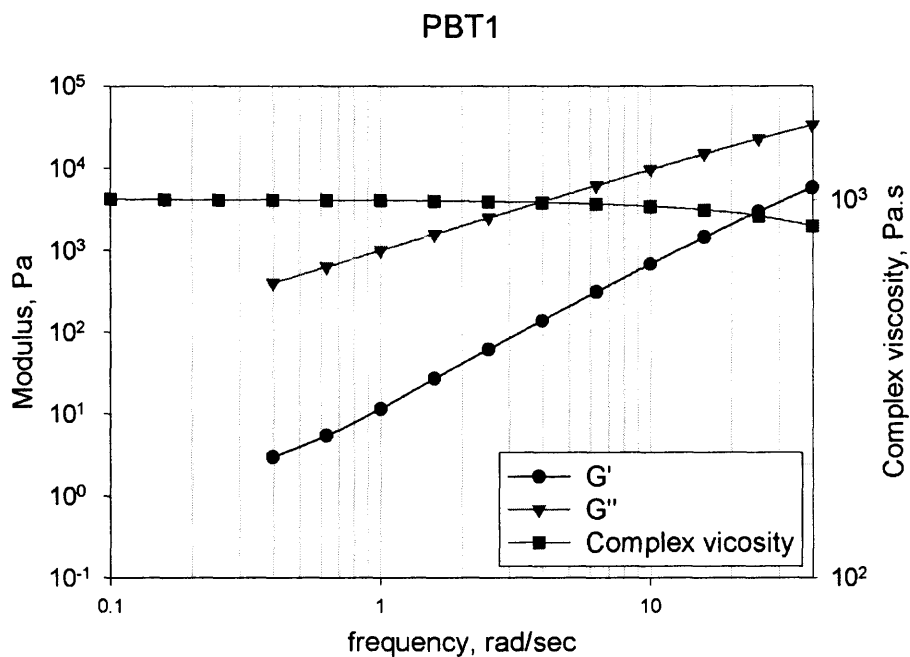
Figure 4.1 Moduli and complex viscosity vs. frequency curves of PBT1 (250°C).

4.1.1 Effects of CBA Concentration

As a result of experiments with different CBA concentrations, it was found that foamed extrudates showed different behavior between below and above a certain concentration (which is referred to as a critical concentration). At the critical concentration: 1) the density was minimum (or remained constant thereafter), 2) the expansion ratio showed a maximum, and 3) the bubble morphology was changed. As shown in Table 4.1 the critical concentration depended on the screw rpm and weakly on the die temperature.

Table 4.1 Critical Concentration under Different Operational Conditions

Die set temp. / Screw speed	Critical CBA concentration	
	230°C	250°C
30 rpm	1.0 phr*	1.0 phr
50 rpm	2.0 phr	2.0 phr

* the minimum foam density appeared at 2.0 phr while the other criteria were met at 1 phr

As a typical example, Figure 4.2 shows the comparison of the bubble morphology between below and above the critical concentration at the die set temperature of 230°C. Below the critical concentration of 1.0 phr and 2.0 phr, the bubbles were relatively large (500~1500 μm); the number of bubbles, with a narrow size distribution, increased with increasing CBA concentration. The extrudate surfaces of those samples were smooth. On the other hand, above the critical concentration, fewer bubbles with smaller size (10~700 μm) were observed. The extrudates had many small holes on their surface and/or were very rough. Those holes might have induced some errors in the measurements of the foam densities.

	0.5 phr	1.0 phr	2.0 phr	4.0 phr
30 rpm				
50 rpm				
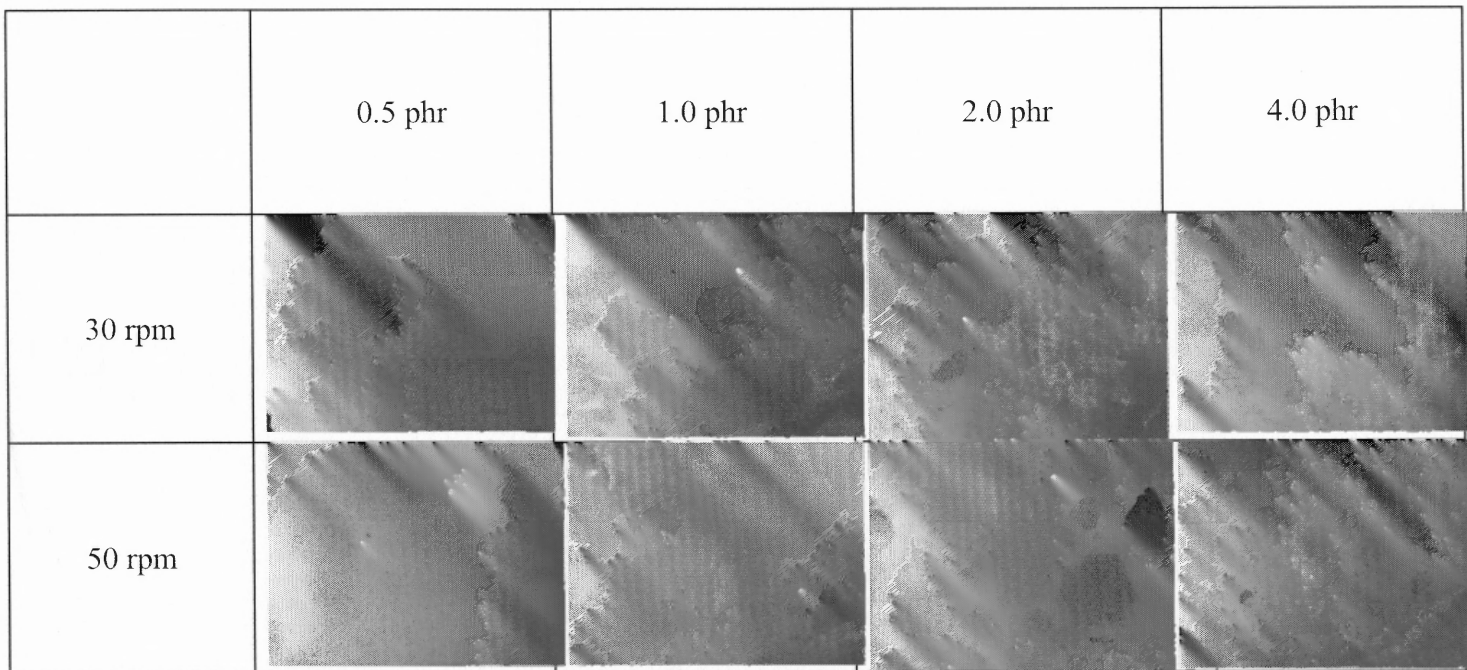
Figure 4.2 The fracture surfaces of the foamed samples as a function of the CBA concentration (die set temp. 230°C) (50 X).

The foam density (Figures 4.3 and 4.4) and the expansion ratio (Figures 4.5 and 4.6) vs. CBA concentration under different operational conditions are presented. Below the critical concentration, the foam densities decreased rapidly with increasing CBA concentration as shown in Figures 4.3 and 4.4, while above the critical concentration the foam density appeared to increase slowly with respect to the CBA concentration. This dependency of the density on the CBA concentration has also been observed in previous polyester foaming studies. For example, Xanthos and Dey (2000) and Xanthos et al. (1998) prepared PET foams with different CBAs and found that CBA concentrations higher than 1.5% did not result in any further reduction of foam density.

The expansion ratio, defined by the ratio of the diameter of the foamed sample over that of the unfoamed extrudate produced at the same conditions, increased with respect to the CBA concentration, but above the critical concentration it showed a decrease (Figures 4.5 and 4.6).
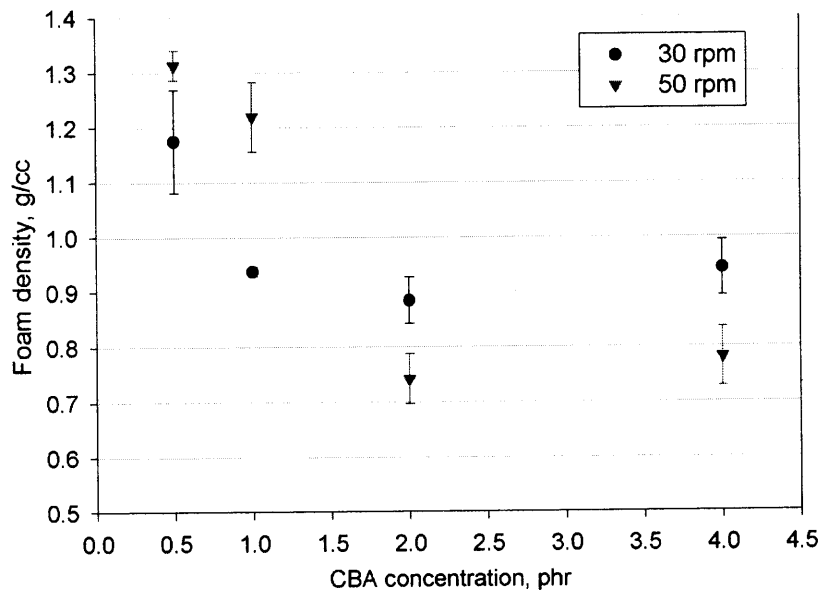
Figure 4.3 The foam density as a function of CBA concentration and screw speed (die set temp. 230°C).
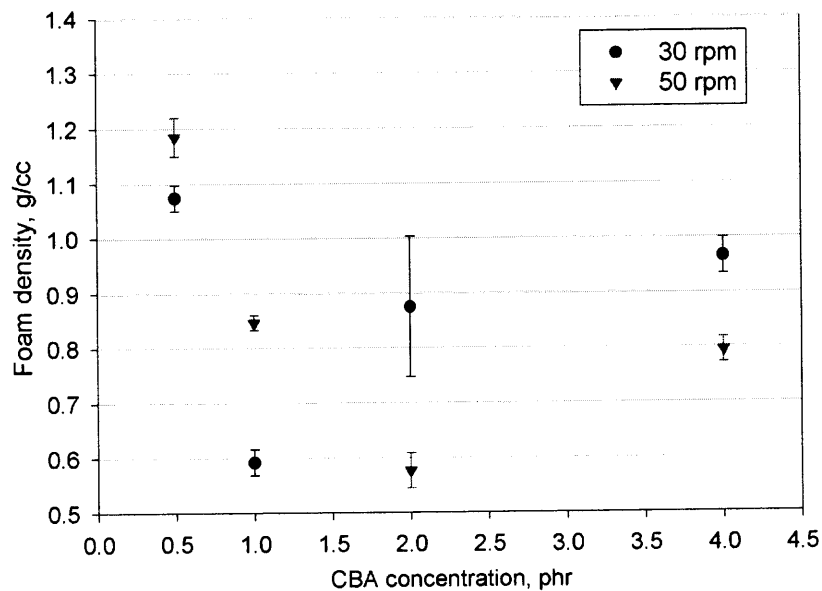
Figure 4.4 The foam density as a function of CBA concentration and screw speed (die set temp. 250°C).
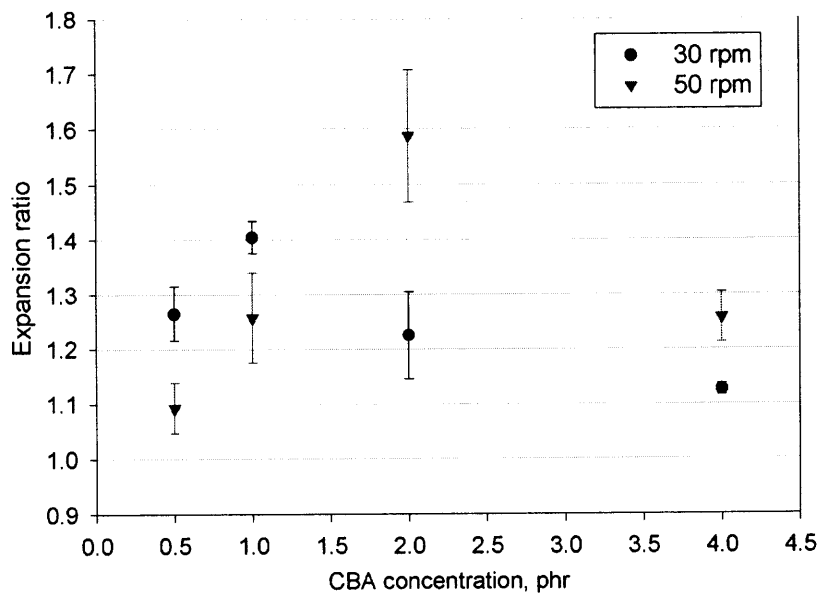
Figure 4.5 The expansion ratio as a function of CBA concentration and screw speed (die set temp. 230°C).
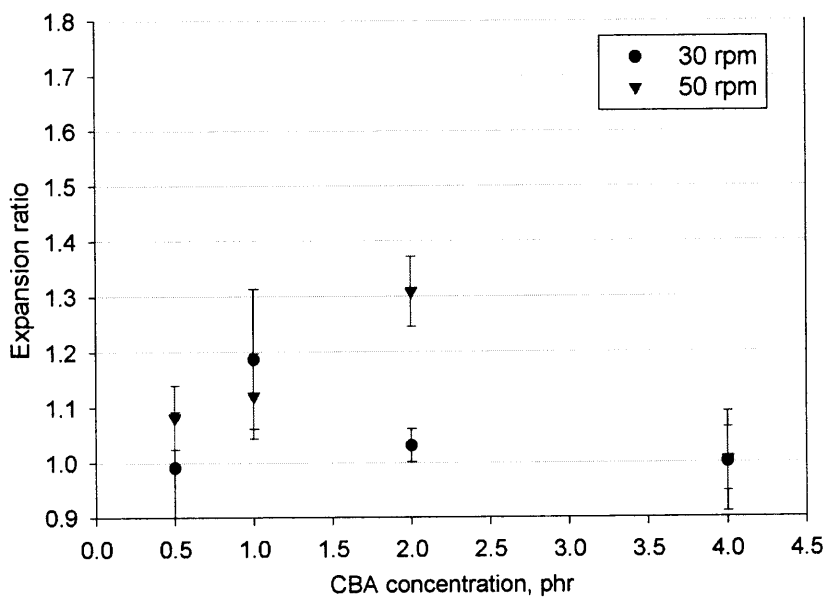
Figure 4.6 The expansion ratio as a function of CBA concentration and screw speed (die set temp. 250°C).

The appearance of a maximum expansion ratio as well as a minimum foam density at the critical concentration is attributed to gas escape, i.e., at the given extrusion conditions, the higher concentration of CBA was expected to generate more nitrogen than would be soluble in the polymer melt, and, then, that excess gas would diffuse out of the PBT matrix during the cooling stage. This is supported by the presence of holes on the surface and the rough surface above the critical concentration. The absence of literature data on the solubility of nitrogen gas into a PBT melt does not allow a quantitative prediction of the concentration where the amount of the produced nitrogen starts to be excessive; however, this hypothesis is in accordance with published data suggesting that excessive amounts of blowing agent might be detrimental to the cell structures (Throne, 1996; Klotzer, 1997; Khemani, 1997; Xanthos 2000a, Jeong et al. 2006a). In addition, the intrinsically low viscoelasticity of PBT1, most probably, allowed the easy escape of the nitrogen gas during the bubble growth stage, in particular, at regions of excessive gas concentrations. Similar results were obtained by Naguib et al. (2004) who showed gas escape from a polypropylene extrudate and reduced expansion ratio at temperatures higher than an optimum one.

4.1.2 Effects of Operational Conditions

Under an assumption that the solubility of nitrogen into PBT1 follows Henry's law (Equation 4.1), an increased solubility was expected at the higher die temperature since, in general, Henry's law constant increases with respect to temperature (an Arrhenius type of dependency).

$$S_g = K_w \cdot P \tag{4.1}$$

where S_c is solubility [cm^3(STP)/g], K_w is the Henry's law constant [cm^3(STP)/g kPa], and P is gas pressure [kPa] at a given temperature. The increased solubility associated with the higher die set temperature resulted in lower foam densities as shown by comparing the foam density curves at a given rpm at 230°C (Figure 4.3) and 250°C (Figure 4.4). The increased solubility in our particular foaming system seemed to have a more pronounced effect on the foam density than any other change induced by the increased die set temperature (e.g. a pressure drop). The higher die temperature caused more extrudate sagging, and, thus, resulted in a decreased expansion ratio as shown by comparing the expansion ratios at a given rpm at 230°C (Figure 4.5) and 250°C (Figure 4.6).

The increase of screw speed resulted in shifting of the critical concentration to a higher value (Table 4.1) as well as lower foam densities at the higher rpm vs. those at the lower one (below the critical concentration).

The effects of the screw speed are related to the decomposition kinetics of the CBA. Figure 4.7 shows a typical decomposition behavior of the Expandex 5-PT in isothermal TGA experiments.
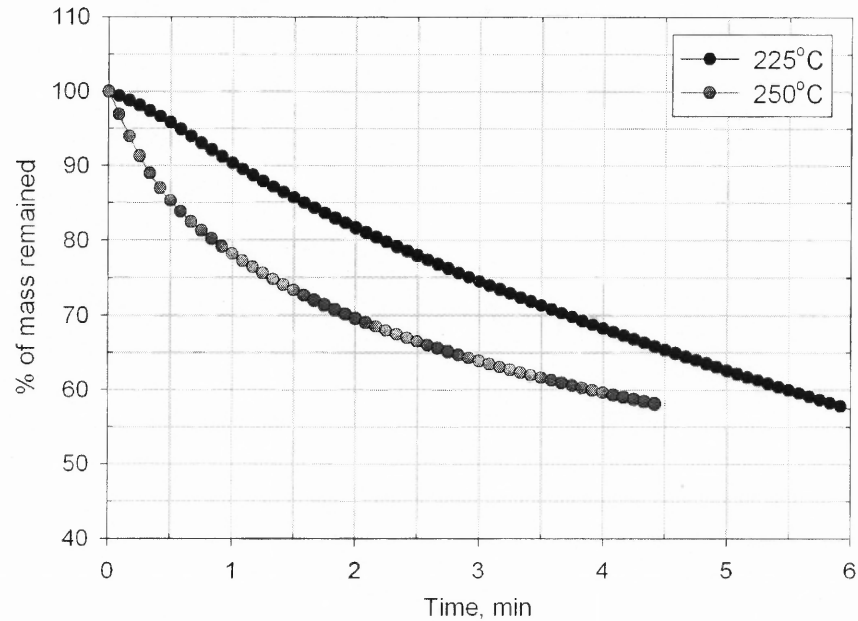
Figure 4.7 Typical thermal decomposition behavior of CBA, Expandex-5PT.

According to product information (Crompton) and literature sources (Hurnik, 2001; Throne 2004b), the nitrogen gas yield of the Expandex 5-PT is 200 ~ 210 ml/g, which is equivalent to about 13% of mass reduction after the onset of the decomposition. Due to removal of the decomposition products by evaporation, the mass kept decreasing during heating. Thus, by heating the CBA started to release nitrogen gas and then after the (almost) completion of the decomposition, the resulting by-products started to evaporate. In other words, there would be about 15% mass reduction (considering evaporation of the decomposition products during nitrogen release) from the onset to the end of the nitrogen release. Under this assumption, 30 seconds at 250°C and 1 min and 30 seconds at 225°C were required to complete the nitrogen release in Figure 4.7.

The residence time at 50 rpm (Section 3.3.1) was not long enough for the completion of the CBA decomposition. Thus, the decomposition continued presumably during the cooling stage of the foamed extrudate at 50 rpm. However, the decomposition,

which involved volume expansion, might have been hindered by the increasing melt strength with respect to time during cooling of the extrudate. Such effects appeared as: 1) lower foam densities at 50 rpm than those at 30 rpm below the critical concentration and 2) the onset of gas escape at a higher concentration, i.e., the amount of gas decomposed from 2.0 phr at 50 rpm is equivalent to 1.0 phr at 30 rpm. However, the increased melt strength allowed higher expansion ratios at 50 rpm as compared to those at 30 rpm.

4.1.3 Crystalline Morphology

SEM pictures of fractured surfaces of a foamed sample (PBT1 / CBA 1.0 phr, die set temp. 250 °C, 30 rpm) are shown in Figure 4.8 and 4.9 in order to compare the effects of foaming on the crystalline morphology. Figure 4.8 shows a morphology unaffected by foaming (away from any bubbles at the fracture surface), while Figure 4.9 shows a totally different morphology at the bubble wall. A similar morphology to that shown in Figure 4.8 could also be found at the fracture surface of the sample without CBA, which confirms that crystalline morphology is highly localized throughout the cross-section of the foamed sample. A spherulitic morphology (Figure 4.9) could be found in all bubble walls at the fracture surface. Further discussion on the different crystalline morphologies will be presented in Section 4.4 after combining the results of extrusion foaming with a PBA.
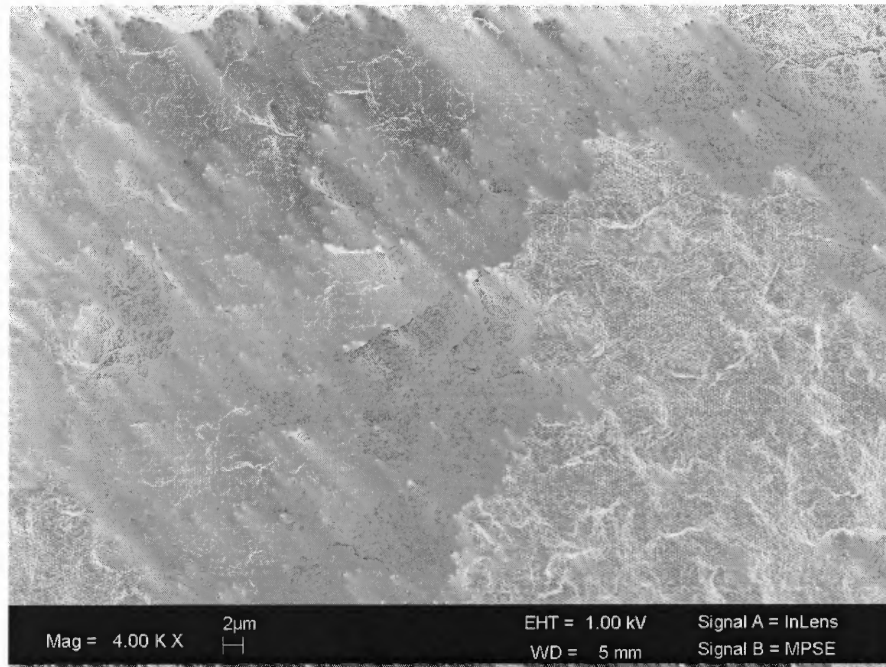
Figure 4.8 Crystalline morphology of the region away from the bubbles in the fracture surface of PBT1/CBA 1phr. Die set temp. 250°C, 30 rpm.
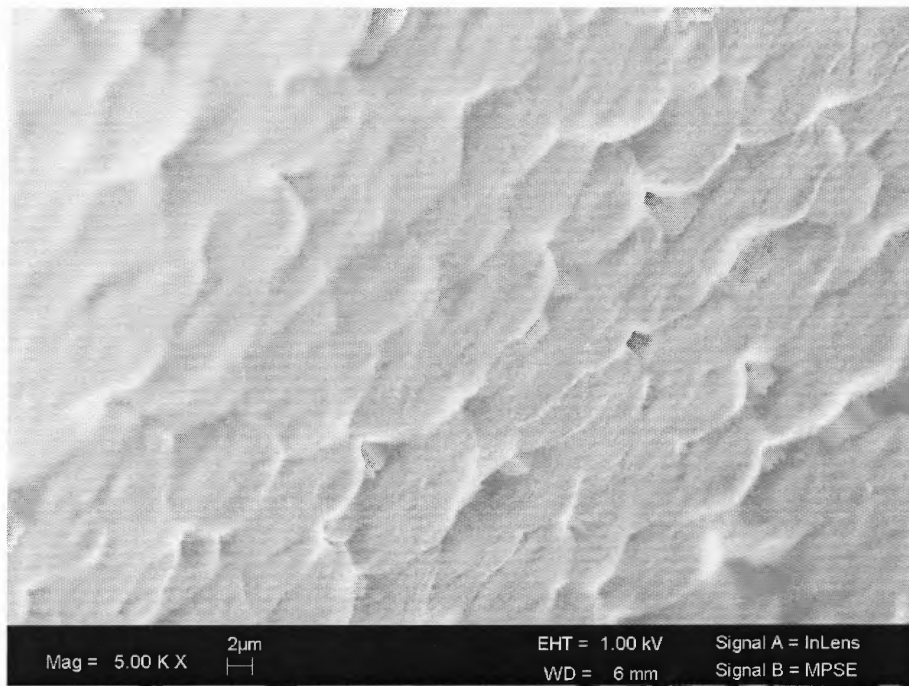
Figure 4.9 Crystalline morphology at a bubble wall of PBT1/CBA 1phr. Die set temp. 250°C, 30 rpm.

4.2 Rheological Modification of PBT

As discussed in Section 2.2 chemical and rheological modification of a linear PBT is required for low density extrusion foaming. The reactive modifier, TGIC, used in this study is expected to react with three PBT functional groups (carboxyl/hydroxyl), thus, resulting in branched and/or partially cross-linked structures. A possible reaction mechanism between a polyester and TGIC is suggested in Figure 4.10 (Dhavalikar et al. 2003; Dhavalikar and Xanthos, 2004).

The PBT2 resin that was used in the modification experiments was expected to be more amenable to rheological modification by reactive processing since it had a lower viscosity than PBT1. Its rheological properties are presented below and compared with those of the modified samples. The sample designation, "as-received", was used in order to distinguish PBT2 pellets (which did not undergo any processing) from the samples processed without the modifier.
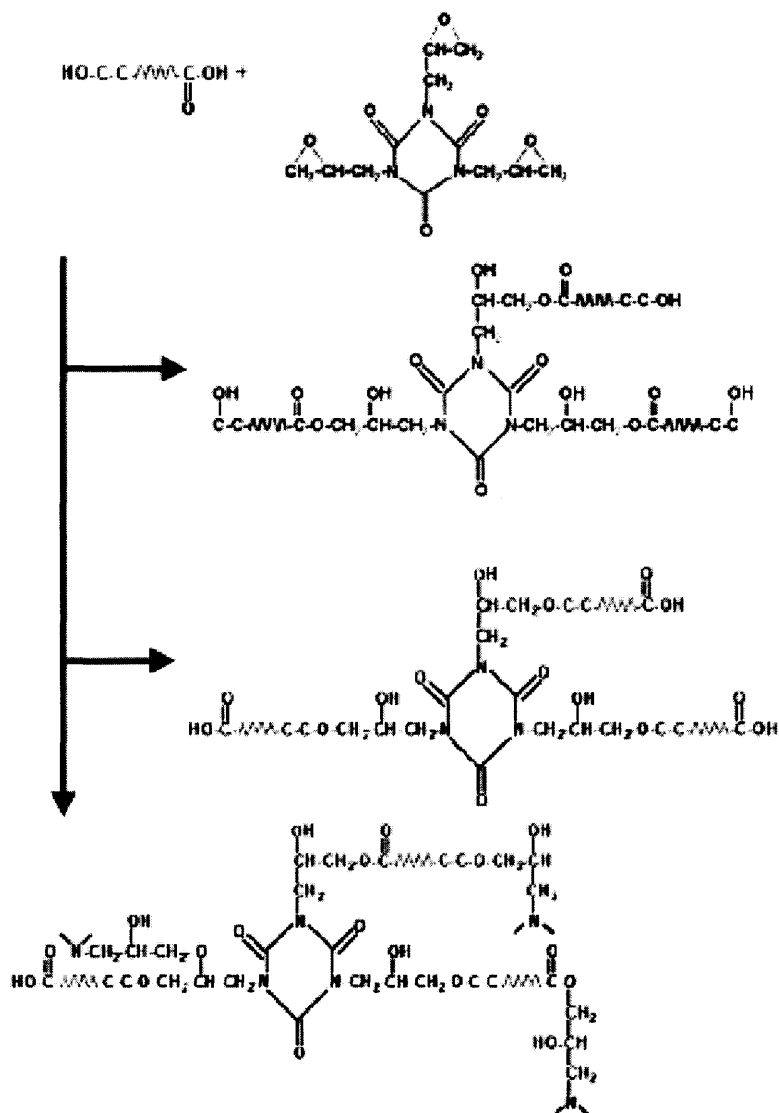
Figure 4.10 Possible polyester/TGIC branching reactions (Dhavalikar et al. 2003; Dhavalikar and Xanthos, 2004).

4.2.1 Modification in Intensive Batch Mixer

Figure 4.11 shows torque-time data obtained with different amounts of TGIC at 50 rpm, 235 °C. The fusion of PBT was complete in the initial stages of the experiment (<200 sec).
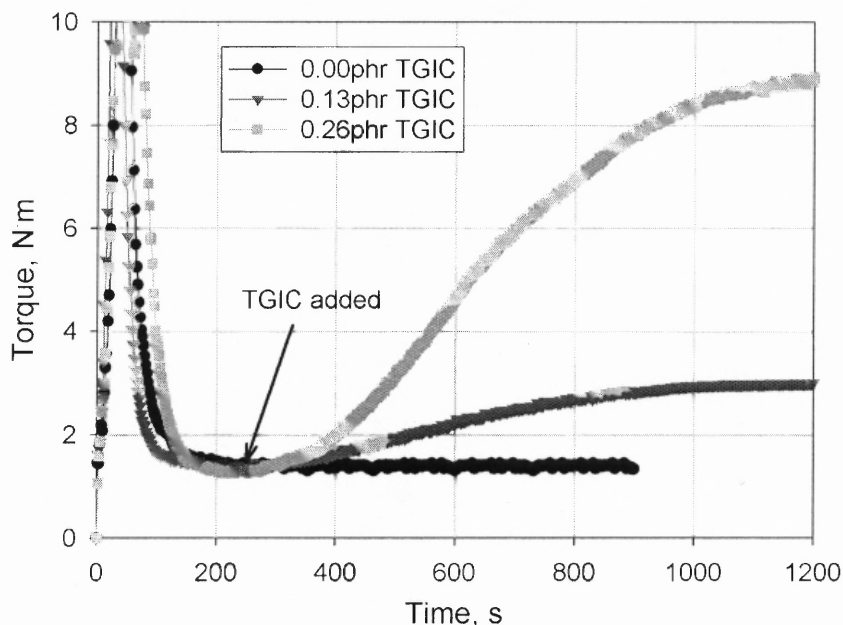
Figure 4.11 Typical torque vs. time data of PBT modification in a batch mixer with TGIC added at different concentrations (mixer set temp. 235°C, rotor rpm 50).

The curve at 0.0 phr TGIC, representing the baseline of the experiments, shows that the possible degradations of PBT, namely, thermal, hydrolytic and thermooxidative, were not significant under the processing conditions, since little decay of torque with respect to time is observed. After adding TGIC, an increase of torque was observed, suggesting an increased degree of branching as well as higher MW as a result of the reaction. Broader MWD is also expected from the increased degree of branching, as suggested by Japon et al. (2000), who performed reactive modification of PET using a tetra-epoxide and found by gel permeation chromatography (GPC) that the MWD of the modified PET was broader than that of the unmodified PET. In the present study, indirect

information on MW and MWD of the modified PBT were obtained from rheological measurements rather than direct GPC analysis in order to minimize solvent toxicity issues. The torque-time relationship in Figure 4.11 shows that the reaction rate is a function of the concentration of TGIC (from 0.13 phr to 0.26 phr); hence, it is applicable to a kinetic analysis, as suggested by Dhavalikar et al. (2003), who fitted the torque curves of the PET modification reaction with TGIC to a pseudo-first order kinetic equation as Equation (4.2).

$$-\frac{d\tau_{batch}}{dt} = k_{batch}\tau_{batch}$$

(4.2)

where τ_{batch} is the torque data from the batch mixer and k_{batch} is the reaction kinetic constant. However, it should be noted that the determined kinetic constant is a function of mixing and diffusion characteristics specific to the batch mixer; so, the constants are not applicable directly to other processes (such as single screw extrusion) with different mixing and diffusion behavior.

The viscosity-frequency curves of samples processed in the batch mixer are shown in Figure 4.12. In the presence of increasing amounts of TGIC, the observed increasing viscosity and shear thinning characteristics provide qualitative information on MW and MWD. The PBT2, "as-received", sample behaves as a Newtonian fluid over the entire measurement range. The PBT modified with 0.13 phr TGIC shows the onset of power-law behavior at an intermediate frequency and Newtonian behavior at lower frequencies. The PBT modified with 0.26 phr TGIC obeys a power-law and is expected to reach a Newtonian plateau at a frequency lower than in the measurement range. The increased Newtonian viscosity (and consequently the increased zero shear viscosity) with respect to the amount of TGIC indicates increased MW; the existence of the onset of

shear thinning is also an evidence of the broader MWD of the modified PBT (Dealy and Wissbrun, 1989c).
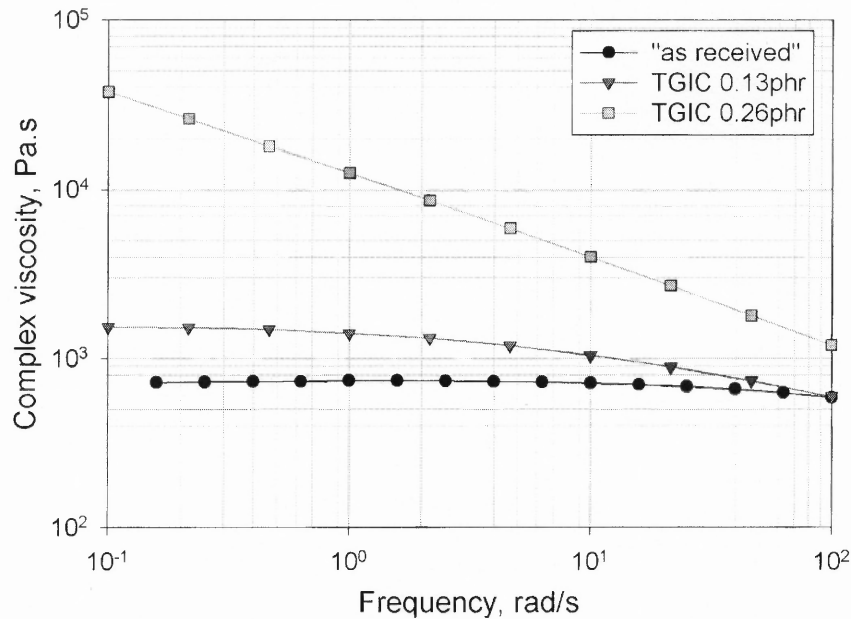
Figure 4.12 Batch mixer samples: effects of amount of modifier on PBT complex viscosity vs. frequency curves (250°C).

The storage modulus (G') and the loss modulus (G'') are shown in Figs. 4.13 and 4.14, respectively. The "as-received" sample shows a very low storage modulus (elasticity), which is a typical behavior of linear polyesters. Owing to the long chain branching as a result of the modification reaction, both G' and G'' increased; however, the G' increase, which was more pronounced than that of G'', resulted in an increased contribution of the storage modulus to the magnitude of the complex viscosity with respect to the concentration of TGIC. For example, in the "as received" pellet sample at 1.0 rad/sec, the contribution of G' to the magnitude of the complex viscosity (designated as $Con\,G'$) as calculated from Equation (4.3) was 0.04%. At the same frequency, for PBT

reacted with 0.13 phr TGIC the contribution of G' increased to 1.6% and at 0.26 phr

TGIC, it became 48.3%.

$$ConG' = \frac{\left(\dfrac{G'}{w}\right)^2}{\left(\dfrac{G'}{w}\right)^2 + \left(\dfrac{G''}{w}\right)^2} \times 100 \qquad (4.3)$$
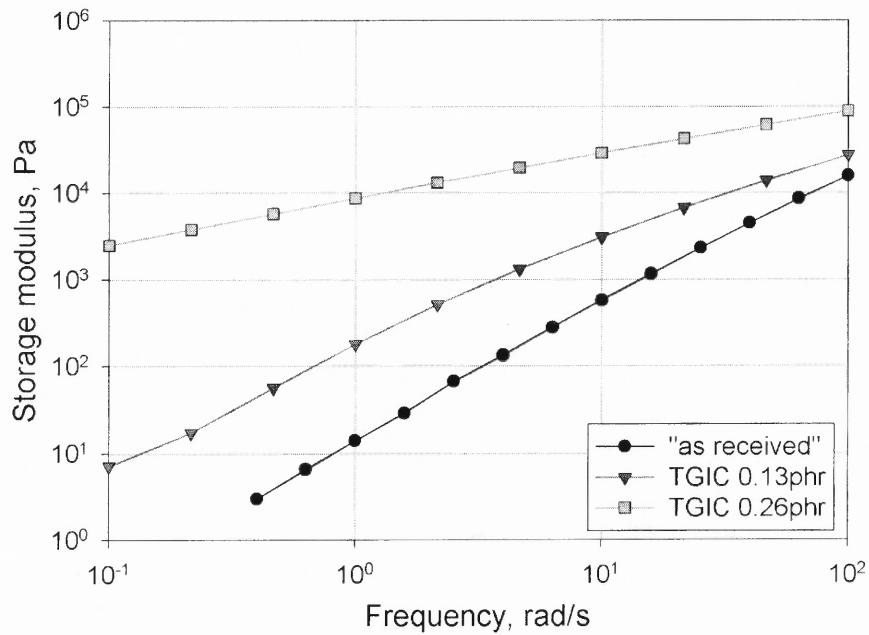
Figure 4.13 Batch mixer samples: effects of amount of modifier on PBT storage modulus vs. frequency curves (250°C).
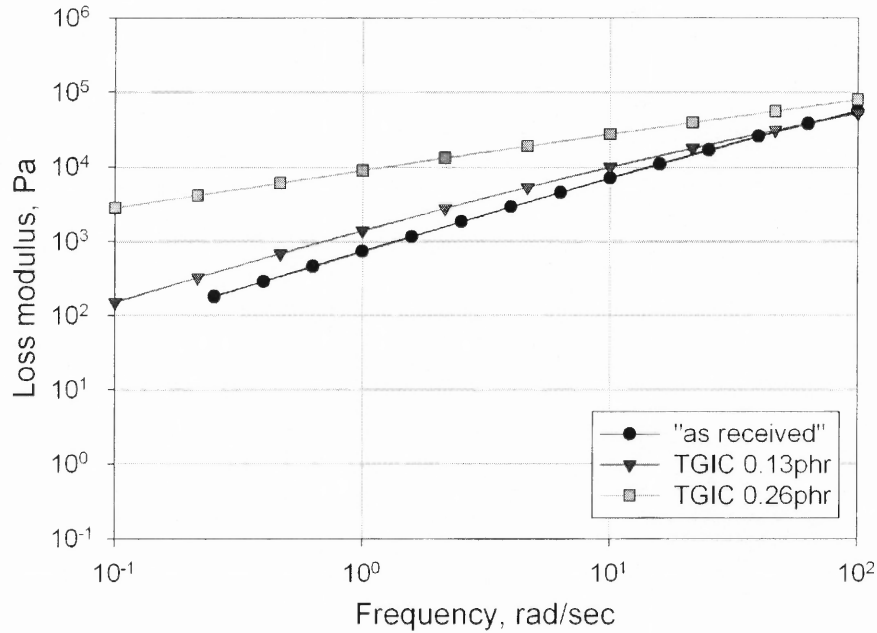
Figure 4.14 Batch mixer samples: effects of amount of modifier on PBT loss modulus vs. frequency curves (250°C).

The increased contribution of G' can be easily visualized from Cole-Cole plots. Harrel and Nakajima (1984) modified an ethylene-propylene copolymer using a peroxide for long chain branching and showed that the curves shifted to the lower right in the Cole-Cole plot as the contribution of G' increased with respect to the degree of branching. Yilmazer et al. (2000) also found the same shifting of the curves in the Cole-Cole plots of linear and branched PET. Figure 4.15 confirms the pronounced increase of G' in the branched PBT resulting in the same curve shifting tendency described above.
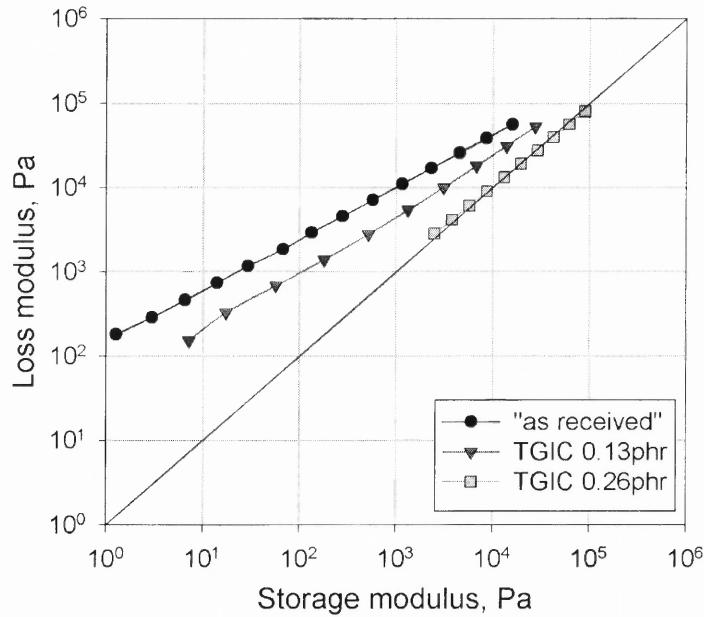
Figure 4.15 Batch mixer samples: effects of amount of modifier on PBT Cole-Cole plot (250°C).

4.2.2 Modification by Reactive Extrusion

4.2.2.1 Degradation. The effects of the TGIC concentration on the samples produced by reactive extrusion are shown in the viscosity curves (Figure 4.16) and the Cole-Cole plot (Figure 4.17). The viscosity curve for extruded samples without TGIC is also included. The extrusion modification reaction showed the same trends as the intensive batch mixer process described above, namely increased viscosity, earlier onset of shear thinning behavior (Figure 4.16) and increased elasticity (Figure 4.17) with respect to the amount of TGIC.
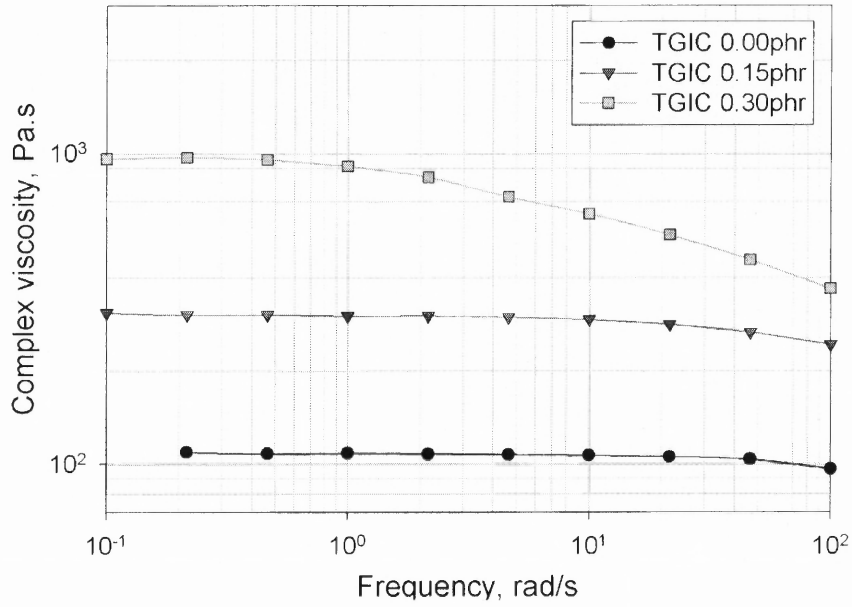
Figure 4.16 Extruder samples: effect of amount of TGIC on PBT complex viscosity vs. frequency curves (250°C).
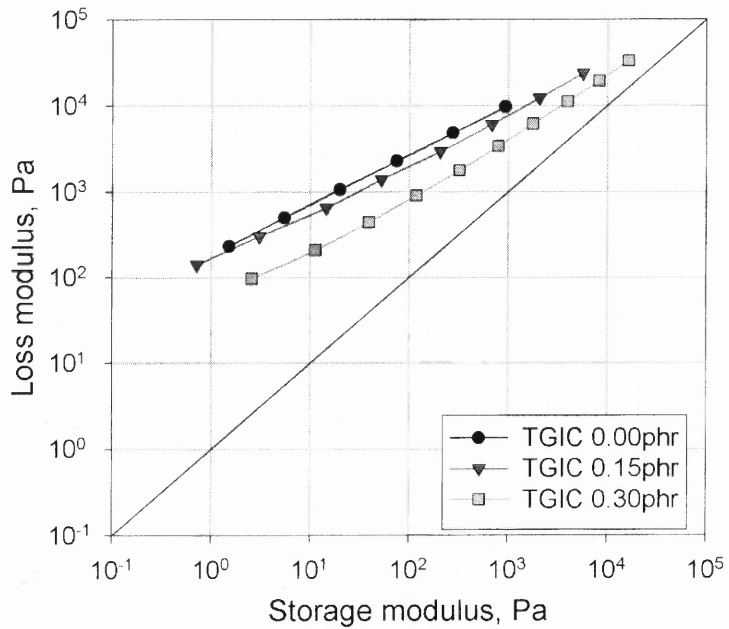
Figure 4.17 Extruder samples: effect of amount of TGIC on PBT Cole-Cole plot (250°C).

However, a noticeable difference appears to exist between the unmodified products of the extruder and those of the intensive batch mixer. All unmodified PBT samples (A, B, and C in Table 4.2) have significantly lower viscosities, as a result of excessive degradation, than the "as-received" pellets, as shown in Figure 4.18. Although similar viscosity data for the unmodified samples processed in the batch mixer are not available, the stability of the torque values for the 0.0 phr TGIC over long periods shown in Figure 4.11 suggests little or no degradation. The lower viscosity of the extruded unmodified PBT is, presumably, the result of PBT degradation, due to: a) the absence of nitrogen blanket in the extruder hopper and b) the presence of aggressive mixing elements in the screw. Besides the pin mixing section (length of 3D) at the end of the screw, specially designed mixing elements (similar to the turbine mixing elements used in twin screw extrusion) with a total length of 12D were present after the melting section of the screw. These aggressive mixing elements, which are suitable for compounding requiring intensive mixing, induce broad residence time distributions and very high shear stresses (or strains). The intensive mixing provided by these special elements was thought to be necessary for completing the modification reaction within a relatively short residence time; however, it is obvious that the PBT resin, which is known to be particularly sensitive to heat and/or shear, underwent excessive degradation. Figure 4.18 and Table 4.2 show that the extent of the degradation reaction increased with residence time (proportional to the reciprocal of feed rate at the same screw speed). Note that the extruded PBT without TGIC was considered as a new baseline in the reactive extrusion experiments.

Table 4.2 Operational Conditions for Studying Reaction and Degradation of PBT in Extruder

	Degradation studies (Figure 4.18)			Case studies (Figures 4.19, 4.20)			Optimization studies (Figure 4.21)	
	A	B	C	Case i	Case ii	Case iii	D	E
Screw, rpm	35	50	50	35	50	50	50	50
Feed rate, kg/hr	3.49	5.91	7.30	1.14	1.14	2.16	2.20	3.05
Min. residence time, s	N/M	N/M	N/M	430	410	265	263	164
TGIC, phr	0.0	0.0	0.0	0.3	0.3	0.3	0.3	0.3

N/M: not measured
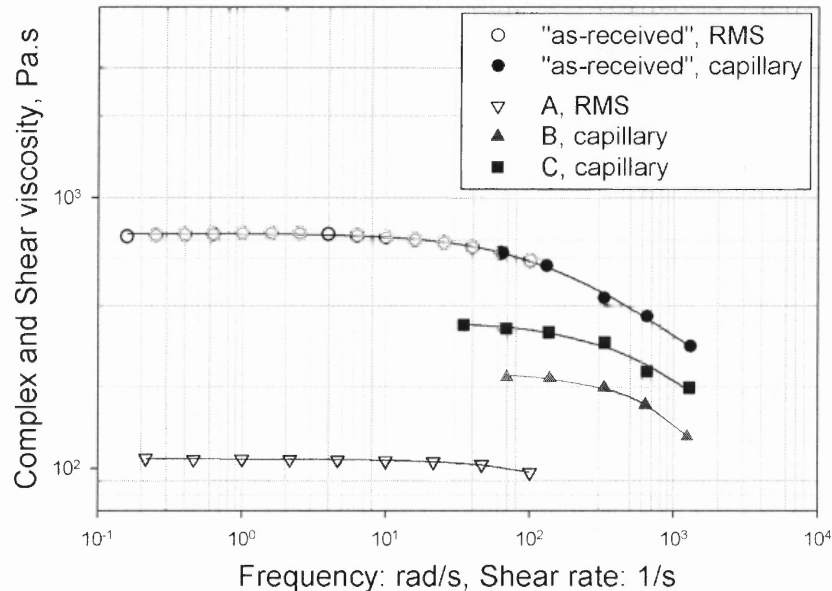
Figure 4.18 Extruder unmodified PBT samples: viscosity vs. frequency (RMS) or shear rate (capillary) curves at 250°C obtained at different operational conditions (see Table 4.2).

4.2.2.2 Case Studies. In the modification by reactive extrusion, there are two competing reactions, namely the desired branching reaction by the modifier, and the inevitable degradation. In order to find a condition where more branching than degradation occurred, the effects of the operational variables (screw speed and feed rate) were investigated. As an example, Cases i, ii and iii (Table 4.2) constitute a series of experiments performed to investigate the effects of the operational conditions at a constant TGIC concentration (0.3 phr). The minimum residence time under each set of operational conditions was measured by using a tracer (colored pellets). The minimum residence time was in accordance with the functional approximation concept for the average residence time, described by Todd (1998). According to this approximation, under starved feed conditions the increase of the feed rate at a constant rpm would affect

the residence time in the filled zone, resulting in a decrease of the average residence time. Increase of rpm at a constant feed rate would reduce the length of the filled zone and consequently decrease slightly the average residence time. A comparison between Case i and Case ii shows the effects of rpm at a constant feed rate. More intensive mixing at a higher screw rpm presumably enhances the modification reaction, and as a result, increased viscosity and elasticity are observed for Case ii in Figs. 4.19 and 4.20, respectively. However, due to the longer residence time in both Cases i and ii, degradation seems to be very pronounced. Note the little increase of viscosity in Case i (even though 0.3 phr TGIC was added) vs. condition A above (Figure 4.18). The effects of the feed rate at a constant screw rpm can also be shown by comparing Case ii and Case iii. Reduced degradation appears to occur in Case iii, primarily due to the shorter residence time. In addition, the higher feed rate of Case iii lengthened the filled zone (increased degree of fill), where much more reaction would take place than in the starved zone. Consequently, the rheological behavior of samples prepared in Case iii (Figs. 4.19, 4.20) suggests that highly branched structures were produced under these operational conditions.
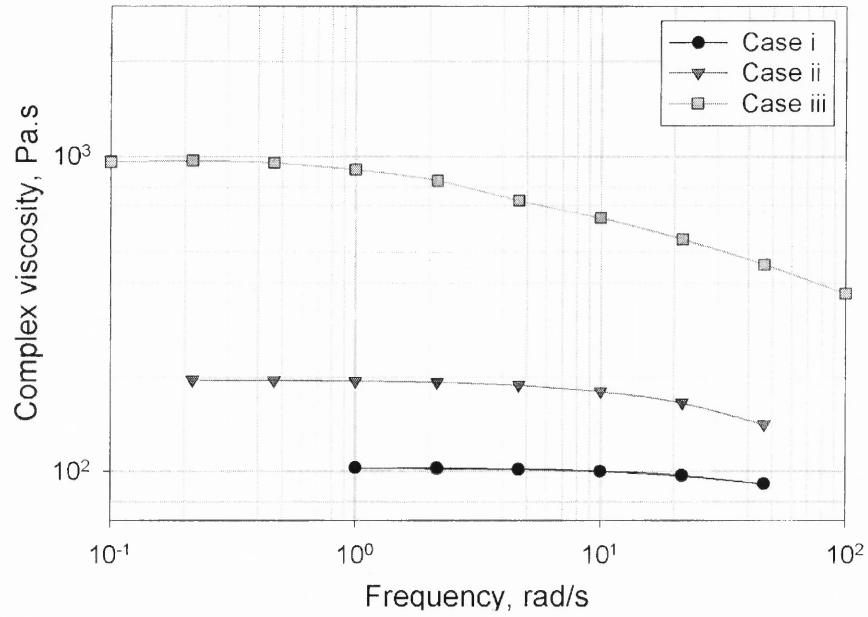
Figure 4.19 Extruder unmodified PBT samples: viscosity vs. frequency (RMS) or shear rate (capillary) curves at 250°C obtained at different operational conditions (see Table 4.2).
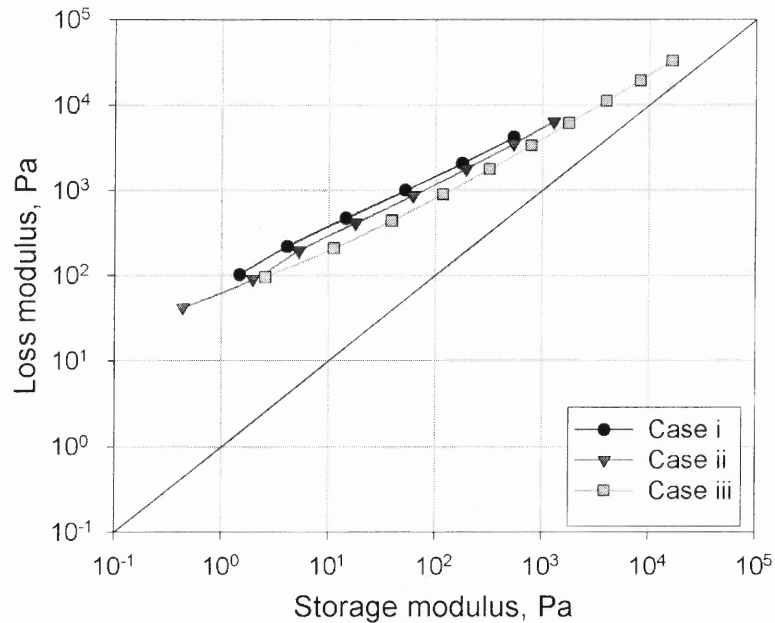

Figure 4.20 Case studies i – iii (see Table 4.2): effects of operational conditions on modified PBT complex viscosity vs. frequency curves (250°C).

4.2.2.3 Optimization. The Case studies in the previous section showed that higher rpm (intensive mixing) and higher feed rate (shorter residence time) favored the branching reaction. Hence, two more conditions (D and E) were examined in order to optimize the preparation of branched PBT in quantities suitable for extrusion foaming as shown in Table 4.2. Figure 4.21 shows that the largest increase of MW and the broadest MWD were obtained for the E condition rather than any other condition in this study. A further increase of the feed rate was shown to provide insufficient reaction at a given TGIC concentration as became evident from the non-uniform extrusion behavior and the poor product quality in subsequent experiments. Thus, the E condition was considered as the optimized condition that would be used for low density extrusion foaming.

An increased melt tension for samples produced under the E condition was also determined (Table 4.3), implying an increased extensional viscosity of the branched PBT. From a rheometric view point, the temperature during the melt tension measurements is not uniform along the spinline, and stress and strain rate depend on the position along the spinline; thus, an exact extensional viscosity cannot be extracted (Gendron and Daigneault, 2000). However, the melt tension is an easily obtainable quantity that enables a qualitative estimation of the extensional viscosity. The extrudate swell ratio is also a sensitive indicator for long chain branching and the presence of high molecular weight molecules in a broad MWD (Koopmans, 1992; Xanthos et al. 2004); the higher ratios at the E condition (Table 4.3) confirm these results.

Table 4.3 Calculated and Measured Viscoelastic Properties of PBT at Different Operational Conditions

Sample	Cross model parameters			Power-law model parameters		Extrudate swell ratio				Melt tension, $*10^{-3}$ N
	$\mu_0 *10^3$ Pa.s	n_c	t_1, s	$M *10^3$ Pa.s	n_p	38.4/s	76.8/s	153.6/s	384.0/s	
"As-received" resin	0.75	0.27	0.0017	2.30	0.71	0.89	1.02	1.14	1.25	3.53
Resin processed at condition D	1.13	0.56	0.054	1.33	0.71	0.90	1.10	1.27	1.50	4.66
Resin processed at condition E	2.62	0.61	0.28	2.51	0.68	1.08	1.29	1.45	1.61	9.70
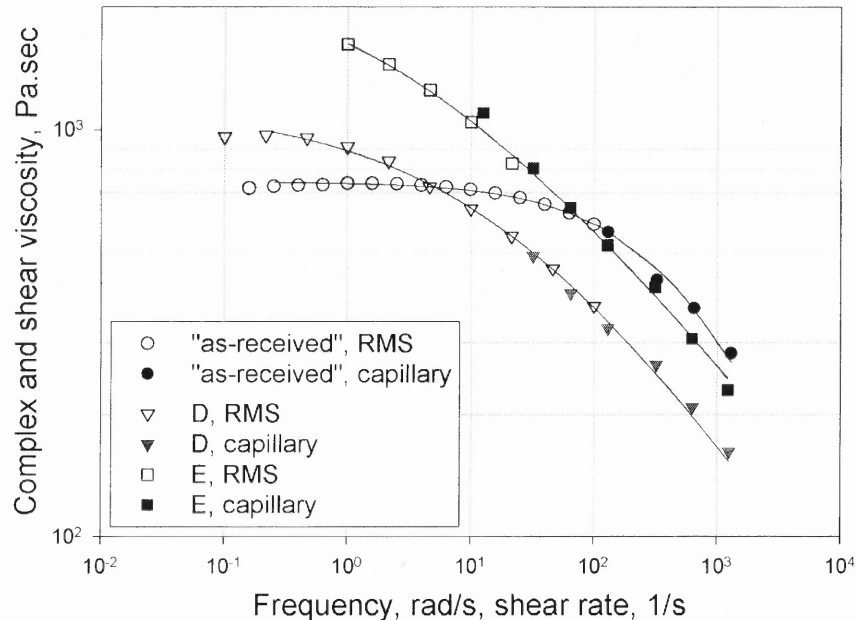
Figure 4.21 "As-received" pellets and extruder modified PBT samples: viscosity vs. frequency (RMS) or shear rate (capillary) at 250°C obtained at different operational conditions (see Table 4.2).

The rheological curves suggest the formation of a broader MWD by reactive extrusion of PBT with TGIC. A detailed explanation is as follows: the reactively modified PBT has an increased number of high MW chains as a result of the branching reaction. On the other hand, the number of lower MW chains increased by degradation during reactive extrusion. This behavior would result in a broad MWD and/or, as a limiting case, a polydispersed MWD (e.g., bimodal distribution) differing from the monodispersed narrow MWD of the linear ("as-received") PBT. The comparison of viscosities between the "as-received" and the branched PBT (E case) in Figure 4.21 is a good example of such differences. The effect of high MW chains is pronounced at the low shear rate region, in which the increased population of high MW chains of the

branched PBT increased the zero shear viscosity. However, at higher shear rates, entanglements of high MW chains and/or the branched structures would be aligned by flow; thus, the effects of those molecules become less significant, and degradation effects become more pronounced (Dealy and Wissbrun, 1989a; 1989c). This is in agreement with the observed lower shear viscosity of the branched PBT above the shear rate of 90 s^{-1}.

4.2.2.4 Parametric Fitting of Constitutive Equations. For a quantitative analysis, a Cross model (Carreau et al. 1997), Equation (4.4) and a power-law model (Carreau et al. 1997), Equation (4.5) were fitted with the parameters shown in Table 4.3.

$$\mu = \frac{\mu_0}{\left(1 + \left|t_1 \dot{\gamma}\right|^{1-n_c}\right)} \tag{4.4}$$

$$\mu = m\left(\dot{\gamma}\right)^{n_p - 1} \tag{4.5}$$

where μ is viscosity and $\dot{\gamma}$ is shear rate. In the Cross model, μ_0 is the Newtonian viscosity, t_1 is a parameter related to the onset of shear thinning, and n_c is a parameter dependent on shear rate; in the power-law model, m is consistency and n_p is the power-law index.

The Cross model, Equation (4.4), is a generalized Newtonian model with three parameters and is an adequate model in the case of a polymer showing Newtonian behavior in the lower shear rate range and shear thinning in the higher shear rate range (applicable to both the unmodified and modified PBTs in this study). The power-law model, Equation (4.5) is a two-parameter, generalized Newtonian model with a widely

used equation to describe the shear thinning behavior. Although the power-law model is only applicable at higher shear rates (> 100/s) for the PBT resins of this study, the calculated parameters can be useful in the simple pressure drop equations to be discussed in Section 4.3.2.

4.2.3 Crystallization Behavior of Modified PBT

Table 4.4 shows the crystallization behavior of several PBT samples as measured by the first cooling DSC scan. The comparison of data of the "as-received", C and B cases gives information on the effects of degradation. Extent of degradation is proportional to the reciprocal of the feed rate as discussed in the previous section. Lower MW chains possess higher mobility, which facilitates their diffusion onto nuclei to form a crystalline phase. This results in higher degree of crystallization (higher heat of crystallization) and faster crystallization kinetics (higher peak, T_c, and onset temperatures). T_c in the absence of reaction at feed rates less than 3.05 kg/hr would follow this trend; In Figure 4.22, the extrapolated curve I intends to show a tendency for further increasing of T_c at feed rates lower than 5.91 kg/hr (B) where more severe degradation conditions would be present, rather than indicate specific values. Similarly, the curve II represents the possibility (as a limiting case) that the effects of the lower MW chains on T_c are not pronounced at feed rates around the value of an end B, with the result of little increase of T_c at values higher than B.

Table 4.4 Crystallization Behavior of "As-received" and Extruded Samples Obtained at Different Operational Conditions (Measured at the First Cooling DSC Scan)

	TGIC, phr	Feed rate, kg/hr	Onset temp. of crystallization, °C	T_c (peak temp.), °C	Heat of crystallization, J/g
"As-received"	-	-	180.4	168.9	44.1
C	0.0	7.30	187.8	182.1	49.7
B	0.0	5.91	189.3	183.7	50.4
E	0.3	3.05	188.1	182.9	50.0
D	0.3	2.20	188.9	183.4	52.2
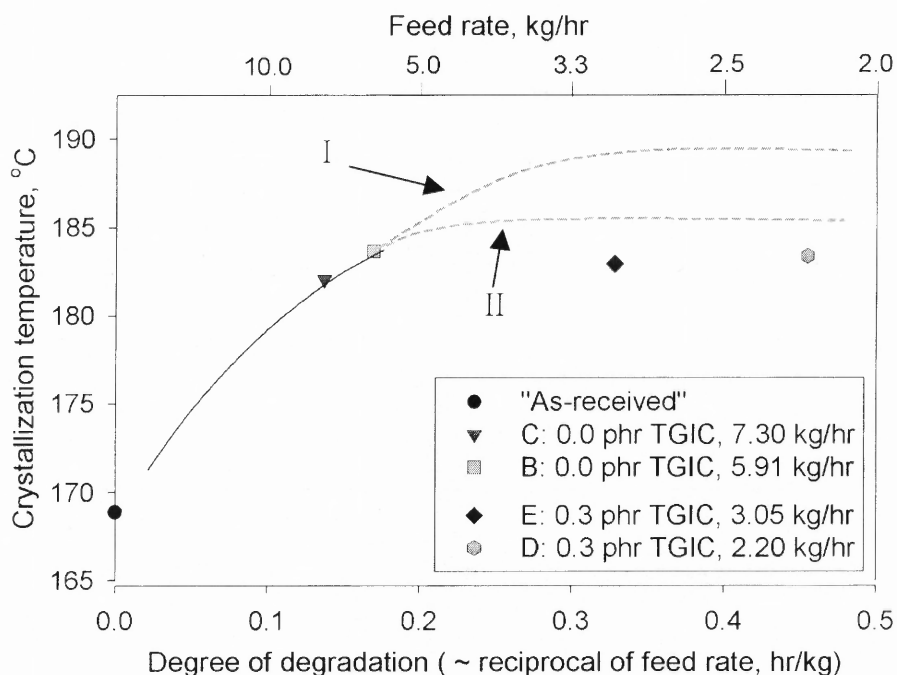
Figure 4.22 Crystallization temperature (peak temperature at 1st cooling scan) vs. degree of degradation (proportional to reciprocal of feed rate) of extruded samples obtained at different operational conditions (see Table 4.4). Dashed lines represent extrapolations.

Note that both curves of extrapolation curves lie above conditions E and D for the chain modified material. Although the feed rate conditions of E and D presumably induced more severe degradation, the branched PBT (E and D) show slower crystallization than the linear one as obtained from the extrapolated curves. This is the result of the presence of high MW chains and/or branched structures formed by reactive modification. A higher concentration of chain entanglements and enhanced interchain interactions induced by the presence of high MW chains and branched structures inhibited the diffusion of chains for crystallization; this results in decreases of T_c as shown qualitatively in Figure 4.2 by the differences of T_c's of the branched PBT (E and D) and the extrapolated T_c of linear PBT extruded under the same conditions. Guo and Chan (1999) measured the crystallization temperatures of the chain extended PBT by chemical modification. They also observed an increased T_c with increasing degree of branching without providing an explanation of this trend. However, there exist more published data on the effects of branching, which resulted in slower crystallization kinetics, with various copolymerized polymers with branched structure based on PBT (Righetti and Munari, 1997), poly(butylene isophthalate) (Finelli et al. 2002), PET (Jayakannan and Ramakrishnan, 1999) and poly(butylene adipate) (Chae et al. 2001).

The effects of branching also appear in the isothermal crystallization behavior. Experimental data of isothermal crystallization of the linear PBT sample (B) and the branched sample (E) were obtained and fitted to the Avrami equation, Equation (2.27), as shown in Figures 4.23 and 4.24.

$$X_c(t) = 1 - \exp[-kt^n] \qquad (2.27)$$

The fitting followed a procedure suggested by Hsu (1991), and a graphic software, SigmaPlot®, was used for non-linear regression. The fitted parameters are shown in Table 4.5. The crystallization kinetic constant, k, of the branched PBT is higher than that of the linear PBT; increased mobility by severe degradation is found to be more significant than structural hindrance of diffusion within the measured temperature range. The Avrami exponents of both PBT samples are between 2 and 3 without showing a significant difference, and this suggests that the nucleation and growth mechanism is independent of the PBT structures. Both PBT samples are nucleated thermally, and circular lamellae would be formed (Wunderlich, 1976). The Avrami exponents of PBT reported by Chou et al. (2001) were in agreement with those of this study.

Table 4.5 Fitted Parameters of Avrami Equation of the Linear and the Branched PBT Samples

	190°C		195°C		200°C	
	k, min^{-1}	n	k, min^{-1}	n	k, min^{-1}	n
C, linear	5.35	2.43	0.63	2.78	0.035	2.94
E, branched	7.68	2.37	0.89	2.82	0.048	2.93
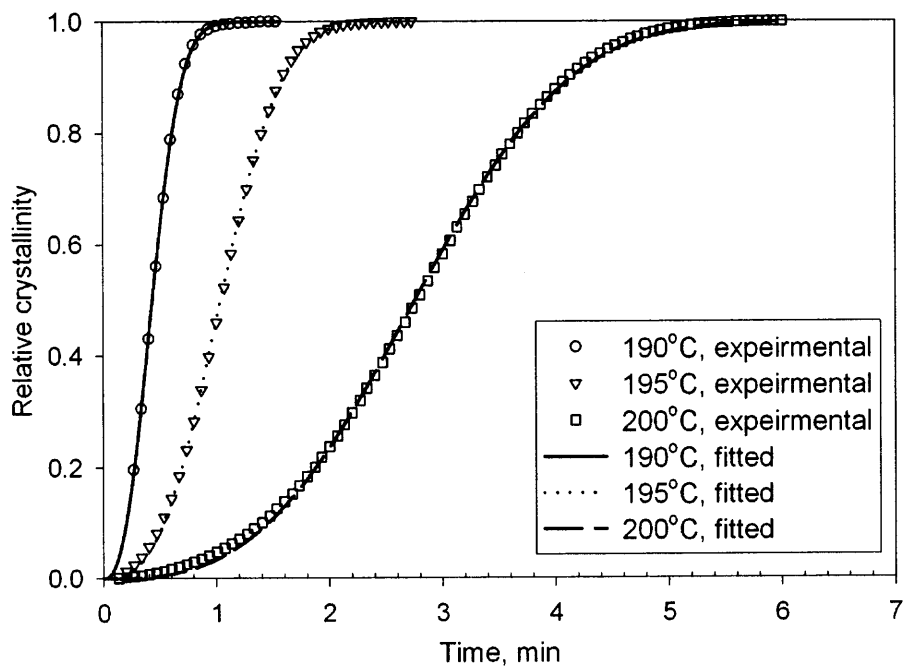
Figure 4.23 Isothermal crystallization behavior of the linear PBT sample.
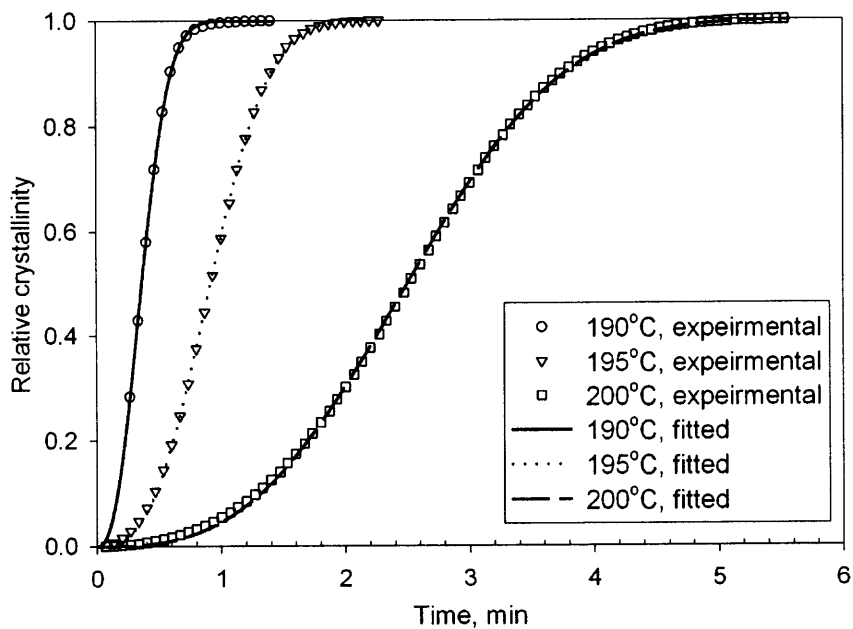
Figure 4.24 Isothermal crystallization behavior of the branched PBT sample.

4.3 Extrusion Foaming of Rheologically Modified and Unmodified PBT with PBA

The PBA extrusion foaming behavior of the two PBTs are compared and discussed in this section. The unmodified PBT was the PBT2 pellets (referred to "as-received" in Section 4.2) whose structure was linear. The modified PBT had a branched structure, and it was produced under the optimized conditions (condition E in Section 4.2.2.3) of this study. Introduction of PBA was necessary to produce low density foams, since extrusion foaming of the branched PBT with CBA resulted in relatively high density foams (the lowest density was 0.68 g/cc) (Jeong et al., 2006b).

4.3.1 Foam Characterization

The PBT modified under the optimized condition E showed better foamability than the unmodified PBT as evidenced by higher density reduction and higher expansion (Table 4.6). The lower expansion ratio of the unmodified foamed extrudate was due to gas escape, since its lower extensional viscosity could not sustain the rapid expanding deformation after the die (strain rates from 1 to 5 s^{-1}) (Gendron and Daigneault, 2000); as a result, there were more chances of cell collapse. Cell morphologies of the PBT foams are compared in Figs. 4.25 and 4.26. Larger cells and thinner walls between cells, evident in the branched PBT foams, indicate less occurrence of cell collapse and coalescence as a result of a pronounced viscoelastic behavior. Spitael and Macosko (2004) have also observed the same tendencies for extrusion foamed linear and branched PP. The branched PP showed strain hardening during measurements of extensional viscosity; as a result, cell coalescence was prevented and foamed extrudates with significantly larger cells were produced.

Table 4.6 Characteristics of Extruded PBT and PET Foams

Sample	PBA	Foam density, g/cm^3	Expansion ratio	Cell density, Cells/cm^3	Crystallinity, %	Onset temperature of crystallization, ^oC	T_c
Unmodified PBT (linear)	Isobutane	0.51	1.86	$2.20*10^7$	28.8	194.7	181.2
Modified PBT (branched)	Isobutane	0.33	3.97	$1.08*10^7$	33.1	198.5	190.0
Unmodified PET* (linear)	Carbon dioxide	0.68~1.23	N/A	N/A	6.5~9.6	N/A	N/A
Modified PET* (branched)	Carbon dioxide	0.20~0.43	N/A	N/A	15~25	N/A	N/A

* N/A: not available
* Information on PET foams was obtained from Xanthos et al. (2000a; 2000b)
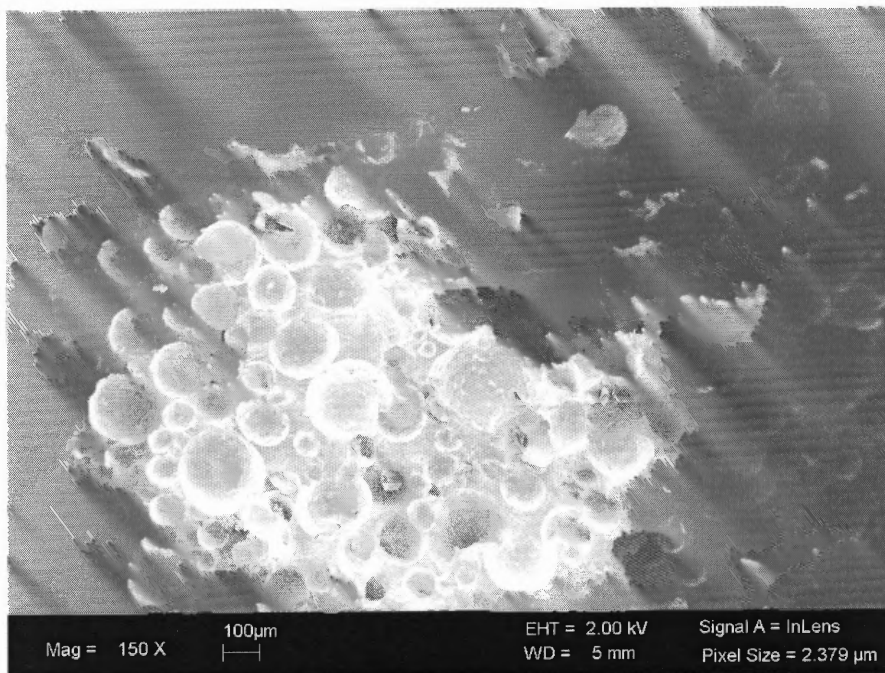
Figure 4.25 Morphology of isobutane foamed, unmodified PBT extrudate.
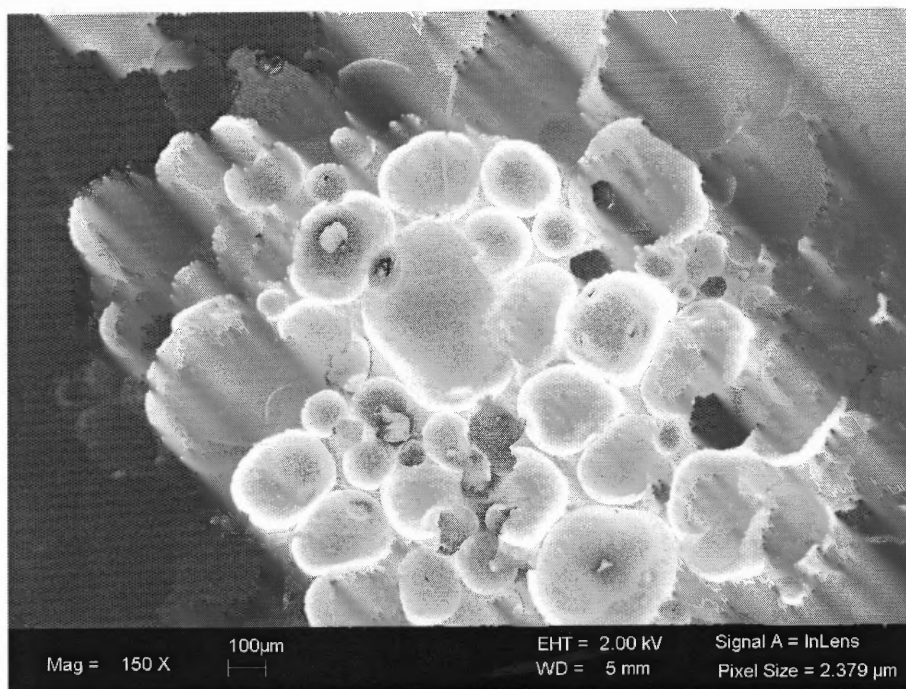
Figure 4.26 Morphology of isobutane foamed, modified PBT extrudate.

The number of cells per unit volume (N_0) of the foamed polymer may be calculated from Equation (4.6) (Matuana et al. 1997):

$$N_0 = \left(\frac{n_{cell} M_{micro}^2}{A_{micro}} \right)^{3/2} \cdot \left(\frac{1}{1-V_f} \right) \tag{4.6}$$

where n_{cell} is the number of cells in the micrographs (see Figures 4.25 and 4.26), M_{micro} and A_{micro} are the magnification and the area of the micrographs, respectively, and V_f the void fraction of the foamed sample defined as:

$$V_f = 1 - \frac{\rho_f}{\rho} \tag{4.7}$$

where ρ is the density of the unfoamed polymer and ρ_f is the foam density. The cell density of the branched PBT foam is lower than that of the unmodified PBT foam in Table 4.6, although the branched PBT foam had less chances of collapse and coalescence as described above. This is possibly due to the effects of: a) cell nucleation rate as a function of a pressure drop rate and b) the crystallization behavior of the particular resin.

4.3.2 Effects of Pressure Drop Rate on Bubble Nucleation

The nucleation rate model by Colton and Suh (1987) predicts that the homogeneous nucleation rate will increase under a higher pressure drop (ΔP) through reduction of the thermodynamic free energy change (minimum work required to form a critical nucleus) in the nucleation step. However, during actual polymer processing, pressure drop cannot occur instantaneously but over a finite residence time in a die. Thus, the pressure drop rate (dP/dt) should be considered. Park et al. (1995) suggested that at a lower pressure drop rate, there exists more time for the gas in the solution to diffuse into the initially

nucleated cells during the residence time in a die; this will lead to a decreased local concentration of the gas adjacent to the nucleated cells to below the critical concentration needed to nucleate additional cells, with the net result of a lower cell density. At a higher pressure drop rate, more cells can be initially nucleated, and there remains a higher possibility for additional nucleation owed to little time available for diffusion. The diffused gas will also contribute to the growth of the initial nuclei.

Equations (4.8) – (4.10) are adopted for calculating the pressure drop rate in a circular channel for a power-law fluid (Bird et al. 1987).

$$-\Delta P = \frac{2mL}{R}\left(\frac{Q\left(3+\frac{1}{n_p}\right)}{\pi R^3}\right)^{n_p} \tag{4.8}$$

$$\Delta t \approx \frac{\pi R^2 L}{Q} \tag{4.9}$$

$$-\frac{dP}{dt} \approx \frac{-\Delta P}{\Delta t} \approx 2m\left(\frac{Q}{\pi R^3}\right)^{n_p+1}\left(3+\frac{1}{n_p}\right)^{n_p} \tag{4.10}$$

where Q is the volumetric flow rate, m and n_p are the power-law parameters (Table 4.3), L is the length of die, and R is the radius of the die.

The wall shear rate at the capillary die during extrusion foaming is about 850~865/s as calculated by Equation (4.11). This is the shear rate range in which both unmodified and modified PBT obey the power-law model (Figure 4.21).

$$\dot{\gamma}_w = \left(\frac{3n_p+1}{4n_p}\right)\cdot\left(\frac{4Q}{\pi R^3}\right) \tag{4.11}$$

The calculated pressure drop rates of the unmodified and modified PBTs in the absence of dissolved gas, as calculated from Equation (4.8), are 103.6 and 95.2 MPa/s,

respectively. Viscosity values for both unmodified and modified PBTs are expected to be lower in the presence of dissolved gases. However, the degree of viscosity reduction would be the same assuming similar gas solubilities. The calculated pressure drop rates for the gas containing melts would, then, be lower, although ranking would be the same. Thus, the lower pressure drop rate of the modified PBT solution would correspond to the lower cell density of the resulting foam.

4.3.3 Effects of Crystallization on Bubble Nucleation

The cell density also depends on the crystallization behavior. Doroudiani et al. (1996) investigated the effect of crystallinity on the gas solubility and the cell morphology in batch foaming experiments. As expected, the crystalline regions of the semi-crystalline polymer did not dissolve gas and this resulted in uneven distribution of the cells. Since the experiments were performed under conditions where the crystalline regions already existed, a direct extrapolation to a process such as extrusion foaming, where foaming and crystallization of the matrix polymer should be considered as simultaneous, is limited. Spitael and Macosko (2004) found a lower cell density, similar crystallinity and a higher onset crystallization temperature for a branched PP vs. a linear PP. They concluded that the higher onset crystallization temperature affected the cell morphology although an explanation of the effects of crystallization kinetics was not given.

The crystallinity of the unmodified PBT foams is lower than that of the modified foams as shown in Table 4.6. Table 4.6 also shows the difference in the onset temperature of crystallization and peak temperature of crystallization (T_c) between the unmodified and modified PBT. The modified PBT is found to have a faster crystallization rate as

determined by the temperature difference between the onset temperature and T_c. A qualitative explanation of the effects of the crystallization on the cell density and morphology is as follows: during cooling of the foamed extrudate, cell nucleation and growth would be "frozen" by the increase of the matrix viscosity following the formation of crystals and loss of gas (reduced solubility). The modified PBT would inhibit further cell nucleation and growth immediately after the onset of crystallization owed to its faster crystallization rate; hence, its observed higher crystallinity. However, in the case of the relatively slower rate of crystallization of the unmodified PBT, the cell nucleation and growth could compete against each other with an end result of lower crystallinity or interference with crystallization. Table 4.6 contains data from earlier work on unmodified and modified PET (Xanthos et al. 2000a; 2000b) that show similar trends.

4.4 Crystalline Morphology and Structures

4.4.1 Microscopy

Crystalline morphologies at the bubble walls of samples foamed with PBA are shown in Figures 4.27 and 4.28. In foamed samples of both the linear (Figure 4.27) and the branched PBT (Figure 4.28), the same crystalline structures are observed. A similar morphology at the bubble walls could also be found in Figure 4.9 for the PBT samples foamed with CBA. Thus, it can be concluded that the crystalline structures are not related to the type of blowing agent.
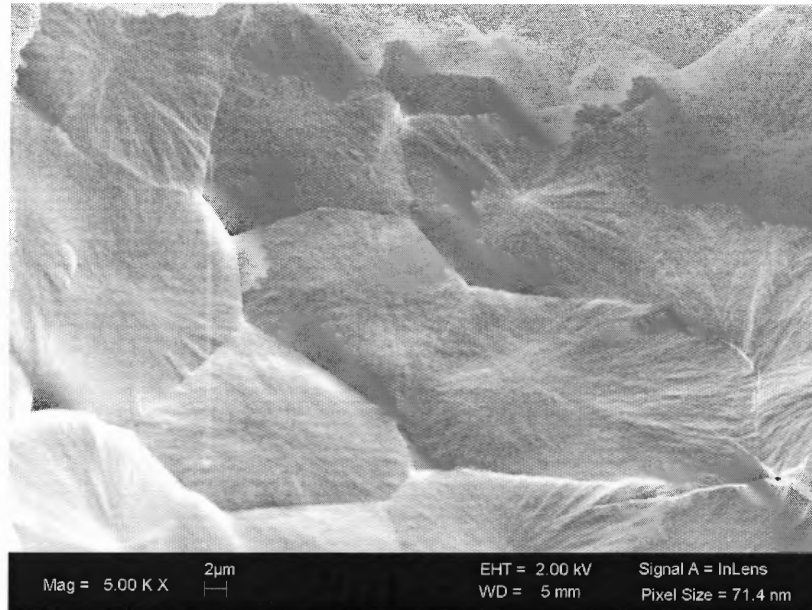
Figure 4.27 Crystalline morphology at a bubble wall of linear PBT foamed with PBA (5,000X).
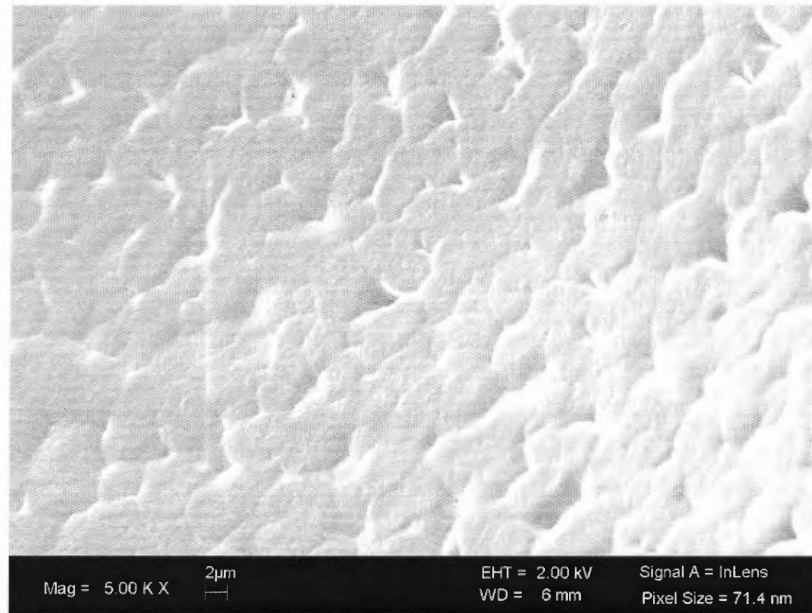
Figure 4.28 Crystalline morphology at a bubble wall of branched PBT foamed with PBA (5,000X).

When polymer melts are crystallized, the most frequently observed structures are spherulites. By using polarized light (with polarizers crossed at 90°), formation of spherulites is easily observed microscopically. In the absence of a crystalline phase, the fields under observation are dark. After the polymer sample reaches a certain crystallization temperature below the melting temperature, then, tiny, bright spots of light appear sporadically. These are sites where crystallization begins, i.e., nuclei. These bright spots are observed to grow radially in two dimensional samples, spherically in three dimensional samples, while nuclei continue to form. Thus, nucleation and growth take place simultaneously. As the spherulites grow, a Maltese cross is observed in each spherulite. As a final step, the spherulites impinge on each other and grow together, forming densely packed polygons in two dimensions and polyhedrons in three dimensions (Schultz, 2001a).

From Figure 4.27, Figure 4.29 (a larger magnification of Figure 4.28) and Figure 4.30 (a much higher magnification of Figure 4.9), this study considers that the observed crystalline morphologies are spherulitic, since: 1) the polygonal geometries are matched with shapes of spherulites observed in usual optical microscopy, 2) it appears that each polygon has grown radially from the center (nucleus), and 3) each polygon shows apparent boundaries as a sign of impingement. Observations 2) and 3) are more evident in Figure 4.30. In the formation of the spherulites at the bubble walls, nuclei have the same age with a fast growth rate, since the boundaries are straight. In the case of nuclei with different ages, the boundaries would have been hyperbolae (Sperling, 2001).
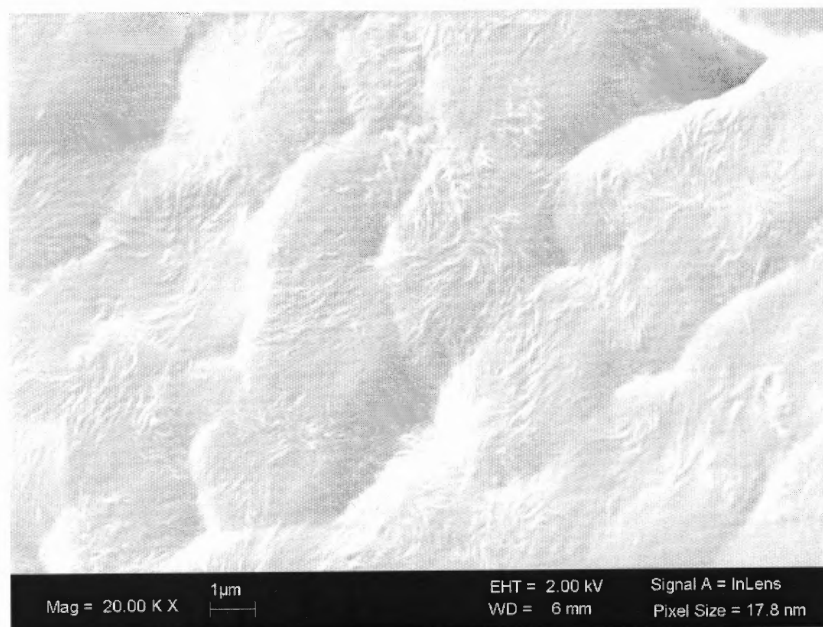
Figure 4.29 Crystalline morphology at a bubble wall of branched PBT foamed with PBA (20,000X).
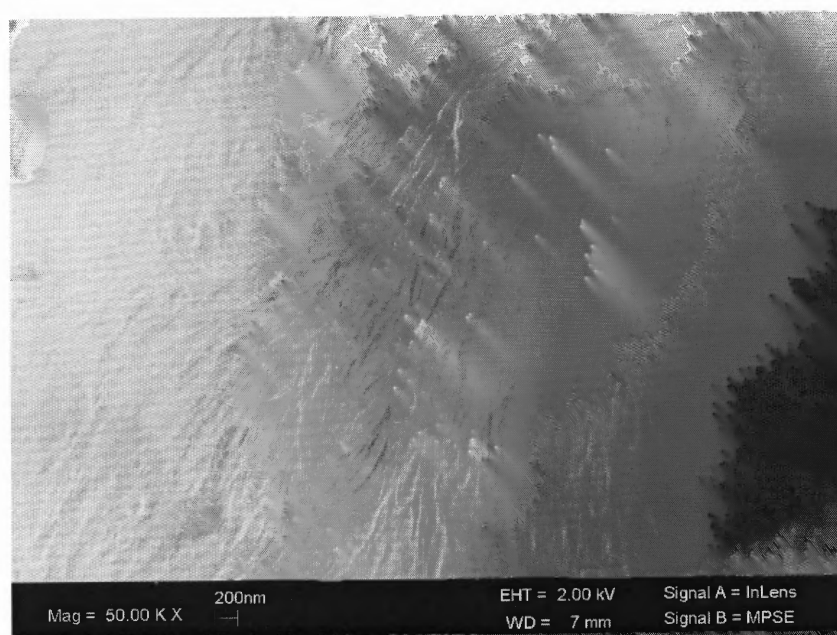
Figure 4.30 Crystalline morphology at a bubble wall of PBT1/CBA 1phr. Die set temp. 250°C, 30 rpm (50,000X).

There exists an apparent difference in the crystalline morphologies at the bubble walls and the fracture surfaces away from the bubble walls (Figure 4.8 in the CBA case and Figure 4.31 in the PBA case). The crystalline morphology at the fracture surface away from the bubble walls (i.e., in a region between two bubbles) appears similar to the fracture surface of the unfoamed PBT extrudate (Figure 4.32).
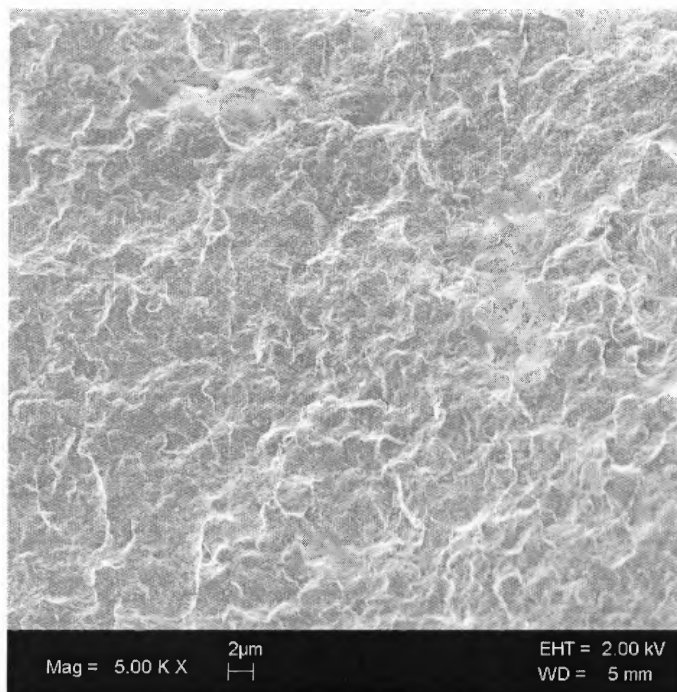
Figure 4.31 Crystalline morphology of the region away from the bubbles in the fracture surface of branched PBT foamed with PBA (50,000X).
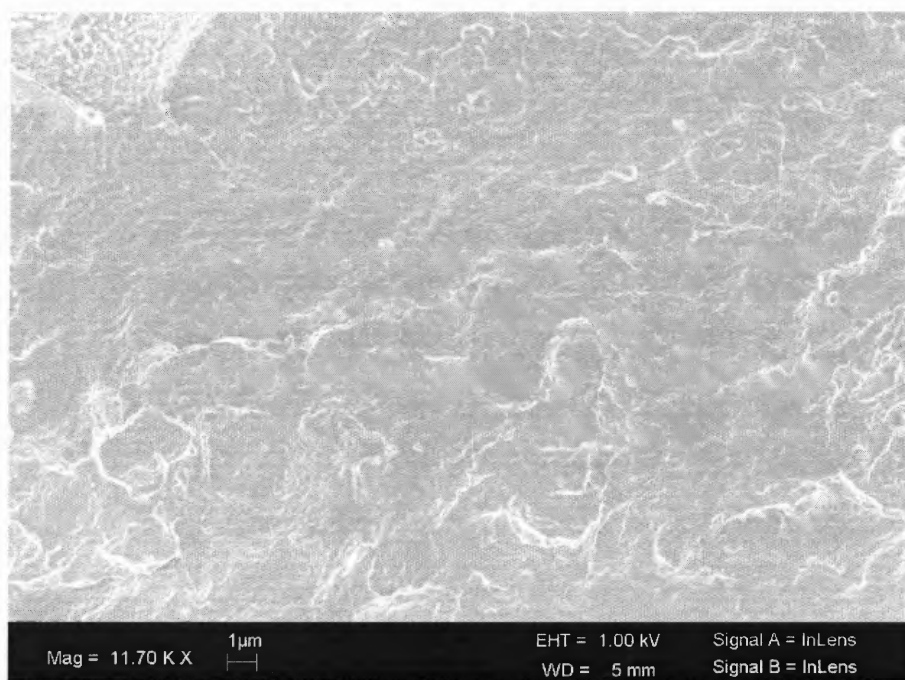
Figure 4.32 Crystalline morphology of the fracture surface of unfoamed PBT extrudate (11,700X).

4.4.2 XRD

XRD patterns (Figure 4.33) show a comparison of the crystalline structures of the unfoamed and foamed PBT. XRD measurements are useful to: (1) determine the crystal structure, (2) establish how processing conditions modify that structure, (3) characterize the degree of crystal orientation relative to some special direction, (4) characterize crystallite size and degree of crystal imperfection, and (5) determine the degree of crystallinity (Schultz, 2001a) by obtaining atomic distances (0.1 − 1 nm), which are equivalent to the dimensions of the unit crystal cell and atomic positions. These are achievable if the full diffraction pattern of a single crystal of a given polymer is available. Different crystalline forms can be distinguished by showing different peak positions in XRD measurements (Malta-Calleja and Vonk). Meanwhile, small-angle X-ray scattering (SAXS) is used to characterize structures of melt crystallized material at a lamellar level. The results of SAXS give information on the periodicity of lamellar stacking, i.e., lamellar thickness (of the order of 10 nm), since larger length scale (5 − 100 nm) are probed. In spite of the different appearances of crystalline morphologies, peak positions of the unfoamed and foamed PBT from XRD measurements are almost identical (Figure 4.33). This suggests that bubble formation induced no apparent change of the crystalline structures or no preferred direction of the crystalline orientation, although such confirmation by a comparison at a larger length scale (lamellar thickness) is not possible in the absence of SAXS data.
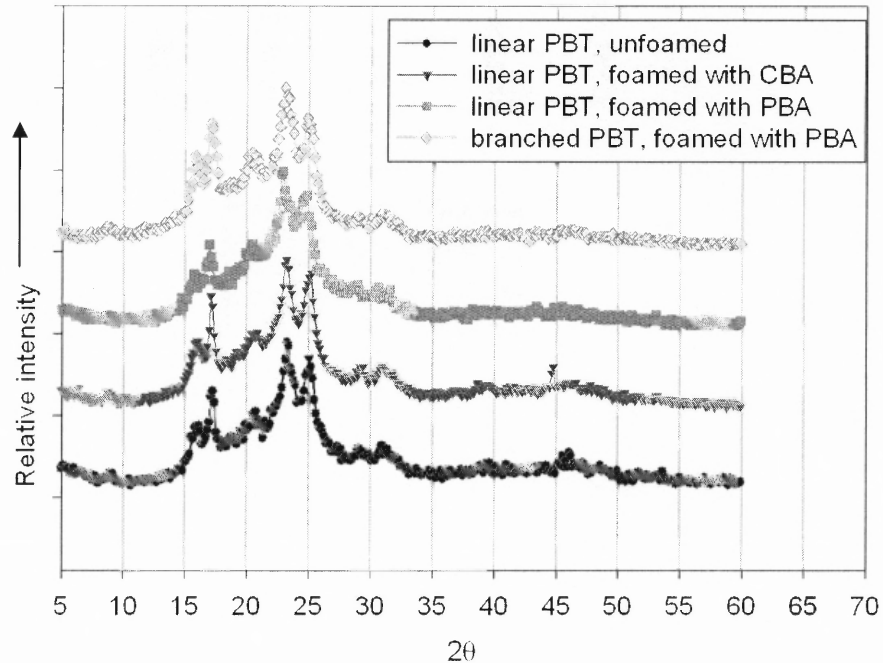
Figure 4.33 XRD results of unfoamed and foamed PBT samples.

4.4.3 Effects of Flow Induced Crystallization

In the section below, attempts are made to relate the spherulitic morphology to flow induced crystallization (FIC). Generally, oriented lamellar structures are expected to be formed by FIC rather than the spherulites which were observed at the bubbles walls. However, the formation of spherulites by FIC may be a characteristic of PBT. Li and de Jeu (2004) performed FIC experiments with a commercial PBT and found that the Avrami exponent did not increase by shear flow by comparison to that under a quiescent condition. As a result, they suggested that PBT formed a spherulitic structure by FIC (not oriented lamellae), although the overall crystallization kinetics were enhanced by the flow.

As mentioned in Section 2.3, bubble formation in a foaming process involves the biaxial deformation (or flow) of the molten polymer matrix during the bubble growth step. The time for bubble growth is typically a few seconds and the corresponding strain rate is in the order of 1 s^{-1} (Gendron and Daigneault, 2000). Bubble formation occurs during a short time period, involving a relatively moderate deformation as compared to the higher deformation in injection molding and spinning where FIC occurs more readily. Thus, in order to confirm that FIC occurs during extrusion foaming, it should be considered that: (1) the deformation by bubble formation is sufficient to form oriented chain segments (i.e., nuclei) and (2) the oriented segments do not relax (disappear) until the foamed extrudate temperature reaches the onset temperature of crystallization.

To the author's knowledge, no data have been reported on the occurrence of FIC during foaming. Only one article, which mentioned FIC as related to foaming (Doelder et al. 2002) is found in the literature. The authors attempted to introduce FIC in their bubble growth model in order to simulate the difference of foaming behavior between nucleated and non-nucleated high melt strength PP; however, the term for FIC by bubble formation was not used during the calculations.

However, there exist modeling (Dai et al. 2006) and experimental (Koscher and Fulchiron, 2002; Deyrail et al. 2002; Li and de Jeu, 2004) results on the occurrence of FIC under relatively low shear strain and shear rates, which are comparable to those in bubble formation. In particular, Deyrail et al. (2002) showed that FIC of PBT at 1 s^{-1} took place at much higher temperatures (210 and 215°C) than the crystallization temperature under a quiescent condition. It should be remembered that bubble formation involves biaxial extensional deformation. Extensional deformations (or flows) are called "strong

flows", since they can generate a high degree of stretching and orientation of the molecules (Dealy and Wissbrun, 1989a). For example, branched polyethylene shows strain hardening behavior under extensional deformation while linear polyethylene does not. However, in a shear flow field, both polyethylenes show shear thinning behavior. In general, the branched molecules should undergo more intensive stretching and orientation in elongational flow fields (Dealy and Wissbrun, 1989b). Considering the occurrence of FIC under the shear rate of 1 s^{-1} by Dai et al. (2006), Koscher and Fulchiron (2002), Deyrail et al. (2002) and Li and de Jeu (2004), it can be inferred that PBT may form the nuclei of FIC more extensively under the biaxial deformation, a "strong flow", occurring during bubble formation.

The bubbles form during a very short time period, and the extrudate containing bubbles is cooled down under quiescent conditions after the end of the bubble growth step. Thus, the relaxation (disappearance) of the nuclei is very critical to the possibility of FIC occurrence by bubble formation. In the present study, reference is made to recent experimental work performed by Azzurri and Alfonso (2005). The authors explained that the nuclei for FIC had a certain "lifetime"; according to their observations, the nuclei formed by flow disappeared gradually by holding above the melting temperature after the cessation of the flow driven by a glass fiber (Figure 4.34). The detailed experimental procedure can be found in the above reference. The authors observed an oriented lamellar structure at short holding times and a spherulitic structure after relatively long holding times, and concluded that the nuclei "lifetime" was proportional to MW (as well as the MWD).
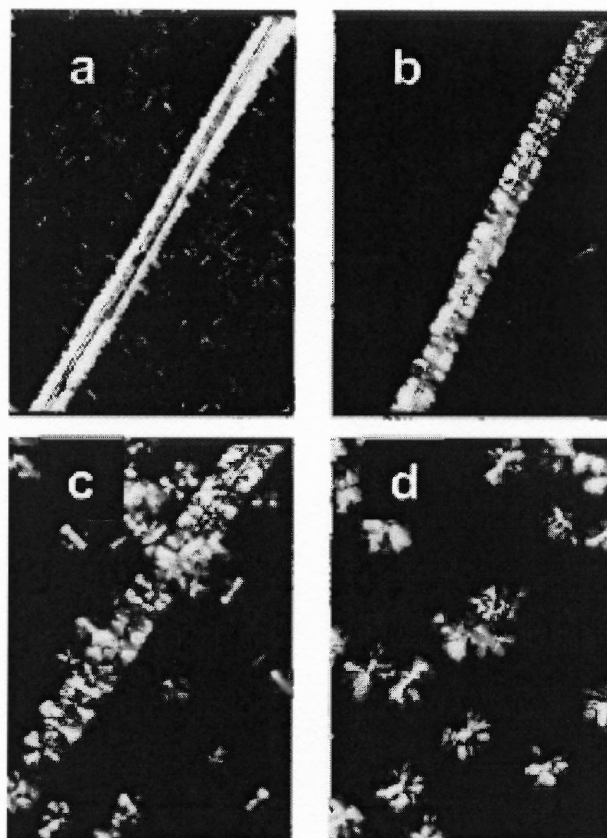
Figure 4.34 Examples of morphological evolution of isotactic poly(1-butene)s after shearing. All samples were sheared and relaxed at 132.5°C and isothermally crystallized at 90 °C. (a) after 6 s, (b) after 60 s, (c) after 420 s, (d) after 690 s (Azzurri and Alfonso, 2005).

Accordingly, FIC by bubble formation may take place if and only if the nuclei formed by the biaxial deformation have a lifetime long enough to be present until the extrudate reaches the temperature corresponding to the onset of crystallization. In other words, the occurrence of FIC by bubble formation depends on a comparison between two time constants: the lifetime of nuclei vs. the time for cooling of the foamed extrudate from the temperature at the die exit to that corresponding to the onset of crystallization.

An elementary calculation of the time for cooling of the foamed extrudate is as follows: the cooling of the extrudate is defined as a one-dimensional heat transfer

problem with cylindrical coordinates. The magnitude of the thermal diffusivity for the PBT foamed extrudate is assumed to be 10^{-4} cm^2/s, considering the experimental results by Lee et al. (1996). As a limiting case, the initial temperature and the temperature at the outer surface are fixed to 235 and 25°C, respectively. The solution of the heat transfer problem with the boundary condition is available in the literature (Bird et al. 2002), and shown schematically in Figure 4.35.
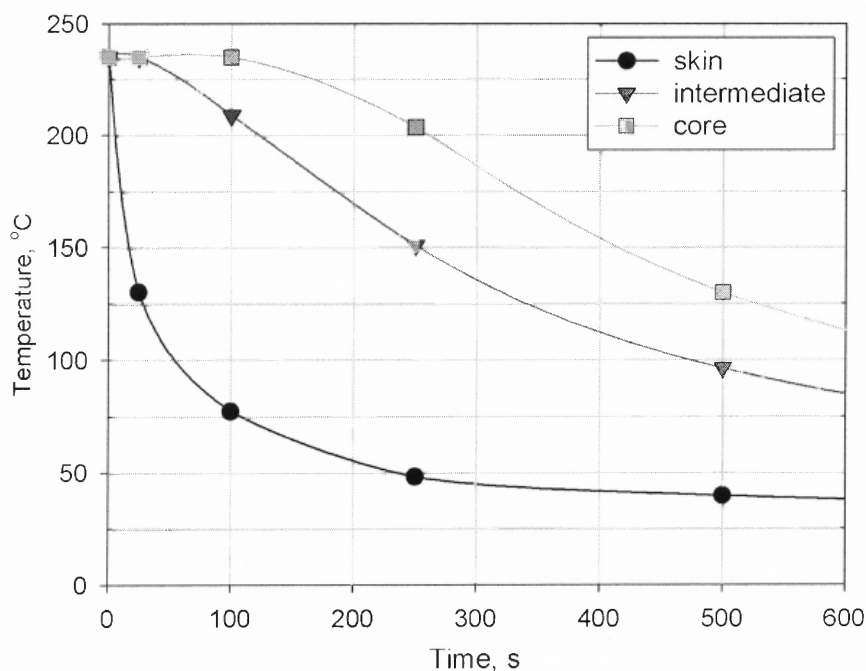
Figure 4.35 Foamed extrudate temperature vs. time. The core is the center of extrudate. The skin and the intermediate are positions away from the center by 90% and 50% of the extrudate radius, respectively.

A quantitative estimation of the onset temperature of crystallization is not possible, due to the absence of information on the increase of the onset temperature by deformation and gas dissolution. A temperature of 200°C is estimated as the increased onset temperature of crystallization. The skin, defined as a position away from the center

by 90% of the extrudate radius, is cooled down to the onset of the crystallization temperature range in less than 20s. At the core, the center of the extrudate requires about less than 5min to reach this onset temperature. At the intermediate position, defined as a position away from the center by 50% of the extrudate radius, it reaches that temperature in about 120 s.

Although work done by Azzurri and Alfonso (2005) is based on observations with a different polymer, the order of magnitude of the lifetime of the precursors can be still obtained. Since the lifetime of the FIC precursors strongly depended on both relaxation temperature and MW, it was difficult to make an average. However, according to an example that was suggested by the authors, it took about 20 s at 142.5°C and 15 hr at 130 °C to erase the memory of flow in the highest MW case. This means that the lifetime was increased by three orders of magnitude with a decrease of 10°C of the relaxation temperature. As compared to the cooling rate of the foamed extrudate above (Figure 4.35), the existence of the precursors when the extrudate reaches the increased onset temperature for crystallization seems to be quite probable. Furthermore, the lifetime scale of the precursors is found to be much longer than reptation times, suggesting that the lifetime of the precursors may be longer than the largest stress relaxation time in the molten state.

Based on the above, it appears that FIC does occur during extrusion foaming, considering the morphological observation of the spherulitic structures at the bubble walls. The molecules oriented by bubble formation relaxed gradually during the cooling stage of the extrudate; however, they were able to survive, thus, contributing to the formation of the spherulitic structure. This is in agreement with the observation by

Azzurri and Alfonso (2005) who showed that the FIC precursors, which were relaxed for a relatively long time period formed spherulites. The smaller spherulites (equivalent to a higher number of the activated nuclei) of the branched PBT foams (Figure 4.28) as compared to the linear PBT (Figure 4.27) provide an additional evidence of the occurrence of FIC. It is well known that formation of nuclei by flow is more pronounced for polymers with longer relaxation times (e.g. higher MW, a branched structure), corresponding to a higher number of nuclei formed under deformation having longer lifetimes (Agarwal et al. 2003; Li and de Jeu, 2004).

CHAPTER 5

CONCLUSIONS AND RECOMMENDATIONS

The scientific and/or engineering interpretation of experimental data generated in this study provided a thorough understanding of reactive processing based on fundamentals of extrusion, as well as information on reactivity and tendency toward degradation of a specific polymer, namely, PBT. This enabled the optimization of processing parameters required to obtain polymer with the desired viscoelastic properties for low density foaming. This is an important contribution, since previous investigations have focused on single elementary steps, as for example reactivity of modifiers or physical/chemical properties of the products, rather than the integrated process. In addition, it should be noted that the effects of crystallization kinetics and crystallinity on extrusion foaming that were extensively investigated in this work, provided comprehensive understanding of the entire foaming process; such information has been limited in the published literature to, mostly, batch foaming. The possibility of occurrence of flow induced crystallization in foaming is also discussed for the first time; this could initiate future studies addressing the combined foaming and flow induced crystallization topics.

Conclusions on specific topics in the thesis are as follows;

Extrusion foaming of PBT with a high temperature CBA was found to depend on processing parameters such as screw speed and die set temperature. These parameters were related to the decomposition kinetics of the CBA and solubility of nitrogen. The unmodified PBT showed low melt strength that allowed partial gas escape from the foamed extrudate. Foaming with CBA limited the reduction of density to levels around

0.6 g/cc under all testing conditions. The establishment of a relationship between foam characteristics (foam density and expansion ratio) and processing parameters is valuable in optimizing properties of the products foamed with CBA.

Reactive modification of PBT to produce a branched structure was accomplished using conventional polymer processing equipment. From a preliminary study in an intensive batch mixer, the reaction of PBT with a trifunctional epoxide (TGIC) was shown to convert a linear PBT to a branched structure with increased MW and a broadened MWD, as suggested from rheological measurements.

The modification reaction was also successfully carried out in a single screw extruder. However, PBT degradation was found to compete against the branching reaction, thus, becoming a considerable parameter to be dealt with through optimization of the extrusion operational conditions. From studies with rpm and feed rate as variables, intensive mixing within an appropriate (relatively short) residence time, was found to favor the modification reaction.

Optimization studies of operational conditions during reactive processing are often not performed or discussed in the literature, although optimization would make possible to scale up a reactive system developed in a lab scale as well as provide the opportunity to improve the quality of the extruded product. Optimized extrusion conditions developed in this study are directly related to the identification of specific viscoelastic characteristics (viscosity, elasticity, extrudate swell, melt strength) required for low density foaming of the branched end product.

The branched product made under the optimized conditions showed good foamability in extrusion by PBA injection. A low density foam (0.33 g/cc) of the

modified PBT was obtained at a high expansion ratio. However, the faster crystallization kinetics after conversion to a branched structure inhibited further cell nucleation and growth, thus, resulting in a lower cell density than in the unmodified PBT foam.

The effects of MW and presence of linear/branched chains on crystallization kinetics were investigated. Degradation occurring during processing induced increased mobility that resulted in faster crystallization kinetics. Branched structure produced by reactive modification had the opposite effects. The parameters of the Avrami equation provided information on the nucleation and crystal growth mechanism of PBT.

A different crystalline spherulitic morphology at the bubble walls (versus that in bulk) was observed in samples foamed with either CBA or PBA, suggesting the formation of morphologies following different crystallization mechanism. However, XRD results showed that there was no difference in the crystalline structures between bubble walls and bulk and no sign of the existence of crystal orientation.

The occurrence of flow induced crystallization during bubble formation was investigated by considering experimental data generated in this work. A definite conclusion on its occurrence was not possible in this study due to the absence of additional supporting experimental and theoretical information; however, the increased number (smaller sizes) of spherulites observed in the branched PBT indicated that the formation of nuclei required to form spherulitic morphology was closely related to the polymer structure, which is one of the parameters known to affect flow induced crystallization.

The following are recommendations for further work.

✓ Changes of solubility and diffusivity of PBA by chemical modification of PBT need to be investigated. The different molecular structures in the modified polymer may involve different free volumes and PBA/polymer affinity resulting from the presence of new end groups.

✓ Experimental investigation on flow induced crystallization under biaxial deformation would be useful. Rather than row structures produced by uniaxial or shear deformation, regular patterns with two dimensional orientation (e.g., spherulitic structure at the bubble walls) could be possibly produced by biaxial deformation.

REFERENCES

P. Agarwal, R. Somani, W. Weng, A. Mehta, L. Yang, S. Ran, L. Liu and B. Hsiao, "Shear-induced crystallization in novel long chain branched polypropylenes by in situ rheo-SAXS and –WAXD", *Macromolecules*, **36**, 5226 (2003)

M. Amon and C. Denson, "A study of the dynamics of foam growth: analysis of the growth of closely spaced spherical bubbles", *Polym. Eng. Sci.*, **24**, 1026 (1984)

E. Andrews; P. Owen and A. Singh, "Microkinetics of lamellar crystallization in a long chain polymer", *Proc. Roy. Soc. Lond.*, **A. 324,** 79 (1971)

A. Arefmanesh and S. Advani, "Diffusion-induced growth of a gas bubble in a viscoelastic fluid", *Rheol. Act.*, **30**, 274 (1991)

M. Avrami, "Kinetics of phase change. I. General theory", *J. Chem. Phys.*, **7**, 1103 (1939)

M. Avrami, "Kinetics of phase change. II. Transformation-time relations for random distribution of nuclei", *J. Chem. Phys.*, **8**, 212 (1940)

M. Avrami, "Kinetics of phase change. III. Granulation, phase change, and microstructure", *J. Chem. Phys.*, **9**, 177 (1941)

P. Azzurri and G. Alfonso, "Lifetime of shear-induced crystal nucleation precursors", *Macromolecules*, **38**, 1723 (2005)

D. Baldwin, C. Park and N. Suh, "A microcellular processing study of poly(ethylene terephthalate) in the amorphous and semicrystalline states. Part I: Microcell nucleation", *Polym. Eng. Sci.*, **36**, 1437 (1996a)

D. Baldwin, C. Park and N. Suh, "A microcellular processing study of poly(ethylene terephthalate) in the amorphous and semicrystalline states. Part II: Cell growth and process design", *Polym. Eng. Sci.*, **36**, 1446 (1996b)

F. Balta-Calleja and C. Vonk, *X-ray scattering of polymers*, Elsevier, Amsterdam (1989)

D. Bikiaris and G. Karayannidis, "Chain extension of polyesters PET and PBT with N,N'-bis(glycidyl ester) pyromellitimides. I.", *J. Polym. Sci.: Part A: Polym. Chem.*, **33**, 1705 (1995)

D. Bikiaris and G. Karayannidis, "Chain extension of polyesters PET and PBT with two new diimidodiepoxides. II.", *J. Polym. Sci.: Part A: Polym. Chem.*, **34**, 1337 (1996)

D. Bikiaris and G. Karayannidis, "Synthesis and characterization of branched and partially crosslinked poly(ethylene terephthalate)", *Polym. Intern.*, **52**, 1230 (2003)

R. Bird, C. Curtiss, R. Armstrong and O. Hassager, Ed., Chapter 4 in *Dynamics of Polymeric Liquids*, Vol. I, John Wiley and Sons, Inc., New York (1987)

R. Bird, W. Stewart and E. Lightfoot, Chapter 12 in *Transport Phenomena*, 2nd edition, John Wiley and Sons, Inc., New York (2002)

M. Blander and J. Katz, "Bubble nucleation in liquids", *AICHE J.*, **21**, 833 (1975)

M. Bradley and E. Phillips, "Novel foamable polypropylene polymers", *Proc. of SPE Ann. Techn. Conf.*, Vol. I, 717 (1990)

P. Carreau, D. De Kee, and R. Chhabra, Chapter 2 in *Rheology of Polymeric Systems: Principles and Applications*, Hanser/Gardner Publications, Inc., Cincinnati (1997)

H. Chae, B. Kim, S. Im and Y. Han, "Effect of molecular and branch structure on the crystallization and rheological properties of poly(butylene adipate)", *Polym. Eng. Sci.*, **41**, 1133 (2001)

L. Chen, X. Wang, R. Straff and K. Blizard, "Shear stress nucleation in microcellular foaming process", *Polym. Eng. Sci.*, **42**, 1151 (2002)

J. Chiou, J. Barlow and D. Paul, "Plasticization of glassy polymers by CO_2", *J. Appl. Polym. Sci.*, **30**, 2633 (1985a)

J. Chiou, J. Barlow and D. Paul, "Polymer crystallization induced by sorption of CO_2 gas", *J. Appl. Polym. Sci.*, **30**, 3911 (1985b)

R. Chou, C. Chang, T. Yu, Y. Tseng and M. Wu, "Crystallization kinetics of poly(1,4-butylene-co-ethylene terephthalate), *Polym. Int.*, **50**, 213 (2001)

J. Colton and N. Suh, "The nucleating of microcellular thermoplastic foam with additives: Part I: Theoretical considerations", *Polym. Eng. Sci.*, **27**, 485 (1987)

Crompton Corp., Product Data Sheet of Expandex® 5-PT

S. Dai, F. Qi and R. Tanner, "Strain and strain-rate formulation for flow-induced crystallization", *Polym. Eng. Sci.*, **46**, 659 (2006)

J. Dealy and K. Wissbrun, Chapter 3 in *Melt Rheology and its role in Plastics Processing: Theory and Applications*, Van Nostrand Reinhold, New York (1989a)

J. Dealy and K. Wissbrun, Chapter 6, *ibid.* (1989b)

J. Dealy and K. Wissbrun, Chapter 10, *ibid.* (1989c)

S. Dey and D. Todd, "Viscosity of blowing agent laden polymer", *Proc. of SPE Ann. Techn. Conf.*, Vol. III, 3122 (2004)

Y. Deyrail, R. Fulchiron and P. Cassagnau, "Morphology development in immiscible polymer blends during crystallization of the dispersed phase under shear flow", *Polymer*, **43**, 3311 (2002)

R. Dhavalikar, M. Yamaguchi and M. Xanthos, "Molecular and structural analysis of a triepoxide-modified poly(ethylene terephthalate) from rheological data", *J. Polym. Sci.: Part A: Polym. Chem.*, **41**, 958 (2003)

R. Dhavalikar and M. Xanthos, "Parameters affecting the chain extrusion and branching of PET in the melt state by polyepoxides", *J. Appl. Polym. Sci.*, **87**, 643 (2003)

R. Dhavalikar and M. Xanthos, "Monitoring the evolution of PET branching through chemorheology", *Polym. Eng. Sci.*, **44**, 474 (2004)

P. Dimitrakopoulos, J. Brady and Z. Wang, "Short- and intermediate-time behavior of the linear stress relaxation in semiflexible polymers", *Phys. Rev. E*, **64**, 050803(R) (2001)

C. Doelder, R. Sammler, R. Koopmans and A. Paquet, "Modeling foam growth in semi-crystalline thermoplastics", *Cellular Polymers*, **21**, 99 (2002)

S. Doroudiani, C. Park and M. Kortschot, "Effect of the crystallinity and morphology on the microcellular foam structure of semicrystalline polymers", *Polym. Eng. Sci.*, **36**, 2645 (1996)

C. Duplay, B. Monasse, J. Haudin and J. Costa, "Shear-induced crystallization of polypropylene: influence of molecular structure", *Polym. Int.*, **48**, 320 (1999)

G. Eder, H. Janeschitz-Kriegl and S. Liedauer, "Crystallization processes in quiescent and moving polymer melts under heat transfer conditions", *Prog. Polym. Sci.*, **15**, 629 (1990)

L. Finelli, N. Lotti and A. Munari, "Influence of branching on the thermal behavior of poly(butylene isophthalate), *J. Appl. Polym. Sci.*, **84**, 2001 (2002)

P. Flory, "Thermodynamics of crystallization in high polymers. I. Crystallization induced by stretching", *J. Chem. Phys.*, **15**, 397 (1947)

GE Plastics, Technical brochure of *"GE Engineering structural foam design & processing guide"*, Pittsfield, MA 01201

R. Gendron and L. Daigneault, Chapter 3 in *Foam Extrusion: Principles and Practice*, S.T. Lee, Ed., Technomic Publishing Company, Lancaster, Pa (2000)

W. Gibbs, *The Scientific Papers*, Vol. 1, Dover, New York (1961)

S. Goel and E. Beckman, "Generation of microcellular polymeric foams using supercritical carbon dioxide. I: Effect of pressure and temperature on nucleation", *Polym. Eng. Sci.*, **34**, 1137 (1994)

H.P. Grace, "Dispersion phenomena in high viscosity immiscible fluid systems and application of static mixers as dispersion devices in such systems", *Chem. Eng. Commun.*, **14**, 225 (1982)

B. Guo and C. Chan, "Chain extension of poly(butylene terephthalate) by reactive extrusion", *J. Appl. Polym. Sci.*, **71**, 1827 (1999)

J. Han and C. Han, "A study of bubble nucleation in a mixture of molten polymer and volatile liquid in a shear flow field", *Polym. Eng. Sci.*, **28**, 1616 (1988)

Y. Handa, Z. Zhang and B. Wong, "Effect of compressed CO_2 on phase transitions and polymorphism in syndiotactic polystyrene", *Macromolecules*, **30**, 8499 (1997)

E. Harrell and N. Nakajima, "Modified Cole-Cole plot based on viscoelastic properties for characterizing molecular architecture of elastomers", *J. Appl. Polym. Sci.*, **29**, 995 (1984)

J. Hoffman and J. Weeks, "X-ray study of isothermal thickening of lamellae in bulk polyethylene at the crystallization temperature", *J. Chem. Phys.*, **42**, 4301 (1965)

J. Hoffman, G. Davis and J. Lauritzen, *In Treatise on Solid State Chemistry: Crystalline and Noncrystalline Solids*, Plenum, New York (1976)

P. Hsu, Doctoral Dissertation, New Jersey Institute of Technology, Newark, NJ (2001)

D. Hurnik, Chapter 13 in *Plastics Additives Handbook*, 5th edition, H. Zweifel, Ed., Carl Hanser Verlag, Minich (2001)

L. Hyde, L. Kishbaugh and J. Katterman, *SAE Technical paper series*, 2002-01-0717 (2002)

K.H. Illers, "Heat of fusion and specific volume of poly(ethylene terephthalate) and poly(butylene terephthalate)", *Colloid & Polymer Sci.*, **258**, 117 (1980)

H. Inata and S. Matsumura, "Chain extenders for polyesters. I. Addition-type chain extenders reactive with carboxyl end groups of polyesters", *J. Appl. Polym. Sci.*, **30**, 3327 (1985)

H. Inata and S. Matsumura, "Chain extenders for polyesters. II. Reactivities of carboxyl-addition-type chain extenders; bis cyclic-imino-ethers", *J. Appl. Polym. Sci.*, **32**, 5193 (1986a)

H. Inata and S. Matsumura, "Chain extenders for polyesters. III. Addition-type nitrogen-containing chain extenders reactive with hydroxyl end groups of polyesters", *J. Appl. Polym. Sci.*, **32**, 4581 (1986b)

H. Inata and S. Matsumura, "Chain extenders for polyesters. IV. Properties of the polyesters chain-extended by 2,2'-bis(2-oxazoline)", *J. Appl. Polym. Sci.*, **33**, 3069 (1987a)

H. Inata and S. Matsumura, "Chain extenders for polyesters. V. Reactivities of hydroxyl-addition-type chain extenders; 2,2'-bis(4H-3,1-benzoxazin-4-one)", *J. Appl. Polym. Sci.*, **34**, 2609 (1987b)

H. Inata and S. Matsumura, "Chain extenders for polyesters. VI. Properties of the polyesters chain-extended by 2,2'-bis(4H-3,1-benzoxazin-4-one)", *J. Appl. Polym. Sci.*, **34**, 2769 (1987c)

O. Ishizuka and K. Koyama, "Crystallization of running filament in melt spinning of polypropylene", *Polymer*, **18**, 913 (1977)

S. Japon, Y. Leterrier and J. Manson, "Recycling of poly(ethylene terephthalate) into closed-cell foams", *Polym. Eng. Sci.*, **40**, 1942 (2000)

F. Jay, J. Haudin and B. Monasse, "Shear-induced crystallization of polypropylenes: effect of molecular weight", *J. Mater. Sci.*, **34**, 2089 (1999)

M. Jayakannan and S. Ramakrishnan, "Effect of branching on the crystallization kinetics of poly(ethylene terephthalate), *J. Appl. Polym. Sci.*, **74**, 59 (1999)

B. Jeong, M. Xanthos and Y. Seo, "Extrusion foaming behavior of PBT resins", *J. Cell. Plast.* **42**, 160 (2006a); *Proc. of SPE Ann. Techn. Conf.*, Vol. II, 2604 (2005)

B. Jeong, M. Xanthos and K. Hyun, "Reactive extrusion of PBT for low density foaming", *Proc. of SPE Ann. Techn. Conf.*, Vol. I, 983 (2006)

P. Jerschow and H. Janeschitz-Kriegl, "The role of long molecules and nucleating agent in shear induced crystallization of isotactic polypropylenes", Int. Polym. Proc., VII, 72 (1997)

A. Keller, "Usual orientation phenomena in polyethylene interpreted in terms of the morphology", *J. Polym. Sci.*, **15**, 31 (1955)

K. Khemani, pp. 54-80 in *Polymeric Foams-Science and Technology*, K. Khemani, ed., ACS Symposium Series 669, Washington D.C. (1997)

K. Kim, A. Isayev and K. Kwon, "Flow-induced crystallization in the injection molding of polymers: a thermodynamic approach", *J. Appl. Polym. Sci.*, **95**, 502 (2005)

R. Klotzer, D. Paul and B. Seibig, "Extrusion of microcellular foams and application", *Proc. of SPE Ann. Techn. Conf.*, Vol. II, 2042 (1997)

R. Koopmans, "Extrudate swell of high density polyethylene. Part I: Aspects of molecular structure and rheological characterization methods", *Polym. Eng. Sci.*, **32**, 1741 (1992)

J. Kornfield, G. Kumaraswamy and A. Issaian, "Recent advances in understanding flow effects on polymer crystallization", *Ind. Eng. Chem. Res.*, **41**, 6383 (2002)

E. Koscher and R. Fulchiron, "Influence of shear on polypropylene crystallization: morphology development and kinetics", *Polymer*, **43**, 6931 (2002)

V. Kumar and N. Suh, "A process for making microcellular thermoplastic parts", *Polym. Eng. Sci.*, **30**, 1323 (1990)

V. Kumar and J. Weller, "Production of microcellular polycarbonate using carbon dioxide for bubble nucleation", *J. Eng. Ind.*, **116**, 413 (1994)

G. Kumaraswamy, A. Issian and J. Kornfield, "Shear-enhanced crystallization in isotactic polypropylene. 1. Correspondence between in situ rheo-optics and ex situ structure determination", *Macromolecules*, **32**, 7537 (1999)

S. T. Lee, "Shear effects on thermoplastic foam nucleation", *Polym. Eng. Sci.*, **33**, 418 (1993)

S. T. Lee, N. Ramesh and G. Campbell, "Study of thermoplastic foam sheet formation", *Polym. Eng. Sci.*, **36**, 2477 (1996)

S.T. Lee, Chapter 4 in *Foam Extrusion: Principles and Practice*, S.T. Lee, Ed., Technomic Publishing Company, Inc., Lancaster, PA (2000)

L. Li and W. de Jeu, "Shear-induced crystallization of poly(butylene terephthalate): a real-time small-angle X-ray scattering study", *Macromolecules*, **37**, 5646 (2004)

T. Loontjens, "Modular approach for novel nanostructured polycondensates enabled by the unique selectivity of carbonyl biscaprolactam", *J. Polym. Sci.: Part A: Polym. Chem.*, **41**, 3198 (2003)

J. Martini, Masters Thesis, Massachusetts Institute of Technology, Cambridge, MA. (1981)

J. Martini, N. Suh and F. Waldman, "Microcellular closed cell foams and their method of manufacture", US Patent No. 4,473,665 (1984)

L. Matuana, C. Park and J. Balatinecz, "Processing and cell morphology relationships for microcellular foamed PVC/wood-fiber composites", *Polym. Eng. Sci.*, **37**, 1137 (1997)

J. Moitzi and P. Skalicky, "Shear-induced crystallization of isotactic polypropylene melts: isothermal WAXS experiments with synchrotron radiation", *Polymer*, **34**, 3168 (1993)

H. Naguib, C. Park and N. Reichelt, "Fundamental foaming mechanisms governing the volume expansion of extruded polypropylene foams", *J. Appl. Polym. Sci.*, **91**, 2661 (2004)

K. Nakamura, T. Watanabe, K. Katayama and T. Amano, "Some aspects of nonisothermal crystallization of polymer. I. Relationship between crystallization temperature, crystallinity, and cooling conditions", *J. Appl. Polym. Sci.*, **16**, 1077 (1972)

A. Nogales, B. Hsiao, R. Somani, S. Srinivas, A. Tsou, F. Balta-Calleja and T. Ezquerra, "Shear-induced crystallization of isotactic polypropylene with different molecular weight distributions: in situ small- and wide-angle X-ray scattering studies", *Polymer*, **42**, 5247 (2001)

C. Park, D. Baldwin and N. Suh, "Effect of the pressure drop rate on cell nucleation in continuous processing of microcellular polymers", *Polym. Eng. Sci.*, **35**, 432 (1995)

C. Park and L. Cheung, "A study of cell nucleation in the extrusion of polypropylene foams", *Polym. Eng. Sci.*, **37**, 1 (1997)

N. Pogodina, H. Winter and S. Srinivas, "strain effects on physical gelation of crystallizing isotactic polypropylene", *J. Polym. Sci. Part B. Polym Phys*, **37**, 3512 (1999)

Pollmann Austria, Technical brochure on *Foam injection molding at Pollmann*, Karlstein, Austria

N. Ramesh, D. Rasmussen and G. Campbell, "Numerical and experimental studies of bubble growth during the microcellular foaming process", *Polym. Eng. Sci.*, **31**, 1657 (1991)

N. Ramesh, Chapter 5 in *Foam Extrusion: Principles and Practice*, S.T. Lee, Ed., Technomic Publishing Company, Inc., Lancaster, PA (2000)

N. Righetti and A. Munari, "Influence of branching on melting behavior and isothermal crystallization of poly(butylene terephthalate), *Macromol. Chem. Phys.*, **198**, 363 (1997)

J. Schultz and J. Petermann, "Transmission electron microscope observations of fibrillar-to-lamellar transformations in melt-drawn polymers. I. Isotactic polypropylene", *J. Colloid Polym. Sci.*, **262**, 294 (1984)

J. Schultz, B. Hsiao, J. Samon, "Structural development during the early stages of polymer melt spinning by in-situ synchrotron X-ray techniques", *Polymer*, **41**, 8887 (2000)

J. Schultz, Chapter 4 in *Polymer Crystallization: The Development of Crystalline Order in Thermoplastic Polymers*, Oxford University Press, Inc., New York (2001a)

J. Schultz, Chapter 6, *ibid.* (2001b)

J. Schultz, Chapter 8, *ibid.* (2001c)

Sigma-Aldrich, Product Catalogue, Milwaukee (2004)

K. Song, W. Li, J.O. Eckert Jr., D. Wu, and R.E. Apfel, *J. Material Sci.*, **34**, 5387 (1999)

L. Sperling, Chapter 6 in *Introduction to Physical Polymer Science*, John Wiley & Sons, Inc., New York (2001)

P. Spitael, Doctoral Dissertation, Univ. of Minnesota, Minneapolis, MN (2003)

P. Spitael and C. Macosko, "Strain hardening in polypropylenes and its role in extrusion foaming", *Polym. Eng. Sci.*, **44**, 2090 (2004)

M. Takada, M. Tanigaki and M. Ohshima, "Effect of CO_2 on crystallization kinetics of polypropylene", *Polym. Eng. Sci.*, **41**, 1938 (2001)

M. Takada and M. Ohshima, "Effect of CO_2 on crystallization kinetics of poly(ethylene terephthalate), *Polym. Eng. Sci.*, **43**, 479 (2003)

V. Tan and M. Kamal, "Morphological zones and orientation in injection-molded polyethylene", *J. Appl. Polym. Sci.*, **22**, 2341 (1978)

J. Throne, "Is your thermoplastic polymer foamable?", *Proc. Foam Conference 96*, LCM Public Relations, Somerset, NJ (1996)

J. Throne, Chapter 1 in *Thermoplastic Foam Extrusion: An Introduction*, Carl Hanser Verlag, Munich (2004a)

J. Throne, Chapter 2, *ibid.* (2004b)

D. Todd , Chapter 1 in *Plastics Compounding; Equipment and Processing*, D. Todd, <u>Ed</u>, Carl Hanser Verlag, Munich (1998)

D. Todd, C. Gogos and D. Charalampopoulos, "Helical barrel rheometer", US Patent No. 5,708,197 (1998)

B. Wunderlich, Chapter 6 in *Macromolecular Physics*, Vol. 2, Academic Press, Inc., London (1976)

M. Xanthos, Q. Zhang, S. Dey, Y. Li and U. Yilmazer, "Effects of resin rheology on the extrusion foaming characteristics of PET", *J. Cell. Plast.*, **34**, 498 (1998)

M. Xanthos and S. Dey, Chapter 12 in *Foam Extrusion: Principles and Practice*, S.T. Lee, Ed., Technomic Publishing Company, Inc., Lancaster, PA (2000)

M. Xanthos, U. Yilmazer, S. Dey and J. Quintans, "Melt viscoelasticity of polyethylene terephthalate resins for low density extrusion foaming", *Polym. Eng. Sci.*, **40**, 554 (2000a)

M. Xanthos, S. Dey, Q. Zhang and J. Quintans, "Parameters affecting extrusion foaming of PET by gas injection", *J. Cell. Plast.*, **36**, 102 (2000b)

M. Xanthos, M. Young, G. Karayannidis and D. Bikiaris, "Reactive modification of polyethylene terephthalate with polyepoxides", *Polym. Eng. Sci.*, **41**, 643 (2001)

M. Xanthos, in *Handbook of Thermoplastic Polyesters*, S. Fakirov Ed., Wiley-VCH, Weinheim, p815-831 (2002)

M. Xanthos, C. Wan, R. Dhavalikar, G. Karayannidis and D. Bikiaris, "Identification of rheological and structural characteristics of foamable poly(ethylene terephthalate) by reactive extrusion", *Polym. Intern.*, **53**, 1161 (2004)

U. Yilmazer, M. Xanthos, G. Bayram, V. Tan, "Viscoelastic characteristics of chain extended/branched and linear polyethylene terephthalate resins", *J. Appl. Polym. Sci.*, **75**, 1371 (2000)

K. Yoon and O. Park, "Diffusion of butanediol in poly(butylene terephthalate) (PBT) melt and analysis of PBT polymerization reactor with surface renewal", *Polym. Eng. Sci.*, **35**, 703 (1995)

Q. Zhang and M. Xanthos, Chapter 4 in *Polymeric Foams: Mechanisms and Materials*, S.T. Lee, ed., CRC Press, New York (2004)